Polymères électrostrictifs à forte déformation : méthode d'élaboration et modélisation

Masae Kanda

To cite this version:

Masae Kanda. Polymères électrostrictifs à forte déformation : méthode d'élaboration et modélisation. Other. INSA de Lyon, 2011. English. NNT : 2011ISAL0067 . tel-00701539

HAL Id: tel-00701539
https://theses.hal.science/tel-00701539
Submitted on 25 May 2012

N° d'ordre 2011-ISAL-0067 Année 2011

Thèse

High strain electrostrictive polymers: elaboration methods and modelization

By

Masae KANDA

A thesis submitted in fulfilment
of the requirements for the degree of

Doctor of Philosophy

School of doctorate: Electronic, Electrotechnic and Automatic (E.E.A.)

INSA-Lyon
Lyon, France
21 July 2011

Advisory Committee:

Dr.	Yves BERNARD	Université Paris 11, Assoc. Prof. (HDR)	Reviewer
Prof.	Yoshitake NISHI	Tokai University, Japan	Reviewer
Dr.	Gilbert TEYSSEDRE	Laplace, UMR5213 Université Paul Sabatier, Toulouse, Directeur of reseach (CNRS)	Committee Member
Dr.	Eric DUHAYON	Université de Toulouse, Assoc. Prof.	Committee Member
Prof.	Daniel GUYOMAR	LGEF, INSA-Lyon	Advisor
Dr.	Kaori YUSE	LGEF, INSA-Lyon, Assoc. Prof.	Co-Advisor

Laboratoire de recherche :
Laboratoire de Génie Electrique et Ferroélectricité (LGEF) de l'INSA de Lyon

INSA Direction de la Recherche - Ecoles Doctorales – Quinquennal 2011-2015

SIGLE	ECOLE DOCTORALE	NOM ET COORDONNEES DU RESPONSABLE
CHIMIE	**CHIMIE DE LYON** **http://www.edchimie-lyon.fr** Insa : R. GOURDON	M. Jean Marc LANCELIN Université de Lyon – Collège Doctoral Bât ESCPE 43 bd du 11 novembre 1918 69622 VILLEURBANNE Cedex Tél : 04.72.43 13 95 directeur@edchimie-lyon.fr
E.E.A.	**ELECTRONIQUE, ELECTROTECHNIQUE, AUTOMATIQUE** **http://edeea.ec-lyon.fr** Secrétariat : M.C. HAVGOUDOUKIAN eea@ec-lyon.fr	M. Gérard SCORLETTI Ecole Centrale de Lyon 36 avenue Guy de Collongue 69134 ECULLY Tél : 04.72.18 60 97 Fax : 04 78 43 37 17 Gerard.scorletti@ec-lyon.fr
E2M2	**EVOLUTION, ECOSYSTEME, MICROBIOLOGIE, MODELISATION** **http://e2m2.universite-lyon.fr** Insa : H. CHARLES	Mme Gudrun BORNETTE CNRS UMR 5023 LEHNA Université Claude Bernard Lyon 1 Bât Forel 43 bd du 11 novembre 1918 69622 VILLEURBANNE Cédex Tél : 04.72.43.12.94 e2m2@biomserv.univ-lyon1.fr
EDISS	**INTERDISCIPLINAIRE SCIENCES-SANTE** **http://ww2.ibcp.fr/ediss** Sec : Safia AIT CHALAL Insa : M. LAGARDE	M. Didier REVEL Hôpital Louis Pradel Bâtiment Central 28 Avenue Doyen Lépine 69677 BRON Tél : 04.72.68 49 09 Fax : 04 72 35 49 16 Didier.revel@creatis.uni-lyon1.fr
INFOMATHS	**INFORMATIQUE ET MATHEMATIQUES** **http://infomaths.univ-lyon1.fr**	M. Johannes KELLENDONK Université Claude Bernard Lyon 1 LIRIS - INFOMATHS Bâtiment Nautibus 43 bd du 11 novembre 1918 69622 VILLEURBANNE Cedex Tél : 04.72. 43.19.05 Fax 04 72 43 13 10 infomaths@bat710.univ-lyon1.fr
Matériaux	**MATERIAUX DE LYON**	M. Jean-Yves BUFFIERE Secrétaire : Mériem LABOUNE INSA de Lyon École Doctorale Matériaux Mériem LABOUNE Bâtiment Antoine de Saint-Exupéry 25bis Avenue Jean Capelle 69621 VILLEURBANNE Tel : 04 72 43 71 70 Fax : 04 72 43 72 37 ed.materiaux@insa-lyon.fr
MEGA	**MECANIQUE, ENERGETIQUE, GENIE CIVIL, ACOUSTIQUE (ED n°162)**	M. Philippe BOISSE Secrétaire : Mériem LABOUNE Adresse : INSA de Lyon École Doctorale MEGA Mériem LABOUNE Bâtiment Antoine de Saint-Exupéry 25bis Avenue Jean Capelle 69621 VILLEURBANNE Tel : 04 72 43 71 70 Fax : 04 72 43 72 37 mega@insa-lyon.fr Site web : http://www.ed-mega.com
ScSo	**ScSo*** M. OBADIA Lionel Sec : Viviane POLSINELLI Insa : J.Y. TOUSSAINT	M. OBADIA Lionel Université Lyon 2 86 rue Pasteur 69365 LYON Cedex 07 Tél : 04.78.69.72.76 Fax : 04.37.28.04.48 Lionel.Obadia@univ-lyon2.fr

*ScSo : Histoire, Geographie, Aménagement, Urbanisme, Archéologie, Science politique, Sociologie, Anthropologie

Résumé

De façon générale la thèse porte sur les matériaux dits intelligents et plus particulièrement sur les polymères electroactifs et/ou electrostrictifs. Ces matériaux présentent un fort couplage electro-mécanique et sont par ailleurs très flexibles et très légers. Ils se déforment lorsqu'ils sont soumis à un champ électrique et peuvent générer un courant ou un champ lorsqu'ils subissent une déformation mécanique. C'est dire qu'ils peuvent être utilisés soit comme actionneurs mécaniques souples, soit en récupération d'énergie sur l'énergie vibratoire.

Le sujet de thèse portait sur :

- le développement d'une nouvelle méthode, peu coûteuse, de réalisation de films polymère électrostrictifs à partir de micelle déjà formées et permettant une meilleure dispersion des particules de carbone.
- L'augmentation de la permittivité, afin d'augmenter le couplage électro-mecanique en chargeant le polymère avec des particules conductrices et/ ou par bombardement électronique.
- La modélisation mathématique des phénomènes observés et les projections afin d'améliorer les caractéristiques de ces derniers.

Le premier chapitre est une introduction aux systèmes couplés reliant les propriétés mécaniques et les propriétés électriques entre elles (piézoélectricité, polymères électro-actifs, polymères ioniques…). L'objectif de ce chapitre est également de choisir le type de polymère le plus adapté à la réalisation d'actionneurs flexibles ou de récupérateurs d'énergie. Notre choix s'est porté sur les élastomères diélectriques et, en particulier les polyuréthanes.

Le second chapitre porte principalement sur la réalisation des films polymères. La déformation électrostrictive augmentant, dans une certaine limite, avec la permittivité diélectrique, nous avons donc décidé d'introduire des charges dans la matrice polymère afin d'augmenter la permittivité. A ce stade, nous avions le choix entre des charges diélectriques ou des charges conductrices. En raison du contraste de permittivité entre le polymère et les charges diélectriques et de la masse ramenée, nous avons opté pour l'introduction de charges conductrices (noir de carbone), qui changent peu la densité de masse pour des variations relativement importantes de la permittivité mais qui présentent une forte conduction près de la percolation. C'est à dire qu'il faut choisir ou développer un procédé de réalisation du polymère composite qui permet une bonne dispersion des charges dans la matrice. Afin de pouvoir réaliser, in fine, des films de surface importante, tout en ayant une bonne dispersion, nous avons introduit le carbone sous forme de micelles préformées. En l'occurrence nous avons mélangé des encres d'écriture avec le polyuréthane et choisi une technique de type « solution-cast » pour réaliser les films. Une amélioration de la déformation d'un facteur 1,6 a ainsi été obtenue par introduction de noir de carbone à 0.89 vol%.

Le troisième chapitre porte sur la modélisation des phénomènes, menée en collaboration avec l'encadrant, et en particulier sur la saturation de la polarisation, ce qui implique directement une saturation de la déformation electrostrictive et une limitation de la course des actionneurs. En modélisant la polarisation comme une fonction non-linéaire

dépendant de deux variables (la permittivité bas niveau et un champ de saturation), on décrit correctement :

- les effets de saturation des niveaux
- le processus qui limite l'augmentation de la déformation avec la permittivité
- la dépendance de la déformation en fonction de l'épaisseur
- les effets liés aux pertes diélectriques et/ou électrostrictives.
- les écarts importants entre la formulation en champ électrique et la formulation en polarisation ; cette dernière respectant mieux la physique du phénomène.
- La distorsion des courants et la variation de la conductivité avec le champ électrique.
- L'évolution fortement non-linéaire de la permittivité avec le champ
- La connexion très forte entre la permittivité équivalente du film et la déformation de ce dernier.
- Les effets de croissance ou de décroissance de la déformation avec l'épaisseur de ce dernier.

La modélisation nous a amené à supposer l'existence d'un gradient de propriété dans le sens de l'épaisseur. Etant donné que les simulations sont en bon accord avec les expérimentations, on peut considérer que l'hypothèse est valide. Plusieurs modèles, en régime linéaire et non-linéaire, ont été développés à partir de cette hypothèse.

Le quatrième chapitre présente une comparaison approfondie entre les films en pure polyuréthane et ceux chargés avec des particules conductrices. La comparaison porte non seulement sur des mesures mécaniques et électriques mais également sur des mesures en XRD ou en DSC afin de détecter un niveau de cristallisation lié aux segments durs présents dans le polymère. Il semblerait que le taux de cristallisation dépende de l'épaisseur du film et que les films minces auraient un taux de segments durs plus élevé que les films épais, ce qui augmenterait la déformation. En ce qui concerne les composites, nous avons montré que la méthode de fabrication proposée permet d'obtenir une bonne dispersion des particules et ceci sans avoir recours à la dispersion par ultrasons de puissance et sans utiliser la tournette. Une dispersion importante a ainsi été observée visuellement. C'est donc un résultat important car il devient alors possible d'obtenir des films de grande surface présentant une bonne dispersion des particules conductrices. Les courbes de déformation en fonction de l'épaisseur pour différents taux de charge confirment ce résultat. Des déformations de l'ordre de 50 % ont ainsi été obtenues.

Le cinquième chapitre porte sur l'effet lié à l'injection de charges électriques, par corona ou par bombardement électronique, sur la déformation électrostrictive. Si les résultats obtenus par effet corona ne sont pas convaincants, ceux obtenus par bombardement électronique (Homogeneous Electron Beam Irradiation (HEBI)) sont très intéressants. En effet, on gagne un facteur de l'ordre de 2 sur la déformation et le bombardement électronique semble réduire les pertes de façon très conséquente. Par contre l'effet diminue rapidement avec le temps puisqu'on note une réduction conséquente de l'effet après 2 mois.

Mots-clés:
Polymères électro-actifs, Composites, Actionneurs, Effet d'épaisseur, Permittivité, Micelle

Abstract

In a general manner, the present thesis focuses on the so-called smart materials, especially on electroactive polymers and / or electrostrictive. These materials exhibit a strong electro-mechanical coupling and are also very flexible and very light. They deform when subjected to an electric field and can generate a current or an electric field when subjected to mechanical deformation. That means that they can be used either as flexible mechanical actuators, or as energy harvester on ambient vibrations sources.

The thesis focused on:
- development of a new method for inexpensive electrostrictive polymer film production with carbon black (CB) already formed micelle that allows a good CB particles dispersion in the matrix
- increasing the permittivity in order to increase the electro-mechanical coupling by loading the polymer with conductive particles and / or electron beam irradiation.
- Mathematical modeling of the observed phenomena and projections to improve the characteristics of the films in terms of strain level.

The first chapter is an introduction to coupled systems linking the mechanical and electrical properties with one another (piezoelectrics, electroactive polymers, ionic polymers ...). The purpose of this chapter is to choose the type of polymer that is best for the realization of flexible actuators or energy recovery. Our choice fell on dielectric elastomers and more specifically on polyurethanes.

The second chapter focuses on the of polymer films making. Since the electrostrictive strain increases, to a certain limit, with the dielectric permittivity, I decided to incorporate fillers in the polymer matrix in order to increase the permittivity. At this point, I had a choice between dielectric or conductive fillers. Due to the permittivity contrast and added mass between the polymer and the dielectric charges, I opted for the introduction of conductive fillers (CB), which change little for the mass density for large permittivity variations but which exhibit high conductivity near percolation threshold. This means that I must choose or develop a method for producing the polymer composite that provides a good dispersion of fillers in the matrix. In order to realize, ultimately, well dispersed large-area films, I introduced the carbon in the form of preformed micelles. In this case I mixed writing inks with polyurethane and chosen a technical type "solution-cast method” to make the films. The strain enhancement of a factor of 1.6 was obtained by doping 0.89 vol% CB composite.

The third chapter focuses on the modeling aspect, established with the help of adviser, in particular the saturation of the polarization which directly implies a saturation of the electrostrictive strain and, consequently a limit of the actuator stroke. Modeling the polarization as a nonlinear function depending on two variables: the permittivity and a saturation field, leads to a good description of
- the effects of saturation levels,
- the process that limits the increase of deformation with the permittivity,
- the dependence of the deformation on the film thickness,
- the effects related to dielectric and / or electrostrictive losses,

- the significant differences between the formulation in terms the electric field and polarization formulation which is compliant with the physics of dielectrics,
- the strong distortion of currents and the variation of conductivity with the electric field,
- the highly non-linear permittivity behavior with the electric field,
- the strong connection between the film equivalent permittivity and its strain,
- the effects of growth or decay of the strain with the thickness of the latter.

The modeling led us to assume the existence of a property gradient in the thickness direction.

Given that the simulations are in good agreement with experiments, we can consider that the hypothesis is valid. Several models in linear and nonlinear have been developed based on that assumption.

The fourth chapter presents a detailed comparison between the pure polyurethane films and those loaded with conductive particles. The comparison includes mechanical and electrical measurements as well as XRD or DSC measurement to detect a level of crystallization associated with hard segments present in the polymer. It seems that the crystallization depends on the film thickness. Thin films would have a hard segment rate higher than the thick films, which would increase the strain. Regarding composites, I have shown that the proposed manufacturing method enables a good dispersion of particles without recourse to the ultrasonic mixing and without using spin-coating. High dispersion level was visually confirmed. It is therefore an important result because it then becomes possible to obtain large area films with good conductive particles dispersion. Looking at the strain curves versus the film thickness, for different loading rates, confirms this result. Strains of the order of 50 % were reached.

The fifth chapter deals with the effect of electric charge injection by corona and electron beam irradiation methods on the electrostrictive strain. Besides the results obtained by corona effect which are not convincing, those by homogeneous electron beam irradiation (HEBI) are very interesting. Indeed, the electrostrictive strain after HEBI has been multiplied more than 2. It seems also that the HEBI strongly reduces the losses in material. In the comparison with corona treatment of which the effect decreases within a few hours, it was confirmed experimentally that the effect by HEBI decreases less rapidly with time as I noted a substantial reduction of the effect after 2 months.

Keywords:
Electrostrictive polymer, Composite, Actuator, Thickness effect, Permittivity, Micelle

Acknowledgments

I would like to express my sincere gratitude to my supervisor, Professor Daniel Guyomar for providing me this precious study opportunity as a PhD student in his laboratory. I especially would like to express my deepest appreciation to my supervisor, Assoc. Prof. Kaori Yuse for her elaborated guidance, considerable encouragement and invaluable discussion that make my research of great achievement and my study life unforgettable.

I would like to thank Professor Laurent Lebrun, Assoc. Prof. Bernoit Guiffard, Dr. Laurence Seveyrat, Assoc. Prof. Agnès Bogner-Van de Moortèle (MATEIS, INSA Lyon) and Mr. Yasuo Miyamoto (Tokai University) for providing help and advices in completing this research. I also would like to specially thank Dr. Pierre-Jean Cottinet and Mr. Komkrid Wongtimnoi for their kindness help and support. I also would like to specially thank Assoc. Prof. Mickaël Lallart for his kindness help and support of French language.

Thanks also go to Mr. Frederic Defromerie and Ms. Veronique Perrin for machining the art-like device for my design and experiment. I also would like to thank Ms. Evelyne Dorieux, secretary of Laboratory for her supporting. I also would like to thank Mr. Michael C. Faudree (Tokai University) for his correction of English.

In addition, I would like to thank my colleagues in the Génie Electrique and Ferroélectricité laboratory (Dr. Xingjun Wang, Dr. Chatchai Putson, Mr. Jiawei Zhang, Mr. Kaixiang Li, Ms. Hongying Zhu, Ms. Dan Wu, Mr. Qin Liu and Ms. Yi-Chieh Wu).

I will not be able to list the names of all whom I feel grateful to, but I would like to express my gratitude to all of the members of LGEF and Nishi laboratory, scientific and administrative for their help and support during my work.

I would like to acknowledge LGEF, INSA Lyon and Tokai University.

I am also very grateful to the Japanese Government Support for a Long-term Study Abroad scholarship under the Project for Establishing Core Universities for Internationalization by the Minister of Education, Culture, Sports, Science and Technology (MEXT) for making my Ph.D. study possible by the financial support. I would like to thank Professor Hirohisa Uchida and Ms. Kumiko Tanaka (Tokai University) for their kindness help and support of my scholarship.

I would like to thank most sincerely the Professor Yoshitake Nishi (Tokai University) and Assoc. Prof. (HDR) Yves Bernard (Université Paris 11), for reviewing my manuscript. I want them to know how much their comments will be appreciated.

Finally I would like to extend my great thanks to my father, mother and sisters for their endless love, understanding, support, encouragement and sacrifice throughout my study.

Table of Contents

Chapter 1
General introduction

Chapter 2
Material, Fabrication procedure and experimental set up of electroactive polyurethane composites

Chapter 3
Modeling the electrostritive films behaviors

Chapter 4

Part 1: Polyurethane films

Part 2: Composites films

Chapter 5
Effect of injecting a charge of film on electroactive strain

Nomenclature

A	area of surface
A_0	strain free surface
A_1	side surface of the first layer
C	capacitance
C_n	capacitance of each layer
C_0	speed of light in vacuum
d	piezoelectric charge constant
D	electric flux density
D_{th}	electron beam irradiation depth
E	electric field
Ee	irradiation voltage
E_{con}	second strain derivative vanishes
E_{max}	maximum electric field
E_{sat}	saturation electric field
F_1	force of the first layer
I	current
I_n	current in each layer
I_0	current for the free strain case
L	total film thickness
L_n	thickness of each layer
L_1	skin film thickness
l_0	mass thickness
M	electrical-field-related-electrostriction coefficient
p	actuation pressure
P	polarization
P^*	apparent polarization
P_r	remnant polarization
Q	polarization-related-electrostriction coefficient
R	resistance
s	elastic compliance
S	strain
$S_{\mathrm{electrostriction}}$	mechanical strain response
$S_{Maxwell}$	Maxwell stress
S_{max}	maximum strain
s^E	elastic compliance at constant field
T	mechanical stress
u	total deformation in 1-direction
V	voltage
$\dot{V}$	voltage derivative
Y	Young modulus
ε	Permittivity
ε_{eq}	equivalent permittivity
ε^T	remains constant

ε_r	relative permittivity
ε_0	space permittivity (8.854×10^{-12} F/m)
ε_1	permittivity in the skin layer
ε_2	permittivity in the inner layer
μ_0	permeability in vacuum
γ	coefficient
ν	Poisson ratio coefficient
σ	conductivity
ρ	density
χ	electric susceptibility
χ_e	frequently

Introduction

Electroactive polymers (EAPs) change significantly in size or in shape by electrical stimulation. These polymers have attracted a great deal of attention due to also their many useful properties, such as flexibility, light weight, high mechanical strength, easy processing to large area films and ability to be molded into a various configuration. EAPs exhibit specific characteristics which make them suitable for new types of actuator materials. The high electric field is, however, in general required in order to present large strains of most of EAPs today. The idea was to fabricate films capable of generating a large strain while requiring only a low electric field. The present thesis focuses on the so-called smart materials, especially on electroactive and / or electrostrictive polymers.

In the present thesis, polyurethane (PU) is chosen because its modulus and relative permittivity is higher than that of silicone rubber. Beside, the relative permittivity of copolymer is quite high, but strain of copolymer is smaller than PU. Pure PU elastomers are one of the most important class of polymers due to some remarkable electromechanical characteristics such as large electric field induced strain, high specific energy and fast speed of response. This makes the material very attractive for many electromechanical applications. Many electroactive strain properties of the PU have been investigated but the fundamental mechanisms which are responsible for the electrostriction have not been yet well understood.

Since the electrostrictive strain is increases, to a certain limit, with its dielectric permittivity, I decide to introduce fillers in the polymer matrix in order to increase the permittivity. Conductive fillers, carbon black (CB) nanoparticles, were chosen to make composite films in pure PU matrix in order to increase the effectively in electroactive strain. Since the electric field must vanish inside the conductive particles, electrical charges appear on the particle surface in order to create the applied electric field. These charges create on particle polarization. This polarization is not remnant but indeed vanishes when the applied electric field is removed. This is a great advantage of EAP in front of ferroelectrics. I mix writing inks with PU. Micelle formed CB, directly obtained from nanoink, was used in order to avoid aggregation. Fabrication procedure is a technical type "solution cast method" to make movies. Dispersion condition inside film is observed by Scanning Electron Microscope (SEM) and Transmission Electron Microscope (TEM).

Mathematical modeling on the observed phenomena and projections are carried out to improve the characteristics of the films in terms of strain level. Saturated polarization is taken into account. The modeling is compared with experimental data.

It seems interesting to evaluate the actuation performance of a dielectric material in which electrical charges have been injected. The most well known technique for injecting a charge is the corona treatment. It is, however, famous that their effect would not stay long. As one of the other methods of injecting a charge, there is homogeneous electron beam irradiation (HEBI). I evaluate and explain the effect of these treatments.

Chapter 1
General introduction

1.1 Introduction
1.2 Piezoelectric material
  1.2.1 Principle of piezoelectricity
  1.2.2 Types of piezoelectric
  1.2.3 Mathematical description
1.3 Electroactive polymer (EAP)
  1.3.1 EAP and other sensors/actuators materials
  1.3.2 Historical background
  1.3.3 Types of EAP
  1.3.4 Ionic EAP
    a) Ionic polymer-metal composite (IPMC)
    b) Ionic polymers gel (IPG)
    c) Conductive polymer (CP)
    d) Carbon nanotube (CNT)/polymer
  1.3.5 Electronic EAP
    a) Piezoelectric polymer
    b) PZT particle/polymer
    c) Dielectric elastomer
    d) Electrostricive graft elastomer
    e) Electrorheological fluid (ERF)
1.4 Dielectric elastomer
  1.4.1 Dielectric properties
  1.4.2 Some famous materials of dielectric elastomer
  1.4.3 Electromechanical actuation mechanisms
    a) Electrostriction
    b) Maxwell stress effect
  1.4.4 Actuation pressure
  1.4.5 Application availability
    a) Artificial muscles
    b) Energy harvesting
    c) Robot application

1.1 Introduction

As materials for the transition between mechanical and electrical energy, the piezo element is the most frequent and widely commercialized material due to its numerous advantages, such as its high precision, high electro-mechanical responses, and its elevated response speeds. This conversion from mechanical energy to electric energy exhibited by a piezoelectric material is known as the “direct piezoelectric effect”. Unique properties of piezoelectric enable people to utilize them in a wide range of applications. Nevertheless, drawbacks exist. The piezoelectric materials require a low electric driving field (< 5 MV/m) and in return, they can generate only a small deformation (< 0.2 %) **[1]**.

Polymer actuators demonstrate many advantages, such as soft actuation, easy manufacturing, being light weight and, especially, presenting a large strain rate. Electroactive polymers (EAPs) are used as polymer actuators **[2]**. EAPs are presently capable of generating a large deformation. For example, dielectric polymer actuators can generate large strains when electric dipoles are present within the polymer. It can be noted that these materials constitute some of the most studied polymer actuators. In many research investigations, large strains up to 10-100 % have been easily observed **[3, 4]**. Since the strain of human muscles is limited to around 20 %, these materials would be quite interesting for the fabrication of artificial muscles. Electroactive strain values up to 380 % have even been reported when a silicone rubber has been used as the matrix material **[5]**. This extraordinary result has dramatically increased the potential of EAPs. Nevertheless, it should be noted that these results were obtained under quite high values of the driving electric field, such as 150 MV/m. The fact that such high values are required limits the use of EAPs since few handy electric components can stand to be used together.

Both advantages and drawbacks can depend on the applications, such as the response speed, endurance limit and induced stress. Even so, a reduction of the required energy is desired in order to use EAPs in actuating applications.

With the aim of creating sensor/actuator materials for energy harvesting **[6-8]**, the present thesis research has been devoted to evaluating the strain of intermediate materials between piezo and today’s EAPs. Based on the advantages of these types of materials, the idea was to fabricate films capable of generating a large strain while requiring only a low electric field.

In this chapter, fundamentals of piezoelectric material and EAPs are described.

1.2 Piezoelectric material

1.2.1 Principle of piezoelectricity

In 1880, the first demonstration of the direct piezoelectric effect was given by Pierre Curie and Jacques Curie that an electric potential was generated when crystals were compressed. They demonstrated the effect by using crystals of tourmaline, quartz, topaz, cane sugar, and Rochelle salt (sodium potassium tartrate tetrahydrate, $NaKC_4H_4O_6$-$4H_2O$). The quartz and Rochelle salt exhibited the highest piezoelectricity. However Curies didn’t predict an inverse piezoelectric effect. The inverse piezoelectric effect was mathematically deduced from fundamental thermodynamic principles by Gabriel Lippmann in 1881. The Curies immediately confirmed the existence of the inverse piezoelectric effect, and went on to obtain quantitative proof of the complete reversibility of electro-elasto-mechanical deformations in piezoelectric crystals. The inverse piezoelectric effect corresponds to a distortion at the time of application of an electric field (Figure 1.1).

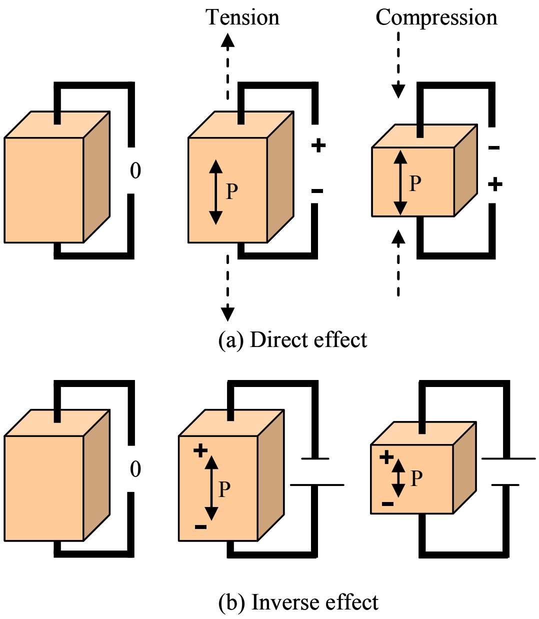

Figure 1.1 Piezoelectric effects.

Lead zirconate titanate (Pb (Zr,Ti)O_3), called PZT in general, is a ceramic perovskite material that shows a remarkable piezoelectric effect. It was found and has been investigated in mid-20th century.

The perovskite materials are of the great importance among all the piezoelectric ceramics because most of the piezoelectric materials used today belong to this family. This structure has a general formula ABO_3 and is described as a simple cubic unit cell with the corners occupied by a large cation ("A", such as Pb, Ba, Ca, K, Na, etc.), a smaller cation ("B", such as Ti, Nb, Mg, Zr, etc.) and oxygen in the face centers, as shown in Figure 1.2.

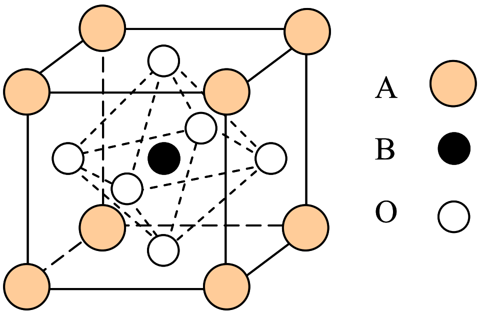

Figure 1.2 Schematic of the perovskite structure (ABO_3).

This structure can also be visualized as corner-linked oxygen octahedral with a small cation sitting in the center (B) of the octahedron and a large cation (A) filling the dodecahedral hole in between the oxygen octahedral.

Figure 1.3 explains the structural function of piezoelectricity by using $BaTiO_3$ **[9]**. The $BaTiO_3$ is one of the first artificial piezoelectric, materials found between natural crystal and artificial PZT. When temperature is above Curie temperature of 129.85 °C, the $BaTiO_3$ is non-polar and becomes cubic form. Below that temperature, structure changes according the temperature, then it is electrically polarized. Firstly, the polarization along a <100> direction appears and the form is spontaneously tetragonally-distorted. On further cooling, it undergoes further phase transformations to <110> polarized orthorhombic at 4.85 °C and then <111> polarized rhombohedral at -90.15 °C. Let us focus on the <100> polarized tetragonal state.

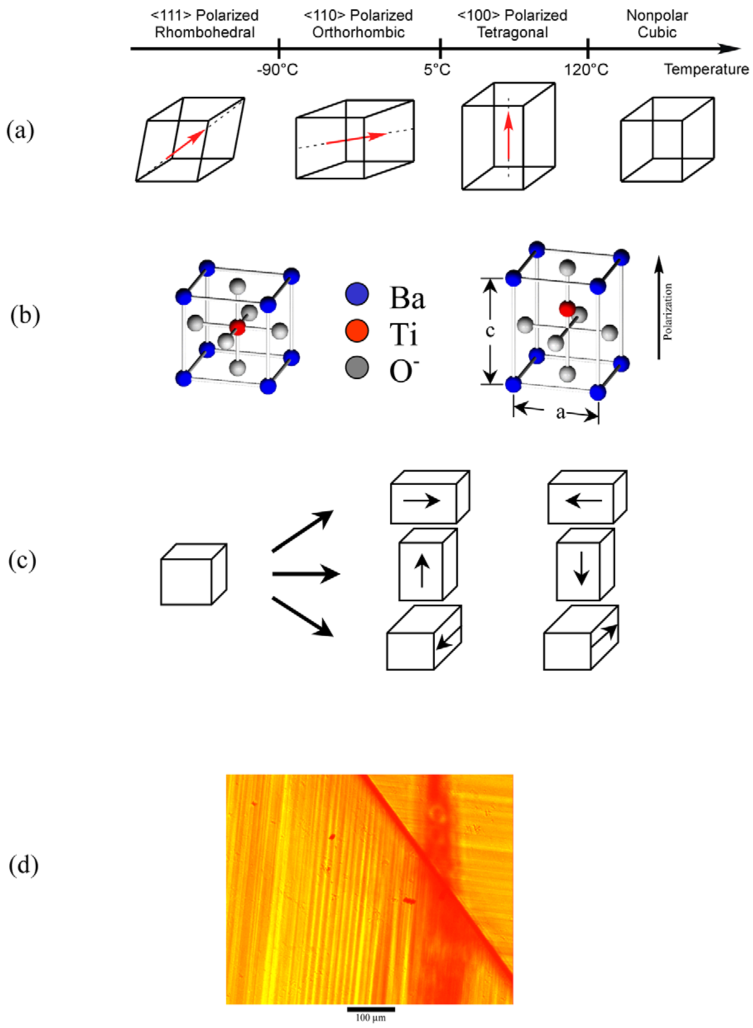

Figure 1.3 (a) Various crystalline phases of $BaTiO_3$; (b) crystal structures of $BaTiO_3$ in their cubic and tetragonal phase; (c) the six tetragonal variants; (d) domain pattern in single crystal $BaTiO_3$ visualized using polarized light microscopy. [9]

1.2.2 Types of piezoelectric

Except for the conductive and semi-conductive materials, all materials create the polarizations when the electric field is applied. They are called 'dielectric' materials. Among them, there are the materials which associate the induced electric field with mechanical deformation. They are called 'piezoelectric' materials. The electro/mechanic conversion phenomena are expressed as direct indirect piezoelectric effects, already mentioned in section 1.2.1. The deformation mechanism by polarization was shown in Figure 1.3 (b).

The detail explanations are omitted here. Figure 1.4 shows polarization, P, versus electric field, E. Among piezoelectric materials, there are the materials which keep the polarizations even after the electrical induction is removed. The materials which have such remnant polarization, P_r, are called 'ferroelectric' materials. Crystal is piezoelectric but not ferroelectric. The $BaTiO_3$ or PZT are piezoelectrics, and at the same time, are ferroelectrics.

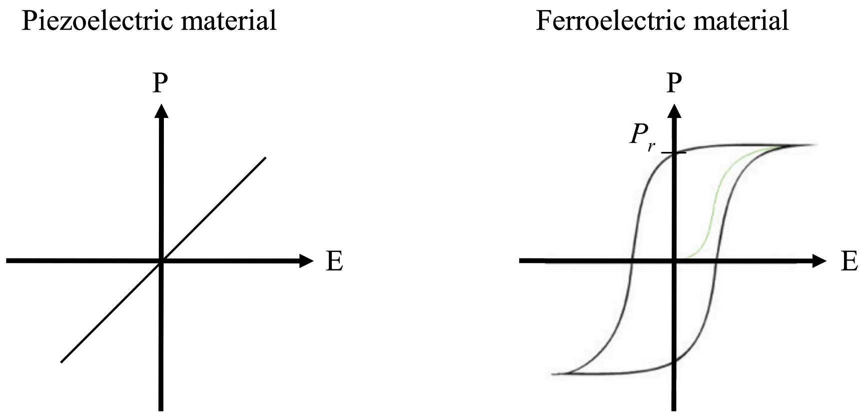

Figure 1.4 Polarization versus electric field.

Figure 1.5 shows strain, *S*, versus electric field, *E*. We can see that ferroelectric materials have hysteresis cycle. Because of the hysteresis, great care has to be paid when using ferroelectrics as sensors/actuators materials. In return, EAPs are attractive because there is no remnant polarization and hysteresis. Their deformation becomes null after the electric field induction is removed.

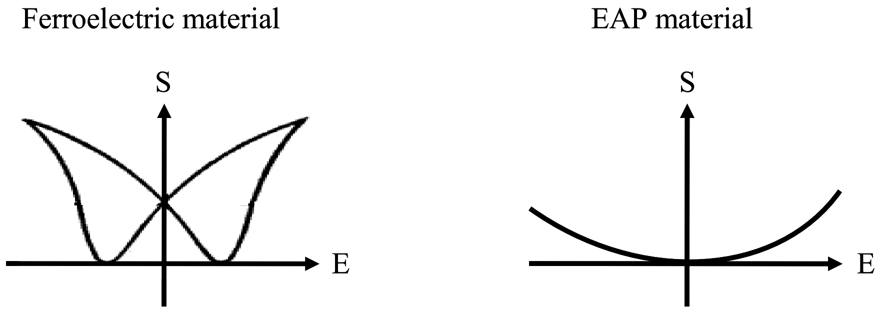

Figure 1.5 Strain versus electric field.

Before start talking about EAP, some general equations used for piezoelectric will be shown in the next section.

1.2.3 Mathematical description

For the direct piezoelectric effect, when a mechanical stress, *T*, is applied to the piezoelectric material the generated charge is proportional to the stress. The general equations that relate the electric to the elastic variables can be written as:

$$D = d^E T + \varepsilon^T E \quad (1.1)$$

Here *D* is dielectric displacement (electric flux density per unit area). *d* is called piezoelectric charge constant (or “piezoelectric constant” in short) that has a unit of coulombs/Newton. It can be understood as induced polarization per unit stress. ε is the permittivity while the stress, *T*, remains constant so it writes ε^T.

For the converse piezoelectric effect, the induced strain, *S*, can be expressed in terms of the applied electric field, *E*.

$$S = s^E T + d^T E \qquad (1.2)$$

In this case, s^E is the elastic compliance at constant field. *d* has a unit of meters/volt. Although this unit of *d* is different from what is used for the direct effect, the coefficient *d* has a numerically identical value to what is shown in equations (1.1) and (1.2). It can be understood as induced strain per unit electric field.

In practice, because piezoelectric materials are anisotropic, the response to an applied electric field or the mechanical force in varies with the direction. Therefore, *d* is actually a tensor and many other physical properties of piezoelectric materials have two subscripts (1, 2 or 3) that indicate the directions of two related quantities. By convention, the subscript 3 denotes the poling direction of the material. 1 and 2 are two arbitrarily chosen orthogonal axes in the plane normal to 3. For piezoelectric charge constant, *d*, the first subscript denotes the direction of polarization generated in the material or the direction of the applied electric field. The second subscript denotes the direction of the applied stress or the induced strain, respectively. For example, d_{31} represents the induced strain along direction 1 (perpendicular to direction 3) per unit electric field applied along direction 3 (see Figure 1.6) **[10]**.

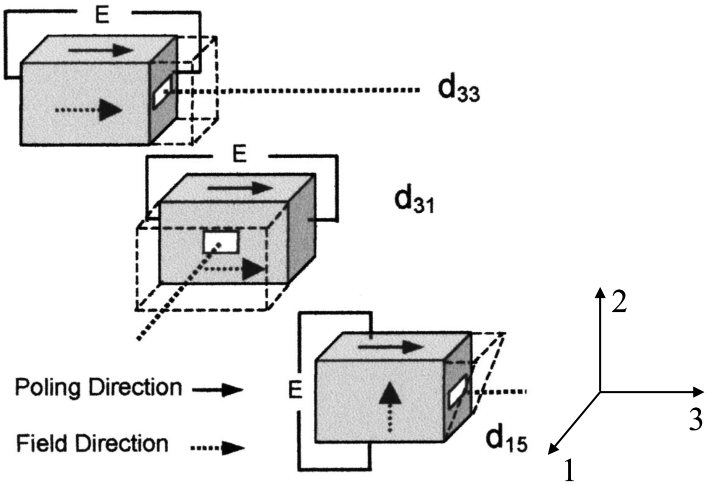

Figure 1.6 Schematic of the measurement system for determining the various piezoelectric coefficients. [10]

1.3 Electroactive polymer (EAP)

1.3.1 EAP and other sensors/actuators materials

Electroactive polymers (EAPs) change significantly in size or in shape by electrical stimulation. These polymers have attracted a great deal of attention due to also their many useful properties, such as flexibility, light weight, high mechanical strength, easy processing to large area films and ability to be molded into a various configuration **[11-14]**.

Actuator is a mechanical device for moving or controlling a mechanism or system. Traditional actuators include pneumatic actuators, electronic actuators, motors, and hydraulic systems. Most of actuators are made from ceramic piezoelectric materials as electroactive ceramic (EAC). However while these materials are able to withstand large forces, striction is limited to fraction of a percent. Consequently, EAP have attracted a great deal of attention as actuators of large deformation (380 %) **[5]**. The weight, limited size, complex transmission, and restrictive shape of such actuators have led researchers to investigate alternative technologies for various applications. Table 1.1 shows comparison between EAP and other actuation technologies **[15]**.

Table 1.1 Comparison between EAP and other actuation technologies. [15]

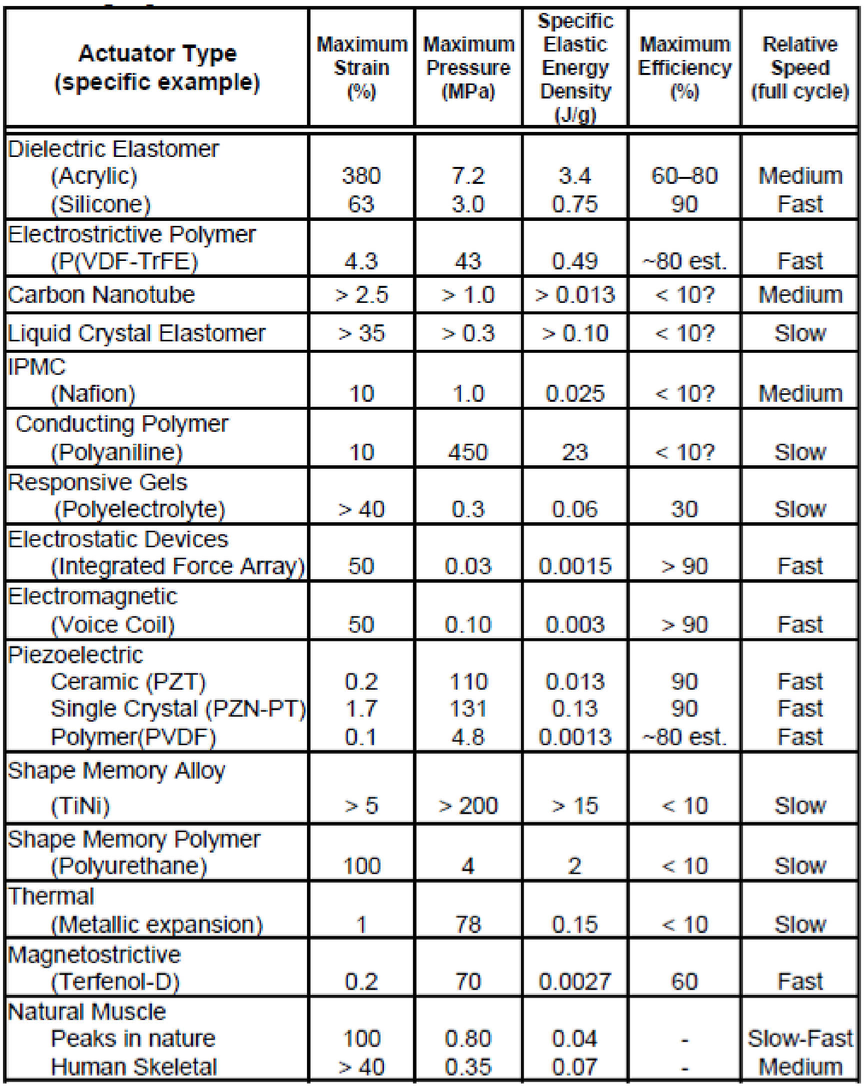

Actuator Type (specific example)	Maximum Strain (%)	Maximum Pressure (MPa)	Specific Elastic Energy Density (J/g)	Maximum Efficiency (%)	Relative Speed (full cycle)
Dielectric Elastomer					
(Acrylic)	380	7.2	3.4	60–80	Medium
(Silicone)	63	3.0	0.75	90	Fast
Electrostrictive Polymer (P(VDF-TrFE)	4.3	43	0.49	~80 est.	Fast
Carbon Nanotube	> 2.5	> 1.0	> 0.013	< 10?	Medium
Liquid Crystal Elastomer	> 35	> 0.3	> 0.10	< 10?	Slow
IPMC (Nafion)	10	1.0	0.025	< 10?	Medium
Conducting Polymer (Polyaniline)	10	450	23	< 10?	Slow
Responsive Gels (Polyelectrolyte)	> 40	0.3	0.06	30	Slow
Electrostatic Devices (Integrated Force Array)	50	0.03	0.0015	> 90	Fast
Electromagnetic (Voice Coil)	50	0.10	0.003	> 90	Fast
Piezoelectric					
Ceramic (PZT)	0.2	110	0.013	90	Fast
Single Crystal (PZN-PT)	1.7	131	0.13	90	Fast
Polymer(PVDF)	0.1	4.8	0.0013	~80 est.	Fast
Shape Memory Alloy (TiNi)	> 5	> 200	> 15	< 10	Slow
Shape Memory Polymer (Polyurethane)	100	4	2	< 10	Slow
Thermal (Metallic expansion)	1	78	0.15	< 10	Slow
Magnetostrictive (Terfenol-D)	0.2	70	0.0027	60	Fast
Natural Muscle					
Peaks in nature	100	0.80	0.04	-	Slow-Fast
Human Skeletal	> 40	0.35	0.07	-	Medium

In particular, EAP is most often compared with actuator technologies such as EAC and shape memory alloy (SMA) actuators. The SMA is known that this material has a larger deformation than piezoelectric materials. However, EAP has a larger deformation than SMA and EAC. The EAP materials are superior to SMA in higher response speed, lower density, and greater resilience. In the late 1990s, it has been demonstrated that some EAP can exhibit up to a 380 % strain **[5]**, which is much more than ceramic and SMA. Issues include high voltage, high efficiency driver circuits, compliant electrodes and reliability **[16]**.

1.3.2 Historical background

Before the details of each type of EAPs will be explained in section 1.3.3-5, their historical backgrounds are briefly introduced here.

The field of EAP emerged back in 1880, when Wilhelm Roentgen designed an experiment in which he tested the effect of an electrical current on the mechanical properties of a rubber band. The rubber band was fixed at one end and was attached to a mass at the other. It was then charged and discharged to study the change in length with electrical current. Sacerdote followed up on Roentgen's experiment by formulating a theory on strain response to an applied electric field in 1899.

Eguchi discovered the first piezoelectric polymer (electrets) in 1925. In 1969, Kawai was able to demonstrate that polyvinylidene fluoride (PVDF) exhibits a large piezoelectric effect. PVDF films are applied as sensors, miniature actuators and speakers. This sparked research interests in developing other conductive polymers systems that would show a similar effect.

In 1977, the conducting polymer of polyacetylene was discovered by Hideki Shirakawa et al. By the late 1980s, a number of other polymers had been shown to exhibit a piezoelectric effect or were demonstrated.

During the 1990s, focus shifted towards truly EAP, which respond directly to an electric stimulus. Pelrine et al. at SRI International have developed dielectric elastomer actuators which give some handsets percentage of strain level **[3-5, 16-19]**.

Besides, Ionic polymer metal composite (IPMC) was shown to have actuator properties in 1992 by Oguro in Osaka, Japan and Shahinpoor. Their co-workers in New Mexico, U.S.A extensively developed the technology.

Zhang et al. have developed copolymers of PVDF of which the energy density was significantly increased.

Recently, two significant new classes of materials with actuator properties have emerged: carbon nanotube filled actuators developed by Baughman et al. in 1999 **[20]**.

Additionally to say, Information on many of these and other EAP research groups can be found on the EAP Web page maintained by Bar-Cohen from the Jet Propulsion Laboratory **[21]**.

1.3.3 Types of EAP

There are numerous types of EAP but most falls into two categories which are ionic and electronic. The ionic EAP materials (gels, polymer-metal composites, conductive polymers and carbon nanotubes) are driven by diffusion of ions and they require an electrolyte for the actuation mechanism. Their major advantage is the requirement for drive voltages as low as 1-2 V. However, they need to be maintained in wet condition. Their response speed is limited because of that mechanism. In contrast, the electronic EAP materials (electrostrictive, electrostatic, piezoelectric and ferroelectric) are driven by electric field. They are able to have a high mechanical energy density and they can be operated in air with no major constraints. However, they require in general a high activation field close to the electrical breakdown level, such as 100 MV/m.

The currently available leading EAP materials are listed in Figure 1.7 and a summary of the advantages and disadvantages of these two groups of materials are listed in Table 1.2 **[22]**. Our work is marked in Figure 1.7. The present thesis dielectric elastomer concerns; pure polyurethane (PU) and that with carbon black (CB) particle fillers.

The ionic EAP and electronic EAP including our working polymer will be introduced briefly in section 1.3.4 and 1.3.5 respectively according to an instruction of Figure 1.7.

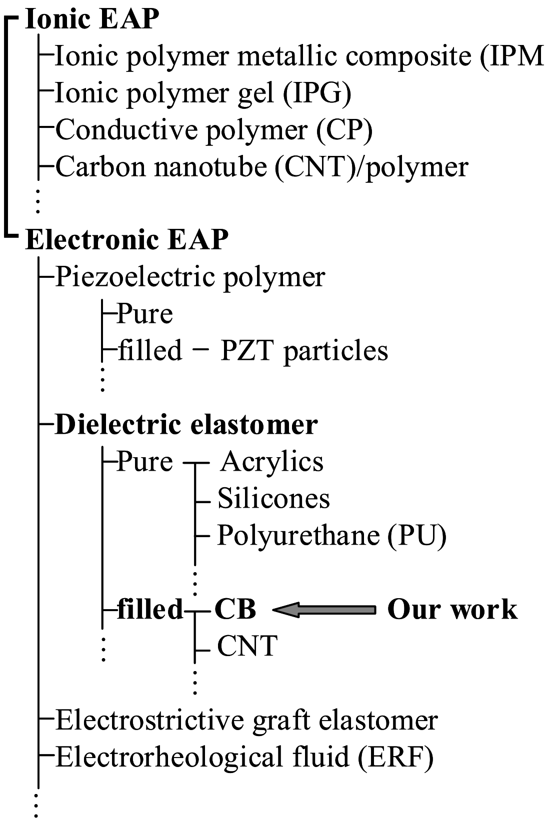

Figure 1.7 List of leading EAP materials.

Table 1.2 Summary of the advantages and disadvantages of the two basic EAP groups. [22]

EAP type	Advantages	Disadvantages
Ionic EAP	- Large bending displacements - Provides mostly bending actuation (longitudinal mechanisms can be constructed) - Requires low voltage	- Except for CP, ionic EAP do not hold strain under DC voltage - Slow response (fraction of a second) - Bending EAP induce a relatively low actuation force - Except for CP, it is difficult to produce a consistent material (particularly IPMC) - In aqueous systems the material sustains hydrolysis at >1.23 V
Electronic EAP	- Long life in room conditions - Rapid response (mSec levels) can hold strain under DC activation - Induces relatively large actuation forces	- Requires high voltages (~150 MV/m) - Requires compromise between strain and stress - Glass transition temperature is inadequate for low temperature actuation tasks

1.3.4 Ionic EAP

The ionic EAPs need to be maintained their wetness. Also their response speed is quite limited. The facts do not agree to the purpose of our work, so that we did not choose ionic but electronic EAP. However, the ionic EAPs are also interesting materials. It is worth to know their mechanism when we study on EAP. They are, so, briefly introduced here.

a) Ionic polymer-metal composite (IPMC)

Ionic polymer-metal composite (IPMC) consist of a thin ionomeric membrane with noble metal electrodes plated on its surface. It also has cations to balance the charge of the anions fixed to the polymer backbone. They are very active actuators that show very high deformation at low applied voltage and show low impedance. IPMC work through electrostatic attraction between the cationic counter ions and the anode of the applied electric field, a schematic representation is shown in Figure 1.8 **[23]**. Typical ionic polymers are Nafion® (perfluorosulfonate, made by DuPont) and/or Flemion® (perfluorocarboxylate, made by Asahi Glass, Japan) **[24]**.

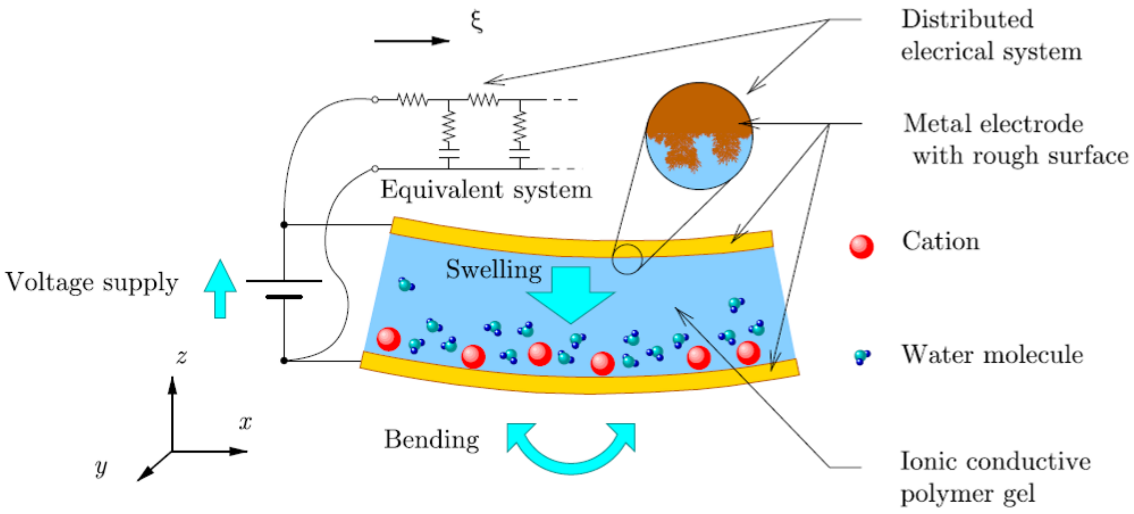

Figure 1.8 Physical structure of IPMC. [23]

Actuation strains of above 3 % have been reported for IPMCs under applied voltages of 7 V **[25]**. Figure 1.9 shows one example of these cantilever-type actuators. Substantial bending is caused as one side of the material contracts and the other expands **[26]**. Reported stresses of actuation by IPMC are as high as 30 MPa **[27, 28]**. As the time variation shown in the Figure 1.9, that response speed is unfortunately quite limited.

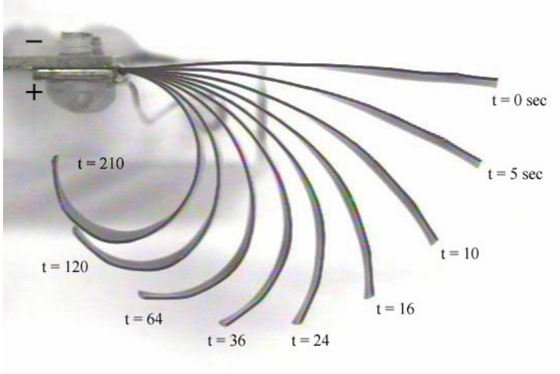

Figure 1.9 Actuation of a Flemion-based IPMC strip as a function of time in seconds.[26]

An IPMC device was developed for use in one of NASA's missions to address the issue of dust on Mars as a dust wiper. It feasibility was demonstrated by removing sawdust from a glass plate. Such a wiper has the potential to serve as a means of removing dust from windows and solar cells using low power, light-weight ionomer films **[29]**.

b) Ionic polymers gel (IPG)

Polymer gels are unique materials in the sense that they can be made to respond to so many different stimuli. In 1970s, the phase transition of polymer gel characterized by its abrupt high volume change was found by Tanaka **[30]**. The stimuli that have been demonstrated to induce abrupt changes in physical properties are diverse, and include temperature, pH, solvent- or ionic composition, electric field, light intensity as well as introduction of specific ions **[31]**. Figure 1.10 shows the shape change of an anionic gel with time under the electric field.

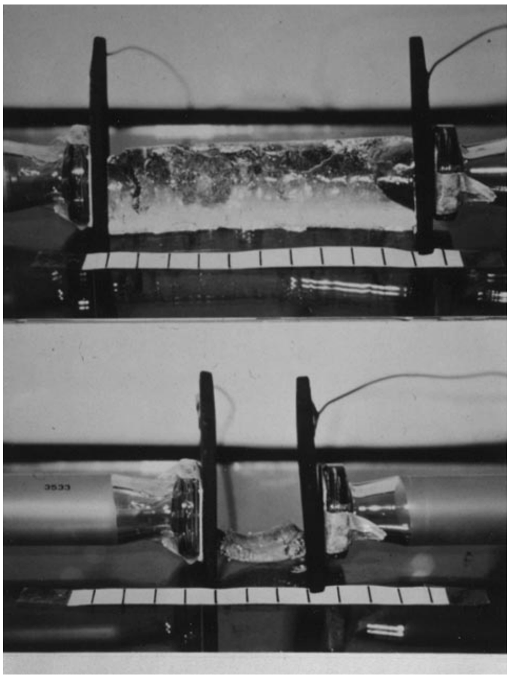

Figure 1.10 Photographs of a poly(2-acrylamido-2-methyl-1-propanesulfonic acid) gel before (upper) and after (lower) imposing an electric field of 15 V for 10 h. [32]

Ionic gels show the higher order of volume change ratio rather than neutral gels on account of the existence of ions in the gel network, and some ionic gels shows thousand times of volume change ratio. Polyacrylic acid gel actuation is shown in Figure 1.11 **[33]**. The deformation of such polymer gels is extremely high, compared with other sensor/actuator materials such as piezoelectrics **[34]**.

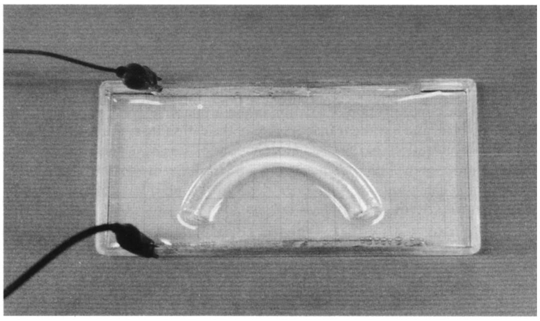

Figure 1.11 Bending of a polyacrylic acid gel rod sodium hydroxide. DC applied field, cathode (negative) at bottom. Gel swells on the anode side and bends toward the cathode. [33]

c) Conductive polymer (CP)

Conductive polymer (CP) is electronically conducting organic materials. Actuation is produced in these polymers due to the electronically change of oxidation state. The flux of ions into and out of these polymers backbone causes deformation of conducting polymers. Conducting polymers with appropriate dopant, such as hydrogen chloride or sulphuric acid, exhibit chemically and electrochemically controllable electronic conductivities. Doping is done in order to have ions that can flow across the covalently bonded conjugated polymer chain. The bending of a conducting polymer sandwich is presented in Figure 1.12 **[34]**. When an electric field is applied to doped conducting polymers with appropriate electrolyte, a reversible exchange of ions takes place between the conducting polymer and the electrolyte. Exchange of ions leads to oxidation or reduction reactions in the conducting polymer, which leads to significant changes in its volume **[35]**. These ions are transferred into and out of the polymer and electrolyte to balance the charges.

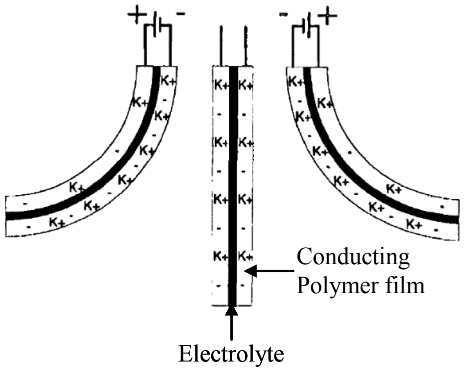

Figure 1.12 Schematic representations of three states during the electromechanical cycle of a rocking-chair-type, bimorph actuator. Both electrodes have the same concentration of dopant (K^+) when the cantilever is undistorted, and electrochemical transfer of dopant between electrodes causes bending either to the right or to the left. [35]

d) Carbon nanotube (CNT)/polymer

The growth and the characterization of carbon nanotube (CNT) have become one of the most active research areas in the field of material science and engineering since its discovery by Iijima in 1991 **[36]**. Carbon nanotubes are fullerene-related nanostructures and can be described as a hexagonal network of carbon atoms (graphite sheet) that has been rolled into a hollow cylinder. The nanotubes can either be open-ended or enclosed with half a fullerene molecule at either end. In general, carbon nanotubes exist in one of the two forms: (1) a single-wall carbon nanotube (SWNT), which consists of a single cylindrical graphite sheet (Figure 1.13 (a)), and (2) a multi-wall carbon nanotube (MWNT) consisting of multiple nested coaxial single-wall nanotubes with an interlayer spacing of 0.34-0.36 nm (Figure 1.13 (b)) **[37, 38]**.

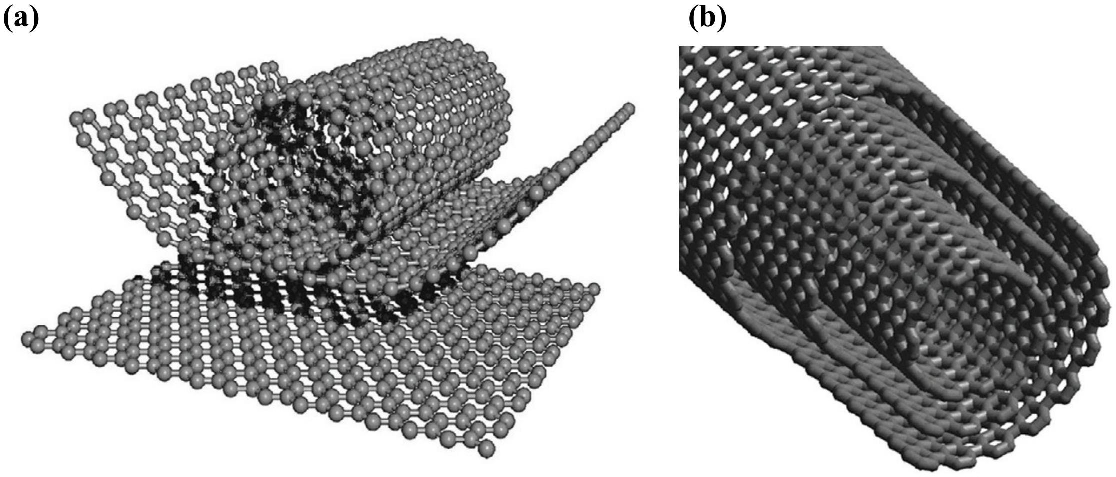

Figure 1.13 (a) A graphene sheet rolled into a nanotube and (b) a MWNT. [37, 38]

Individual SWNT or very long MWNT have exceptional mechanical properties. The mechanical and electronic properties associated with both SWNT and MWNT include high elastic modulus (greater than 1 TPa), thermal conductivity twice as high as diamond, thermal and chemical stable up to 2800 °C in vacuum conditions, high electric current carrying capacity (1000 times higher than copper wires) and excellent field emission characteristics **[39]**. The applications include the use of CNT in reinforcing polymer and ceramic composite materials and electron field emitters for vacuum electronic device such as flat panel display and cathode ray lighting elements.

The response of actuation mechanism of a CNT itself depends on a change in bond length of the carbon-carbon bond due to repulsion between similar charges developed on carbon atoms forming the nanotube. The carbon-carbon bond is suspended in an electrolyte changes length as a result of net charge injection causing the ionic charge balance between the nanotube and the electrolyte (Figure 1.14) **[20]**. The repulsion between similarly positive charged adjacent carbon nuclei results in increase in the C-C bond length, which leads to the increase of the length and diameter of the nanotube **[35]**.

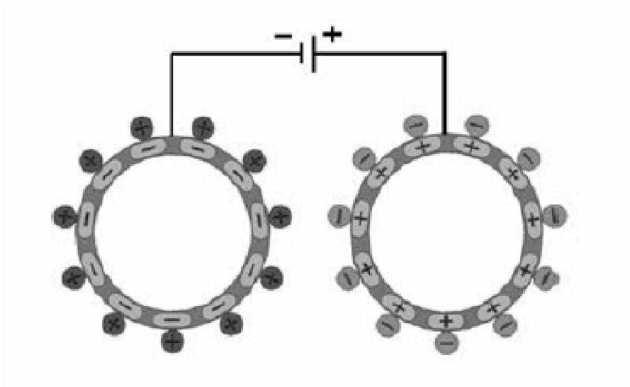

Figure 1.14 Schematic illustration of a charge injection in a nanotube-based electromechanical actuator. [20]

In the use of CNTs ionic polymer, the volume fraction of CNT in polymer is quite high. Consequently, the material becomes extremely stiff and the strain level reminds under a few percentages. Besides, CNTs have been recently used as filler materials in dielectric polymer.

1.3.5 Electronic EAP

An electronic EAP was chosen for the present thesis. First of all, they can be manipulated in air condition. Among many kinds of EAPs, dielectric mechanism was chosen. They have high strain level and their energy density can be high. However, the most significant disadvantage of this type of actuator is the high voltage requirement such as 150 MV/m. Some electronic EAPs will be presented in this section.

a) Piezoelectric polymer

A piezoelectric polymer can be defined as a polymer in which the application of an electric field reverses the direction of spontaneous polarization.

PVDF and its copolymers are the most promising materials of this class. As explained in section 1.3.2, Kawai published the first description of the piezoelectric properties of PVDF in 1969. Many of them have been applied as sensor, transducer, actuator, and underwater acoustic transducer **[40, 41]**. Their electrostrictive strain is nearly 2 %. It is not large as EAP but is enough big compared to traditional electro driven sensors/actuators, PZT, which generates around 0.2 % at maximum. The material has a high elastic modulus (~1 GPa), and the field-induced strain can operate at frequencies higher than 100 kHz. The large electric field such as 200 MV/m is however required instead of a few hundreds MV/m by PZT.

One thing that I want to note is about the studies of the effect of electron irradiation. In 1998, Zhang et al. reported that high-energy electron irradiated P(VDF-TrFE) copolymers exhibit higher electrostrictive response (~ 5 %) **[42-44]**. The topic of electron irradiation will be continued in chapter 5.

b) PZT particle/polymer

In general the PZT generates around 0.2 % at maximum strain **[1]**. Therefore many EAPs are made incorporating with PZT particles in polymer matrixes **[45-48]**.

Researchers have thus tried to increase the permittivity of composite with a large quantity of piezoelectric particles, because a piezo coefficient, *d*, is directly related to the permittivity, ε, of a piezo/polymer composite **[10]**. Due to the huge step in the permittivity difference between the one of polymer matrix and the one of piezoelectric particles, the applied electric field does not ‘enter’ into the high permittivity particles. Consequently, this composite material exhibits poor actuating performances. Furthermore, the resultant composites are quite hard and heavy and they require a high driving energy.

The objective of this thesis is to introduce conductive particles in order to create dipole. Since the electric field must be null inside the particle, a polarization occurs on the particle.

c) Dielectric elastomer

Dielectric elastomer actuators consist of a polymer film sandwiched between two compliant electrodes. A schematic model of the dielectric polymer actuator system is presented in Figure 1.15 **[4]**. When a voltage difference is placed across the top and bottom electrodes, the polymer is compressed in thickness and stretched in area by the electric field pressure **[4, 17]**.

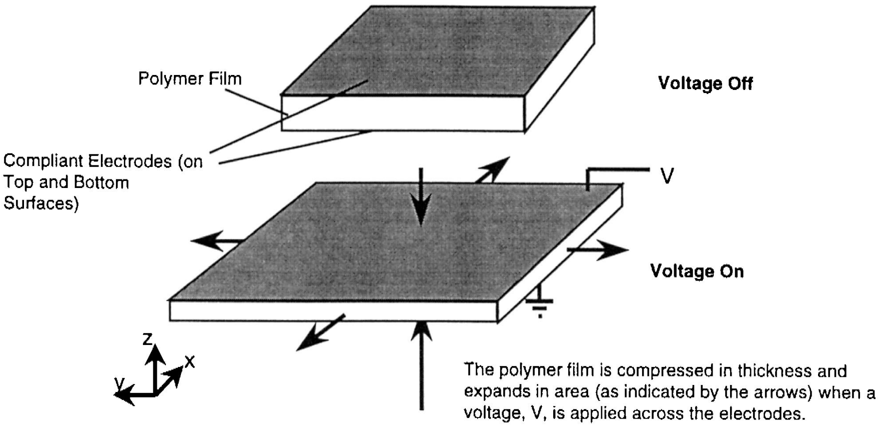

Figure 1.15 EAP actuator systems. [4]

The term electrostrictive strain is used here in the generic sense to describe the stress and strain response of a material to an electric field. Many researchers (particularly those investigating ceramic materials) reserve the term to refer to the strain response of a material in an electric field that arises from field-induced intermolecular forces. The Maxwell strain of dielectric polymer with compliant electrodes results from the electrostatic forces generated between free charges on the electrodes, and is proportional to the square of the electric field. Since the electrostrictive strain results from external electrostatic forces, any elastomeric dielectric material will exhibit electrostrictive strain by this definition, in theory. Thus, it may be argued that actuators based on this technology are more properly considered to be electrostatic. However, as will be shown, the dielectric and mechanical properties of the polymer material determine the magnitude of the stress and strain response.

Figure 1.16 shows the actuation of a circular dielectric elastomer **[18]**. It is acrylic elastomer. As shown in Table 1.1, acrylic and silicon based elastomer are famous for an extremely large strain. It overcomes easily some hundreds of percentage such as 380 %. However this type of polymer typically requires a large actuation voltage to produce high electric fields (hundreds to thousands of volts). The present thesis concerns this kind of dielectric polymer. The elastomer will be explained in the next section, 1.4.

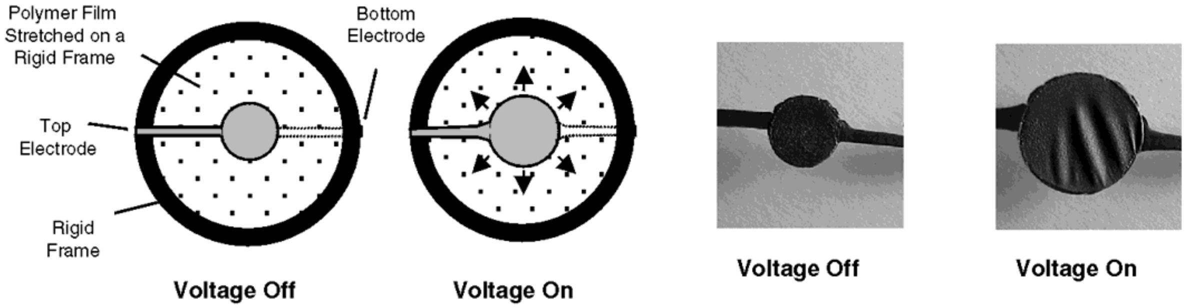

Figure 1.16 Circular strain test and photograph of acrylic dielectric elastomer. [18]

d) Electrostrictive graft elastomer

The electrostrictive graft elastomer is a new type of electroactive polymer developed in NASA Langley research center in 1999. The NASA Langley research center was reported that an electrostrictive graft elastomer exhibits large electric field-induced strain (4 %), shown in Figure 1.17 **[49]**. The 4 % of strain is smaller than dielectric elastomer strain (380 %). Not extraordinary as EAPs but much bigger then PZT, 0.2 % at maximum. The important thing is that there is no hysteresis in this material. However, its required electrical field is quite high, so that the use is limited.

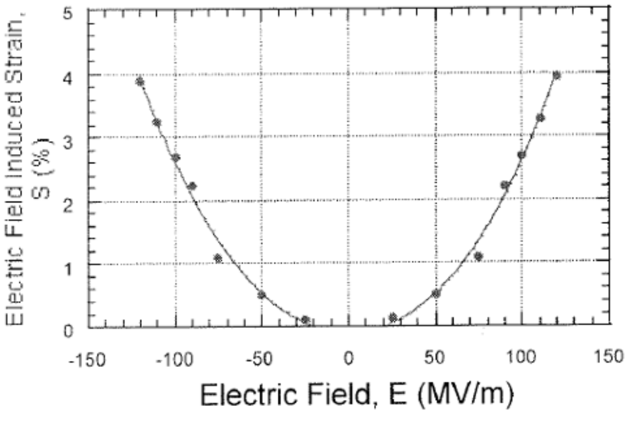

Figure 1.17 Electric field dependence of the induced strain on the graft elastomer. [49]

The graft elastomer consists of two components: flexible backbone chains and crystallisable side chains attached to the backbone, called grafts, shown in Figure 1.18 **[50]**. The grafts on the backbone can crystallize to form physical cross-linking sites for a three-dimensional elastomer network and to generate electric field responsive polar crystal domains. The polar crystal domains are primary contributors to electrostrictive mechanical functionality.

When the materials are under the electrical field, the polar domains rotate to align in the field direction due to the driving force generated by the interaction between the net dipoles and the applied electric field. The rotation of grafts induces the reorientation of backbone chains, leading to deformational change and the polar domains randomize when the electric field is removed, leading to dimensional recovery. The dimensional change generated demonstrates quadratic dependence on the applied electric field as an electrostrictive material does **[49]**.

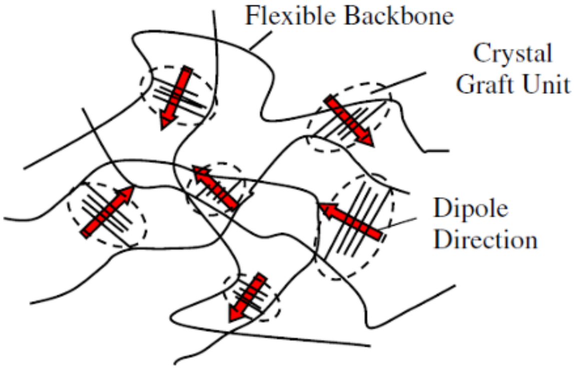

Figure 1.18 Structure of the grafted elastomer. [50]

e) Electrorheological fluid (ERF)

An electrorheological fluid (ERF) is defined as a suspension of a dielectric solid or polymeric particles (the dispersed phase) in an insulative base oil (the continuous phase), which under normal conditions behaves as a Newtonian fluid. On the application of an electric field, the fluid has the ability to transform from a liquid to a plastic state in milliseconds, the fluid viscosity being proportional to the field strength. A widely accepted description of the electrorheological effect states that the dielectric solid particles in the fluid become polarised and form microstructures (chains or clusters) under the presence of an electric field. The unique features of ERF have led to various applications in clutch systems, shock absorption, noise isolation and vibration control **[51]**.

Even some medical applications in biomedicine have been investigated. The majorities of these applications use the fluids in shear mode, whereas the ERF in the tactile array is subjected to both shear and squeeze **[51]**.

1.4 Dielectric elastomer

1.4.1 Dielectric properties

A dielectric material is an electrical insulator that may be polarized by the action of an applied electric field. However, the exact response of a certain material to an applied electric field is quite hard to predict. The actuation diagram was already shown in the Figure 1.15. Here, I will try accurate explication.

When dielectric is placed in electric field, electric charges do not flow through the material, like in conductor, but only slightly shift from their average equilibrium positions causing dielectric polarization, positive charges are displaced along the field and negative charges shift in the opposite direction. This creates an internal electric field which partly compensates the external field inside the dielectric. If a dielectric is composed of weakly bonded molecules, those molecules not only become polarized, but also reorient themselves so that their symmetry axis aligns to the field. If the material is conducting, the electric field will give rise to charge transport, due to which the effects of polarization will be obscured.

A typical model of an insulating material regards the material as composed of small dipoles, which are electrically neutral, but possess internal charge separation. When exposed to an external electric field, the tendency of a single dipole is to align itself with the electric field, such that the positive end points toward lower potential, and the negative end points toward the higher potential **[52]**. When all the dipoles in a material align in this way to an applied electric field, the material is known as a dielectric.

Figure 1.19 (a) depicts the situation when a constant voltage is applied to a set of juxtaposing capacitor plates. Electric field lines may only begin on free positive charges, and end on free negative charges. Thus, surface charge concentration builds up on the capacitor plates. The charge build up continues, until the voltage drop over the capacitor plates matches that of the voltage source. The relation between the amount of free charge, *Q*, and the voltage drop, *V*, is $Q = CV$, where C is the capacitance of the sample. The relative permittivity, ε_r, can be calculated, by assuming that the sample approximated to a simple parallel plate capacitor:

$$\varepsilon_r = (\frac{CL}{\varepsilon_0 A}) \qquad (1.3)$$

The *A* is the area of the plates, and *L* is thickness of the sample.

The constant ε_0 (8.854×10^{-12} F/m), commonly called the space permittivity (or vacuum permittivity, permittivity of free space or electric constant), relates the units for electric charge to mechanical quantities such as length and force.

$$\varepsilon_0 = \frac{1}{\mu_0 C_0^{\ 2}} = 8.854187817...\times10^{-12}(\frac{\mathrm{As}}{\mathrm{Vm}}) = 8.854187817...\times10^{-12}\ (\mathrm{F/\,m}) \qquad (1.4)$$

Here C_0 is the speed of light in vacuum and μ_0 is the permeability in vacuum.

The permittivity, ε, is given by the product of the space permittivity, ε_0, and the relative permittivity, ε_r, by

$$\varepsilon = \varepsilon_0 \varepsilon_r \qquad (1.5)$$

The density of the field lines, *D*, is known as the electric flux density for permittivity and is given by

$$D = \varepsilon_0 \varepsilon_r E = \varepsilon E \qquad (1.6)$$

Here *E* is the electric field between the plates. When a piece of dielectric material is inserted between the plates, Figure 1.19 (b) and (c), the dipoles in the material will reorient as if the positive end of the dipole points toward the negative potential.

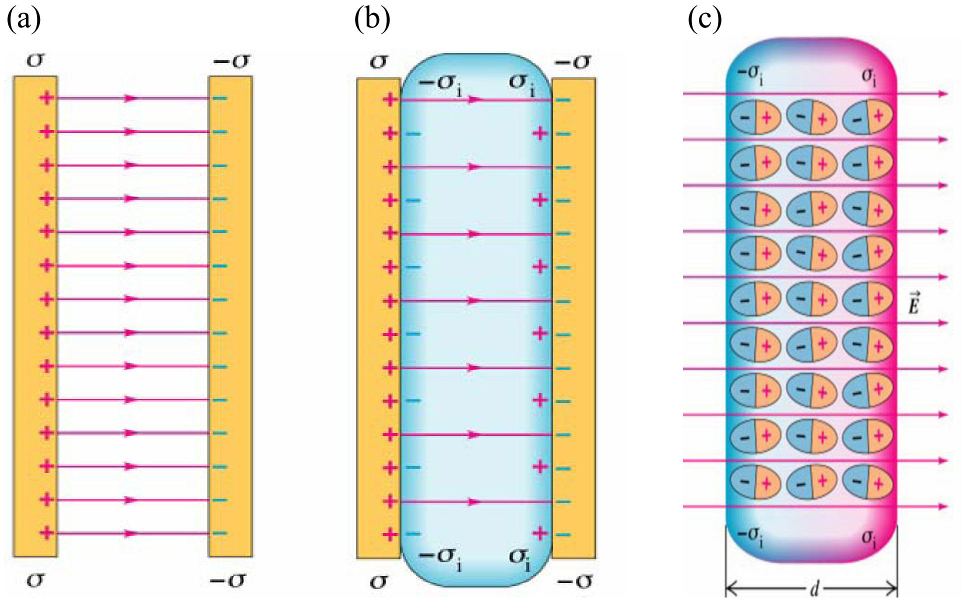

Figure 1.19 (a) Electric field lines with vacuum between the plates. (b) The induced charges on the faces of the dielectric decrease the electric field (c) Polarization of a dielectric in an electric field gives rise to thin layers of bound charges on the surfaces, creating positive and negative surface charge densities. The sizes of the molecules are greatly exaggerated for clarity. (www.physics.sjsu.edu)

A part of the electric displacement originates from the vacuum displacement, and the other part from actual polarization of the dielectric. The electric flux density, *D*, is related to the electric polarization, *P*, by

$$D = \varepsilon_0 E + P \qquad (1.7)$$

The electric susceptibility, χ, (frequently written as χ_e) is the part of the relative permittivity, ε_r, caused by the material,

$$\chi = \varepsilon_r \text{-1} \qquad (1.8)$$

So in the case of a vacuum,

$$\chi = 0 \qquad (1.9)$$

In a homogeneous linear and isotropic dielectric medium, the electric polarization, *P*, is considered to be aligned with and proportional to the electric field, *E*:

$$P = \varepsilon_0(\varepsilon_r \text{-1})E = \varepsilon_0 \chi E \qquad (1.10)$$

Then, the permittivity and electric displacement are rewritten as;

$$\varepsilon = (1+\chi)\varepsilon_0 \qquad (1.11)$$

$$D = \varepsilon_0 (1 + \chi) E \qquad (1.12)$$

The susceptibility, χ, is also often related to the polarizability, α, of individual particles in the medium by the Clausius-Mossotti relation.

$$P = \varepsilon_0 (\varepsilon_r \text{-} 1) E = \alpha E \qquad (1.13)$$

1.4.2 Some famous materials of dielectric elastomer

As can be seen from the Table 1.1, acrylic base EAP has given the extremely high strain level such as 380 %.

Rubber polymers of high relative permittivity caused from a high polarization are able to obtain a large deformation compared to EAPs of other mechanisms. When relative permittivity of material exceeds move then 2.8, under 100 Hz of measurement condition, the generated deformation becomes important. The following polymers are cited in the high relative permittivity; Acrylonitrile/Butadiene copolymer (Nitrile butadiene rubber: NBR), Hydrogenated NBR (HNBR), Acrylic rubber, Polyurethane rubber, Fluoro rubber, Silicone rubber, Chlorosulfonated polyethylene (CSM) rubber, chloroprene rubber (CR) and Ethylene vinyl acetate copolymer (EVA).

Two dielectric elastomers, acrylic and silicone are showing great potential, particularly in relation to strain response. Silicones and acrylic elastomers, both dielectric elastomers, have shown the best performance as artificial muscle actuator materials. The acrylic and silicone rubbers are not crystalline in structure but amorphous. The electromechanical response of these materials is primarily due to the Maxwell stress effect since some crystallinity is required to have an electrostrictive effect beyond that caused by the electrostatic interaction of the electrodes (Maxwell stress). This coupled with their fast response speeds and potentially high efficiencies make them attractive materials for the development of a mechatronic muscle, and off course, as the sensor/actuator material in general.

Acrylic is a pressure sensitive adhesive elastomeric film, which has been a candidate dielectric elastomer material for numerous research projects. This material is commercially available as a pre-cast 1mm thick adhesive on a liner. It is extremely compliant stretching in area before breaking. The handling of this material is easier than that of silicone since the film itself as a double-sided adhesive tape provides gluing, such that electrodes are easy to apply and maintain good contact with the elastomer.

While acrylic elastomer is a powerful material with regard to its strain response, silicone has a faster response time due to lower viscoelastic losses than in acrylic. Silicones can operate at frequencies greater than 1 kHz, while acrylic elastomers currently have an upper limit of 100 Hz. Silicone has better coupling efficiency as well as low creep and good temperature and humidity tolerance making it an attractive actuator material.

However silicone rubber and acrylic can generate high deformation, their driven electric field is quite high. Therefore, in the present thesis, polyurethane (PU) was chosen. Modulus and relative permittivity of PU is higher than that of silicone rubber. Besides, the relative permittivity of copolymer is quite high, but its strain is smaller than PU.

1.4.3 Electromechanical actuation mechanisms

An electromechanical actuation mechanism is a physical process whereby a mechanical system is activated by electricity. Two mechanisms, electrostriction and Maxwell's stress effect are considered prime contributors to the large electric-field-induced strain exhibited by electronic EAPs. The resulting stresses and strains relating to both mechanisms exhibit a quadratic dependence on a low applied electric field.

Su et al. reported that high strain of dielectric elastomer was obtained by space charges. The space charges are considered heterogeneously distributed in the sample and induce a non-uniform field distribution **[53-56]**.

Strain response of an elastomer can be contributed by either dielectric elastomers or graft elastomers or both of them.

a) Electrostriction

Electrostriction arises due to the change in dielectric properties of the material with strain **[57]**. There is a direct coupling between electric polarization, *P*, and mechanical strain response, $S_{\text{electrostriction}}$, which can be expressed as **[58]**:

$$S_{\text{electrostriction}} = QP^2 = ME^2 \qquad (1.14)$$

where *Q* is the polarization-related-electrostriction coefficient, electrical change, and *M* is the electrical-field-related-electrostriction coefficient of the material. It is true only on low electric field regime. For linear dielectrics where $P = \varepsilon_0(\varepsilon_r\text{-}1)E$, equation (1.14) can be written as

$$S_{\text{electrostriction}} = Q\varepsilon^2 E^2 = Q\varepsilon_0{}^2(\varepsilon_r\text{-}1)^2 E^2 \qquad (1.15)$$

Equation (1.14) relates the $S_{\text{electrostriction}}$ in the thickness direction of the film due to electrostriction, the space permittivity, ε_0, the relative permittivity, ε_r, and the applied electric field, *E*.

In order for electrostriction to be present, the material must have some crystallinity in its structure. The likelihood of an electrostrictive effect being present is indicated by an increase in the relative permittivity of the material. The relative permittivity of a material can be measured directly using an impedance analyser.

b) Maxwell stress effect

The Maxwell stress effect is a consequence of a change in electric field distribution inside the dielectric with strain **[59]**. Alternatively this may be interpreted as Coulombs attraction between opposite charges on electrodes.

$$S_{Maxwell} = \mathrm{s}\varepsilon_0\varepsilon_r E^2/2 \qquad (1.16)$$

Equation (1.16) relates the strain in the thickness direction of the film $S_{Maxwell}$ with the elastic compliance, *s*. A study carried out by Ma and Cross **[60]**, suggests that the field-induced strain in acrylic elastomers is due primarily to the Maxwell stress effect, since experimental data closely fits the transverse strain response predicted by equation. Almost all of the slight discrepancy observed in the strain response is attributed to imperfection in experimental setup geometry, since the degree of the electrostrictive behavior determined from dielectric spectroscopy performed on strained films was shown to be smaller than that needed to completely explain the diminished performance of the setup.

1.4.4 Actuation pressure

Dielectric elastomers can only change shape by maintaining a constant volume, consequently the two modes of energy conversion are directly coupled. Stretching in area is mechanically coupled to compression in thickness and vice versa. Thus it makes sense to consider a single effective actuation pressure as derived by Pelrine **[3]**. This actuation pressure, *p*, is defined as

$$p = \varepsilon_0 \varepsilon_r E^2 = \varepsilon_0 \varepsilon_r (\frac{V}{L})^2 \qquad (1.17)$$

where *L* is the film thickness.

The main disadvantage of dielectric elastomer actuators is their high electric field requirement. Voltages can be lowered if the films are thin. However, since it is difficult to produce very thin films uniformly in large areas, the films used are usually in the millimetre thickness range, requiring driving voltages in the kilovolt range. Thus, there are a number of areas of ongoing research, which attempt to increase the actuation pressure of dielectric elastomers while keeping the driving voltage as low as possible **[61]**.

1.4.5 Application availability

Most EAPs are nonlinear in their response to the applied voltage or current. The control of these actuators can be a difficult task. Wet and thermal-phase-change actuators are typically more difficult to control than dry actuators, since their response to an applied voltage or current varies with time.

Actuators based on polymers are limited in their response speed by diffusion processes. As a result, maybe they are difficult to use as actuators for macroscopic robotic applications. However they have many other possible applications for medical purposes, i.e., drug delivery systems and biomimetic energy-transducing devices. It should be noted that all of these wet actuators are generally less energy efficient than the dry ones.

Actuators based on IPMC will most likely be seen in micro applications and biomimetic devices. Their structures are made from nontoxic and, to some degree, biocompatible materials.

Dielectric elastomers have high energy density and are fast acting and energy efficient, as discussed previously. The elastic energy density of electronic polymers exceeds that of traditional electromagnetic actuators such as electric motors and solenoids, suggesting a wide range of potential applications, from pumps to valves to vibration control devices. The muscle-like performance of dielectric elastomers, and to a lesser extent of electrostrictive polymers, suggests applications in biomimetic robots.

a) Artificial muscles

Polymer actuators are relatively compliant. This compliance may be exploited to provide a force control, a difficult task with other actuator technologies. For example, a robot hand designed to grip an item may work by gripping with a given force rather than by moving its fingers to a given position. Due to this fact, EAPs are often referred to as artificial muscles.

They are also good candidates for this object because of its large generated strain. Our muscles are said 20-30 % of strain level. Many types of EAPs can generate around 5-10 % and especially dielectric polymers can have some hundreds. The latter ones have to be reconsidered in terms of force but anyway, EAPs developments for this object are quite active since a while. The driven electric field has to be lowered because not may other electrical components can stand to be used with and because of security in the case of artificial muscles.

b) Energy harvesting

The first object of the present thesis is to make the actuator material which can generate a large strain, more than PZT (0.2 % at maximum), under moderate electric field, less than 20 MV/m.

Besides, the energy harvesting technology has been strongly developed in the laboratory. Until today, PZT has been used as harvesting device. PZT is a great sensor/actuator material in precision, high response speed, generating force, formability and so on as explained in section 1.2, however, that limited strain level, 0.2 % at most, seems difficult to improve again 10 times move. Thus, the use of EAPs as harvester device is quite desired.

Energy harvesting, also referred to as “energy scavenging” or “energy extraction”, can be defined as following, converting ambient energies such as vibration, temperature, light, RF energy, etc. to usable electrical energy by using energy conversion materials or structures, and subsequent storage of the electrical energy for powering electric devices. In other words, the general concept of energy harvesting is to convert energy from the environment that is in an otherwise unusable form or wasted form into a more useful form. This energy is used for other purposes, for example for driving an electrical circuit or for storage in a battery or a large capacitor **[62]**.

As generator materials, piezoelectric PZT devices as well as polymers (PVDF) have been used in the past. This makes it a candidate system for driving wireless sensors **[63]**. Despite a relatively low efficiency factor of about 10 %, the absolute amount of energy is sufficient for driving electrical circuits and a sensor electronics. Researchers have tried to increase the Young modulus of material as energy harvesting, because energy is directly related to the Young modulus, $YS^2/2$. However, the energy is directly related to the strain also. Thus, both Young modulus and strain is important. Consequently, pure PU is interesting in material of energy harvesting, because Young modulus and strain is not low.

A tire pressure monitoring system (TPMS) consists of a wireless pressure sensor inside each tire and a receiver in the car. The TPMS is a key device in preventing a flat tire, which is one of the most frequent causes of car accidents. The TPMS is expected to become one of the most popular electronic products in vehicle applications. In 2000, the US government issued the Transportation Recall Enhancement, Accountability and Documentation (TREAD) act, which mandates car manufacturers to install TPMS in all vehicles sold in the US. In addition, European Union and a number of Asian countries are currently considering the implementation of TPMS-related legislation. The systems currently on the market are powered by a lithium battery, but there are drawbacks to these batteries, such as their limited durability, large size and weight, and pollution of the environment, which has led to them gradually becoming less and less favored by the public. For these reasons, researches into harvesting energy from the environment have grown in the past few years **[64]**.

In this way, many researchers studied to get energy efficiently **[65, 66]**. In addition, the study to use vibration energy harvesting for miniaturization of microelectronics devices was reported in a study team **[67]**.

EAPs are well suited for harvesting energy from human motion. Natural muscles, the driving force for human motion, are typically of low frequency and intrinsically linear; two characteristics where EAPs offer advantages. Human walking is a good example of an application of energy harvesting using human motion. Proof-of-principle heel-strike generators have been built using dielectric elastomer devices. With more development, it will likely become feasible to obtain up to approximately 1–2 J per step **[68]**. The upper limit for energy harvesting without causing discomfort to the walker is estimated at 2–4 W for two shoes, assuming a typical 1-Hz step frequency (Figure 1.20) **[69]**.

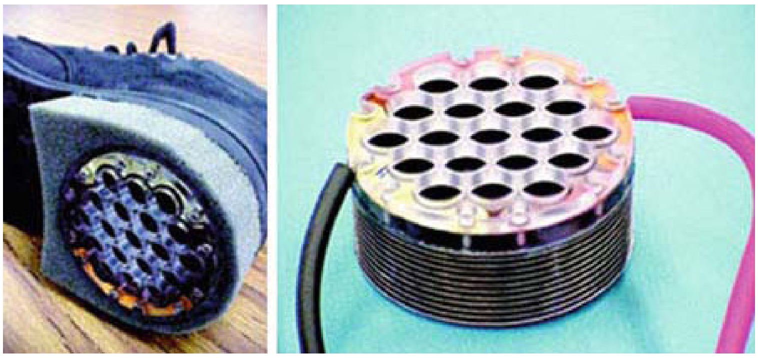

Figure 1.20 Dielectric elastomer heel strike generator. [69]

This amount of power is adequate for portable applications such as cell phone battery charging, and emergency locators for soldiers, as illustrated in Figure 1.21. The figure also provides the orders of magnitude of the powers consumed by various CMOS (complementary metal oxide semiconductor) electronic equipment that could be powered by energy harvesting devices **[70]**.

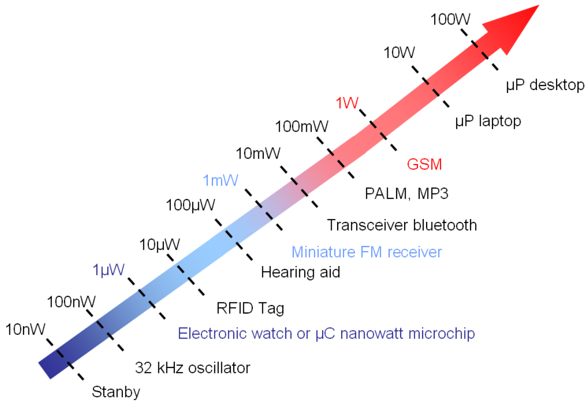

Figure 1.21 Various powers consumed by CMOS electronic devices. [70]

EAPs have demonstrated excellent performances, and numerous applications appear feasible, but challenges remain. EAPs appear most advantageous for applications requiring low or variable frequencies, low cost, and large areas. Currently, piezoelectric (PZT) materials are the most popular for harvesting mechanical energy because of their compact configuration and compatibility with MEMSs (micro-electro-mechanical systems). Nevertheless, there are inherent limitations such as aging, depolarization, and brittleness. In order to overcome these limitations, the use of EAPs seems promising and exciting **[68]**.

c) Robot application

The common applications for EAPs are in the field of robotics in the development of artificial muscles. The robotics is also interesting application. They are, so, briefly introduced here.

The availability of EAP actuators can bend or extend / contract capable of producing unique robotic devices that emulates human hands **[29, 71, 72]**. A robotic arm was developed and programmed for computer control as shown in Figure 1.22 **[73]**. To form a miniature lightweight robotic arm a 5 mm diameter graphite/epoxy rod was used and a rope was connected on the short end of this balanced rod and was used to lower and raise the arm as shown in Figure 1.22. On the right of the rod a gripper was mounted as an end effector using bending EAP fingers and miniature hooks to secure the gripped objects. The rope consisted of a silicone film and it required voltage levels of 30-70 V/µm, which reached between 1000 and 2500 V to produce the levels of several percents actuation strain (shown in Figure 1.23) **[73]**. Since the film is squeezed as a result of the activation, it becomes longer under the electro activation making the rope longer. This longitudinal EAP rope actuated the arm by tilting its balance and the lifting displacement is determined by the ratio between its connection distances from the pivot point compared to the gripper distance. The longitudinal EAP was used here as the equivalent of human muscle with the exception that it becomes longer under activation **[73]**.

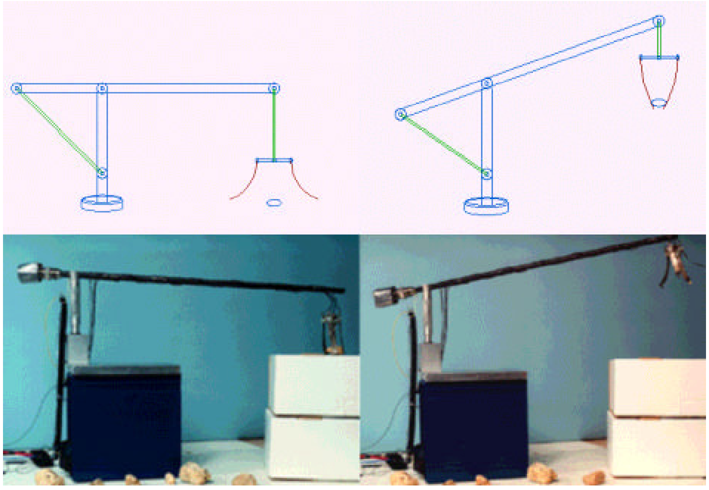

Figure 1.22 A simulated view (top) and a constructed robotic arm, which takes advantage of the capability of longitudinal and bending EAP actuators. [73]

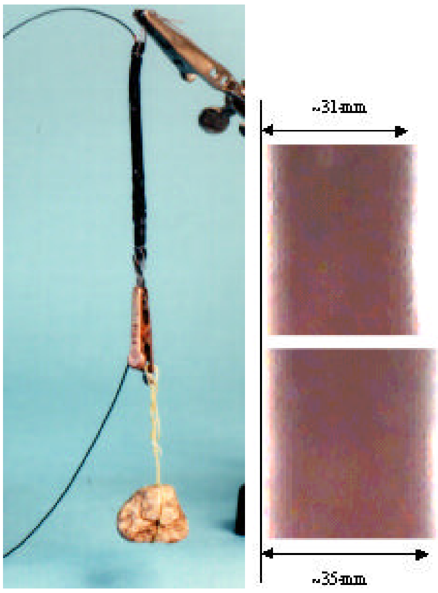

Figure 1.23 Using an electroded silicone film a 12% extension was obtained by electro-activation (right) and in a rope shape the actuator is shown lifting 10.3 g rock (left). [73]

Consequently, dielectric elastomers as EAP are widely used by energy harvesting. Furthermore dielectric elastomers can be used as active actuators on various miniature robotic arm elements.

Chapter 2

Material, Fabrication procedure and experimental set up of electroactive polyurethane composites

2.1 Introduction

Fundamentals of piezoelectric material and EAPs were described in a previous chapter. The piezoelectric materials exhibit small deformation (< 0.2 %) but it requires a low electric driving field (< 5 MV/m) **[1]**.

As explained in chapter 1, electroactive polymers (EAPs) exhibit specific characteristics, such as being lightweight, flexible, and presenting large strains and high mechanical energies, which make them suitable for new types of actuator materials. The high electric field is, however, in general required in order to present large strains of most of EAPs today. Consequently, this electric device cannot be used together other electric devices.

The present chapter, chapter 2, proposes a specific concept and a fabrication method of EAPs which generate large strains under a moderate electrical input. It means to make intermediate materials between piezoelectric materials and EAPs materials today.

In the present thesis, polyurethane (PU) was chosen because its modulus and relative permittivity is higher than that of silicone rubber. Beside, the relative permittivity of copolymer is quite high, but strain of copolymer is smaller than PU.

In addition, conductive fillers, carbon black (CB) nanoparticles, were also chosen to make composite films in pure PU matrix to increase the effectively in electroactive strain. Since the electric field must vanish inside the conductive particles, electrical charges appear on the particle surface in order to crate the applied electric field. These charges create on particle polarization. This polarization is not remnant but indeed vanishes when the applied electric field is removed. Micelle formed CB was used in order to avoid aggregation. First of all, fabrication method and rare electrical output results of such polymeric material are shown.

2.2 Material

2.2.1 Polyurethane (PU)

As mentioned earlier, electrostrictive polymers exhibit quite attractive characteristics. As a result, they have been widely studied either for the purpose of understanding the electrostriction phenomenon or in view of practical applications **[1, 74-76]**. Numerous reports are devoted to the characterizations of the electrostrictive behavior versus applied electric fields **[1, 56, 75]**. Under moderate electric fields (< 20 MV/m), they have been found to produce large strains of up to 10 %, and for this reason they are considered as good candidates for sensor/actuator material **[77]**.

Polyurethane (PU) elastomers are of great interest for a wide range of transducer and sensor/actuator applications when considering their significant electrical-field-induced strains, high specific energy. The other reasons of choice in PU comparing with other electrostrictive polymer were already discussed in chapter 1.

The chosen matrix material, in the present thesis, was from commercially available PU granules. They are polyether-type thermoplastics TPU58888 from Estane Company. The basic knowledge of PU will be explained in this section.

a) PU - general structure

PU is the general name of polymer consisting of a chain of organic units joined by urethane links. PU polymers are formed through step-growth polymerization to react a monomer containing at least two isocyanate functional groups with another monomer containing at least two hydroxyl (alcohol) groups in the presence of a catalyst.

Polyurethane or urethane linkage is produced by reacting an isocyanate group, -N=C=O, with a hydroxyl (alcohol) group, -OH, (Figure 2.1). Polyurethanes are produced by the polyaddition reaction of a polyisocyanate with a polyalcohol (polyol) in the presence of a catalyst and other additives. A polyisocyanate is a molecule with two or more isocyanate functional groups, R^1-(N=C=O) $_{n \geq 2}$ and a polyol is a molecule with two or more hydroxyl functional groups, R^2-(OH) $_{n \geq 2}$. The reaction product is a polymer containing the urethane linkage, -R^2NHCOOR^1- **[78]**. Isocyanates will react with many molecules that contain active hydrogen.

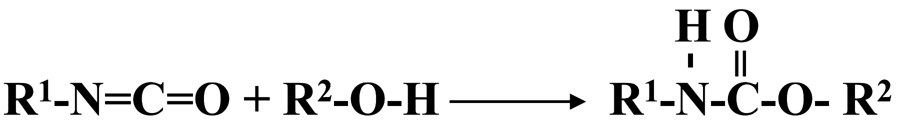

$$R^1\text{-N=C=O} + R^2\text{-O-H} \longrightarrow R^1\text{-}\overset{\overset{\text{H}}{|}}{\text{N}}\text{-}\overset{\overset{\text{O}}{\|}}{\text{C}}\text{-O-}R^2$$

Figure 2.1 Generalized PU reaction.

The first essential component of a PU polymer is the isocyanate. Molecules that contain two isocyanate groups are called diisocyanates. These molecules are also referred to as monomers or monomer units, since they themselves are used to produce polymeric isocyanates that contain three or more isocyanate functional groups. Isocyanates can be classified as aromatic series, such as diphenylmethane diisocyanate (MDI) or toluene diisocyanate (TDI) or aliphatic, such as hexamethylene diisocyanate (HDI) or isophorone diisocyanate (IPDI). An example of a polymeric isocyanate is a polymeric diphenylmethane diisocyanate, which is a blend of molecules with two-, three-, four- or more isocyanate groups.

The second essential component of a PU polymer is the polyol. Molecules that contain two hydroxyl groups are called diols. Those with three hydroxyl groups are called triols, and so on. In practice, polyols are distinguished from short chain or low-molecular weight glycol chain extenders and cross linkers such as ethylene glycol (EG), 1,4-butanediol (BDO), diethylene glycol (DEG), glycerine, and trimethylol propane (TMP). Polyols formed by polyesterification are polyester polyols. The choice of initiator, extender, and molecular weight of the polyol greatly affect its physical state and the physical properties of the PU polymer. Important characteristics of polyols are their molecular backbone, initiator, molecular weight, percent of primary hydroxyl groups, functionality, and viscosity.

b) Thermoplastic PU

Thermoplastic polyurethanes (TPUs) are randomly segmented copolymers composed of hard and soft segments forming a two-phase microstructure (Figure 2.2) **[79-81]**. Generally, phase separation occurs in most TPUs due to the intrinsic incompatibility between the hard segments (HS) and soft segments (SS). The HS, composed of polar materials, can form carbonyl to amino hydrogen bonds and thus tend to cluster or aggregate into ordered hard domains, whereas the soft segments form amorphous domains. Phase separation, however, is often incomplete, i.e., some of the HS are isolated in the soft domains as illustrated schematically in Figure 2.2 **[80]**. In many TPUs, the hard domains are immersed in a rubbery soft segment. Depending on the HS content, the morphology of the hard domains changes from one of isolated domains (Figure 2.2 (a)), to one of interconnected domains (Figure 2.2 (b)) **[79-81]**.

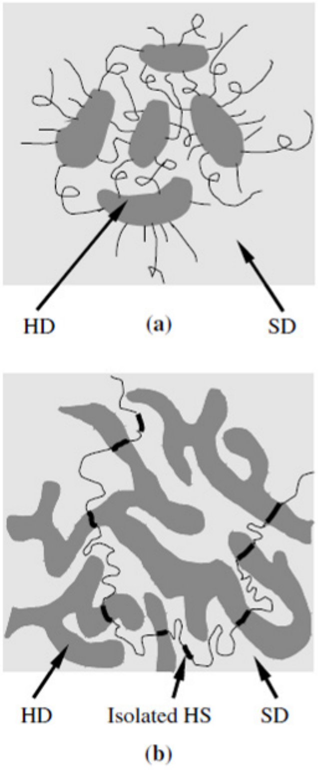

Figure 2.2 Hard domains (HD) and soft domains (SD) of TPUs with (a) low hard segment content [80]; (b) high hard segment content. Isolated hard segments (HS) seen in (b). [79-81]

The presence of hard domains in segmented polyurethanes is very important to the mechanical properties. In segmented polyurethanes, hard domains act as physical crosslinks, playing a role similar to chemical crosslinks in vulcanizates and imparting the material's elastomeric behavior. Since hard domains also occupy significant volume and are stiffer than soft domains, they also function as effective *nano-scale fillers* and render a material behavior similar to that of a composite **[80]**. At room temperature, soft domains are above their glass transition temperature and impart the material its rubber-like behavior, whereas hard domains are below their glassy or melt transition temperature and are thought to govern the hysteresis, permanent deformation, high modulus, and tensile strength. The domain structure also imparts TPUs' versatility in mechanical properties. A wide variety of property combinations can be achieved by varying the molecular weight of the hard and soft segments, their ratio, and chemical type.

c) PU -Estane 58888

The studied PU is a commercial material, Estane 58888-NAT021 provided by Noveon. The structure of PU 58888 is depicted in Figure 2.3. This PU is based on MDI (4,4' methylene bis(phenyl isocyanate)) and BDO (1,4-butanediol) as crystalline form of HS and poly(tetramethylene oxide) as SS **[82]**. The HS content is about 46 wt% and the physical properties depend partially on the phase separation degree between hard and soft phases which are shown in Figure 2.4 **[83]**.

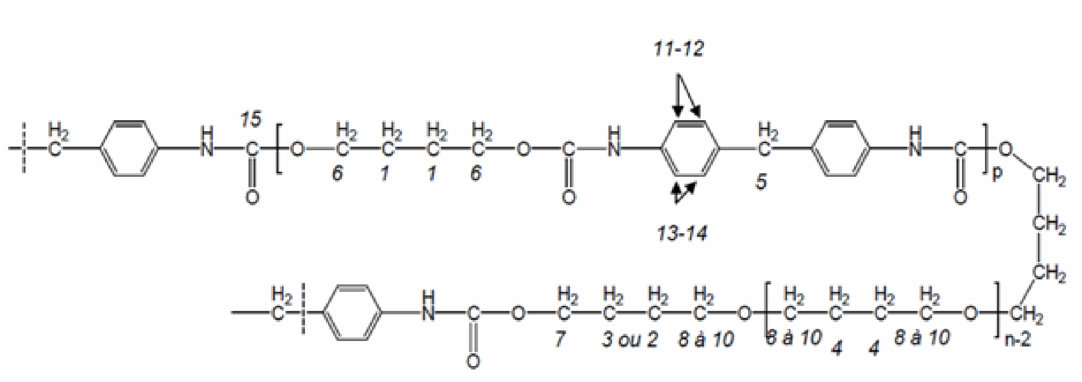

Figure 2.3 Structure of PU - Estane 58888.

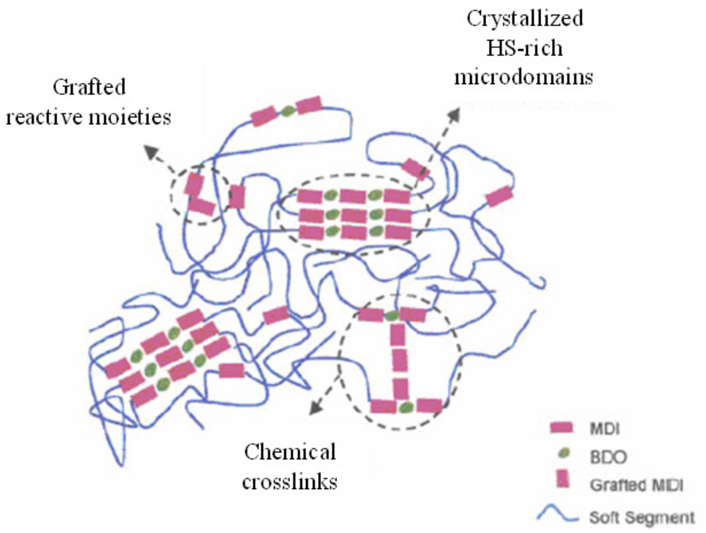

Figure 2.4 Schematic representation of chains urethane and micro-separation of rigid segments. [83]

Linear and segmented polyurethanes, which consist of alternating SS and HS, offer unique possibilities for tailor-made polymers through the variation of the block length and composition. The SS are typical polyether, and polyester and they provide the flexible character of the polymers. These segments are connected by HS formed from the reaction of diisocyanates with diol chain extenders. Thermodynamic immiscibility between HS and SS induces a phase separation and generates a two-phase morphology in these segmented block copolymers. Several physico-chemical properties of PU – Estane 58888 are listed in Table 2.1.

Table 2.1 Physio-chemical properties of PU –Estane 58888.

Characterization	Polyurethane (TPU 58888)
Density (g/cm^3)	1.13
Melting temperature (^{o}C)	160
Breaking stress (MPa)	38
Breaking elongation (%)	640

2.2.2 Conductive particle directly obtained from nanoink

a) Comparison with piezo electric particles

It has recently been shown that the incorporation of nano fillers such as carbon nano tubes into a polymer matrix can greatly enhance the strain versus electric field **[84]**.

Until today, many EAPs are made incorporating with piezo particles and conductive particles in polymer matrices as shown in Table 1.1 in chapter 1 **[45-48, 85]**. The conductive mechanism is different **[1]**. An explanatory schematic is given in Figure 2.5.

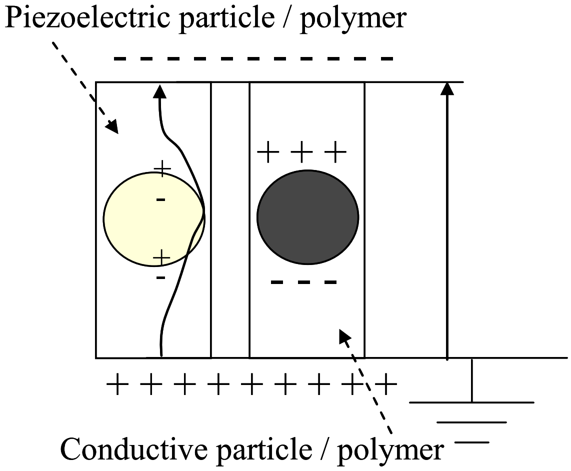

Figure 2.5 A schematic of electric induction for composite films filled with ferroelectric and conductive particles.

A piezo coefficient, *d*, is directly related to the permittivity, ε, of a piezo/polymer composite. Researchers have thus tried to increase the permittivity of composite with a large quantity of piezoelectric particles **[10]**. Due to the huge step in the permittivity difference between the one of polymer matrix and the one of piezoelectric particles, the applied electric field does not ‘enter’ into the particles. Consequently, this composite material exhibits poor actuating performances. Furthermore, the resultant composites are quite hard and heavy and they require a high driving energy.

The conductive material, as opposed to a piezoelectric one, was chosen in the present thesis as the filler material and was incorporated into the polymeric material **[1, 10, 56, 86, 87]**. The concept differs from that of EAPs with piezoelectric fillers. It is believed that the electrons stay on the surface of each conductive particle since the electric field is null inside of conductive particles.

b) Aggregation problem

The incorporation of particles, however, leads one famous disadvantage. It is a dispersion state of particle. Aggregation of particles is called aggregate. With a low volume percentage of fillers, the risk of electric short circuiting caused by aggregates should decrease. The performance in strain, however, is reported higher near the percolation threshold. It is important thus to prevent aggregations.

The famous dispersion methods are sol-gel process, ultrasonic dispersion (sonication), surfactant and micelles formation.

The sol-gel process, also known as chemical solution deposition, is a wet-chemical technique widely used in the fields of materials science and ceramic engineering. Such methods are used primarily for the fabrication of materials (typically a metal oxide) starting from a chemical solution or sol that acts as the precursor for an integrated network or gel of either discrete particles or network polymers. This process is a cheap and low-temperature technique that allows for the fine control of the product's chemical composition.

The ultrasonic dispersion (sonication) can be used to speed dissolution, by breaking intermolecular interactions. It is especially useful when it is not possible to stir the sample.

The surfactants are compounds that lower the surface tension of a liquid, the interfacial tension between two liquids, or that between a liquid and a solid. Surfactants may act as detergents, wetting agents, emulsifiers, foaming agents, and dispersants. Many surfactants can also assemble in the bulk solution into aggregates. Furthermore, particle size also is important. In case of nano size particles, aggregations can easily occur since Van der Waals or other short range forces increase which makes nanoparticles attracts each other.

If nanoparticles have the micelle form previously, they can be dispersed easily in matrix. It is difficult to make the micelle form. However ink is composed of micelles in a fluid has the micelle form. Therefore, micelle form of nanoink was selected in order to avoid this problem.

The dispersion of nanoink will be shown with photos in chapter 4, but some basic information of used nanoink is shown the following.

In the present thesis, a premixed solution with carbon particles, i.e., carbon black (CB) in micelle form was selected **[1]**.

c) Nanoink

The diameters of the nano carbon black (CB) obtained directly from nanoink (SAILOR Ltd., Japan) particles in the composite films were measured by Transmission Electron Microscope (TEM: HF-2200TU, HITACHI). It was confirmed to lie in the range of 15 to 30 nm.

The evaporation temperature of the nanoink was measured by Differential Scanning Calorimetry (DSC: 131Evo, SETARAM, France). The crucible was made of aluminium. The heating rate was 10 °C/min. The samples were measured from 30 to 200 ºC and the first heating curve was registered. The precision of the DSC measurement was 0.1 ºC.

Evaporation temperature of nanoink was found to lie between 86.52 ºC and 152.86 ºC (Figure 2.6). The calculation of the volume fraction was based on the solid densities of the constituents. In general, density of CB nanoparticles is 2.2 g/cm^3.

The weight of the nanoink was measured after drying at 160 ºC at less than atmospheric pressure for 1 h. 100 μl of nanoink was transformed into 8.6 mg of powder. It could thus be determined that the composite film of 200 μl nanoink dispersed into 1 g of polyurethane (PU) signified 0.89 vol% CB nanoparticles/PU **[1]**.

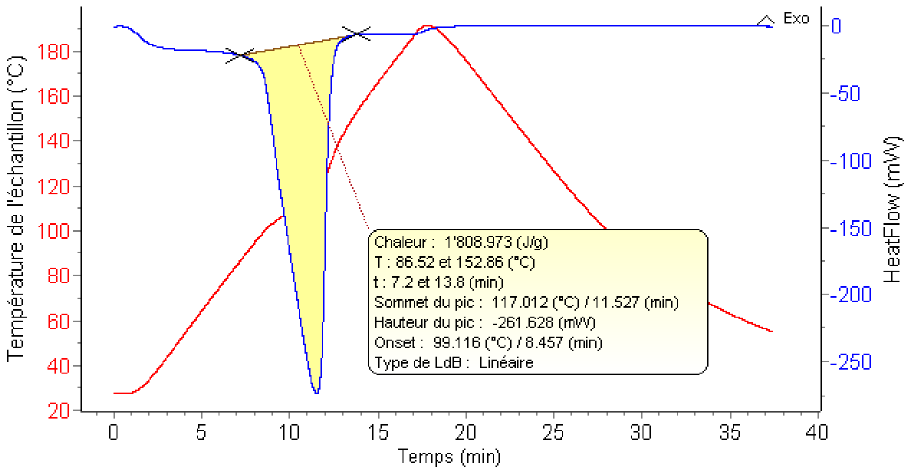

Figure 2.6 Evaporation temperature of nanoink.

2.3 Fabrication procedure

2.3.1 Preparation of pure PU film

The Estane 58888-NAT021 ether based thermoplastic pure PU was selected because of its high level (enrichment) of HS, 46 wt%, and its high electrical stability as discussed in section 2.2.1. Pure PU films were prepared through a simple solution casting method **[1, 56, 86, 87]**.

1 gram of PU granules were first dissolved in 20 ml of *N*, *N*-dimethylformamide (DMF) under mixing at 80 ºC during 45 min until the PU solution became homogeneous. The solution was poured onto a glass plate and dried at 60 ºC for 1 day after solidification from liquid to solid. The obtained films were removed from the plate with ethanol. Subsequently, they were placed in a ventilated oven at 130 ºC for 4 h in order to totally eliminate residual solvent.

For the electromechanical characterization measurements, samples were cut into disc-shaped (25 mm in diameter). The solidification thickness was measured by mechanical comparator (FLORENZA THYEZ, France) in 0.001 µm order. The solidification thickness means the thickness at room temperature just after solidification from liquid to solid. It may strongly affect the perfection and volume fraction of the crystalline form of HS in pure PU. The procedure of the preparation of pure PU films is shown in Figure 2.7.

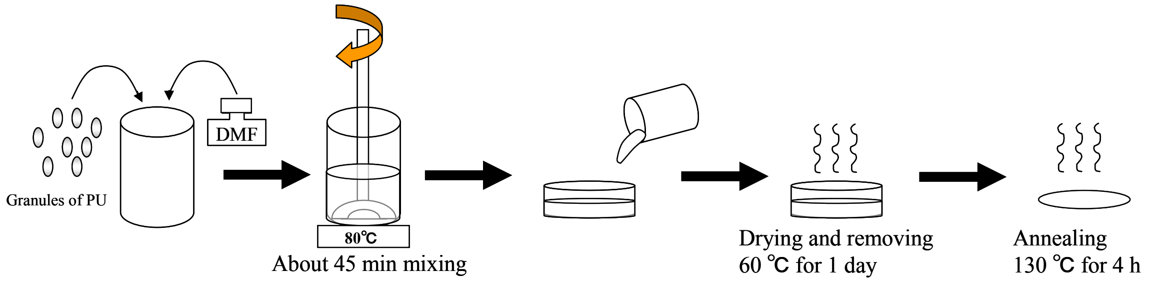

Figure 2.7 Solution casting method of pure PU film.

2.3.2 Preparation of composite film

PU films incorporating with nano CB particles obtained form nanoink are called ‘composite films’ in the present thesis whereas pure PU is just called ‘Pure PU film’.

Composite films comprising a nanoink were also prepared by a simple solution casting method **[1]**. After the confirmation of homogeneous mixture of PU, after 30 min, liquid ink was added then continuously mixed by non magnetic stirring at constant temperature for 40 min.

To the volume fraction of CB fillers content was varied from 12, 50, 100, 200 and 400 µl in 1g of PU granules. They correspond 0.05, 0.22, 0.45, 0.89 and 1.78 vol% or 0.102, 0.425, 0.85, 1.7 and 3.4 wt%, respectively. In the present thesis unit of vol% is used.

Other procedures are the same to the ones of pure PU films. The procedure of composite films is shown in Figure 2.8.

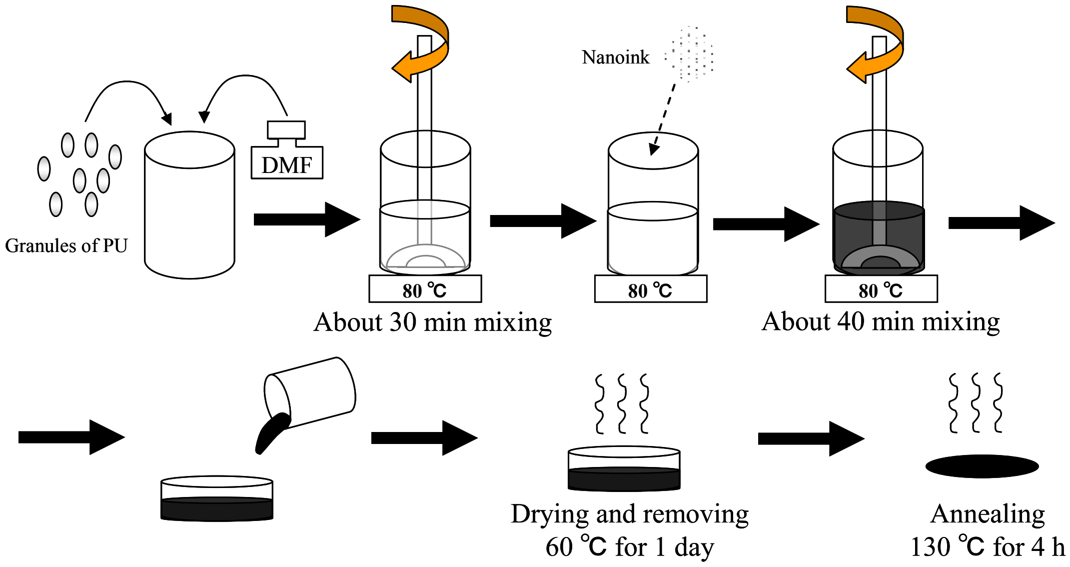

Figure 2.8 Solution casting method of composite film.

2.4 Electrostrictive strain and output current measurement method

Schematic diagram of the interferometer setup and picture are shown in Figure 2.9 and Figure 2.10, respectively.

The electric field-induced electroactive strain, *S*, was measured by a laser interferometer (Agilent 5519A) with a precision on the order of 5 nm. The induced electric field, *E*, was a sawtooth wave for 2-cycle at 0.1 Hz with varying amplitude between 1 and 20 MV/m. The upper limit of the maximum electric field, E_{max}, in the present thesis was 20 MV/m. Therefore, the range from 10 to 20 MV/m is called ‘high electric field regime’ and from 1 to 5 MV/m is in general called ‘low electric field regime’ in the present thesis.

The films were placed on a horizontal brass disc (20 mm in diameter) in order to avoid measuring a parasitic flexural motion, and a second brass disc (20 mm in diameter, 8.582 g) placed on the upper side of the film. It was rendered it possible to apply a bipolar electric field. The mirror (0.875 g) was put on brass disc. A function generator (Agilent 33220A) delivered the corresponding bipolar voltage amplified by a factor of 1000 through a high-voltage lock-in amplifier (Trek 10/10B). The ground current between the sample holder and the ground was measured using a current amplifier (Stanford Research Systems SR570).

In the case of PU, the thickness strain is compressive with an increasing applied electric field due to its negative electrostrictive coefficient, confirmed experimentally in-between the beam measurements. In the present thesis, compressive strain is expressed in positive strain.

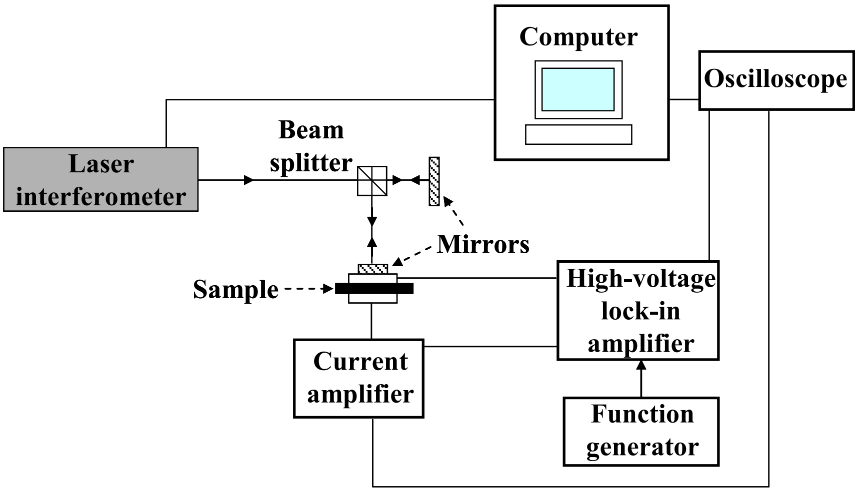

Figure 2.9 Schematic diagram of the interferometer setup.

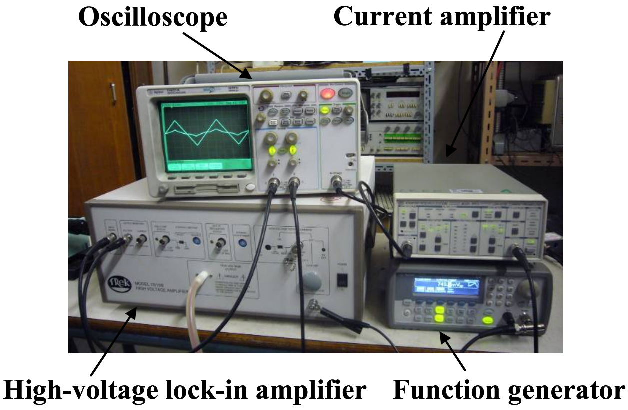

Figure 2.10 Picture of the setup.

2.5 Overview of the results and discussion

Before to see the effectiveness of CB particle doping by the comparison between pure PU and composite films in chapter 4, I put some results of electroactive strain and output currents in the present section to give a brief overview. The results of pure PU and composite film will be more detailed and discussed in chapter 4.

2.5.1 Electrostrictive strain induced by electric field

The results are similar, pure PU and composite films, in the relation of electroactive strain in time domain. First of all, all compressive strains in general, during the evolution of induced electric field. Secondly, they have saturation in high electric field regime. Figure 2.11 shows the typical outcome of the electric field-induced strain of (a) pure PU and (b) 0.89 vol% composite films under 2-cycle of a sawtooth wave electric field with various amplitudes. The image of the electric field is represented in the figure by a bold line.

(a) Pure PU film (40 µm)

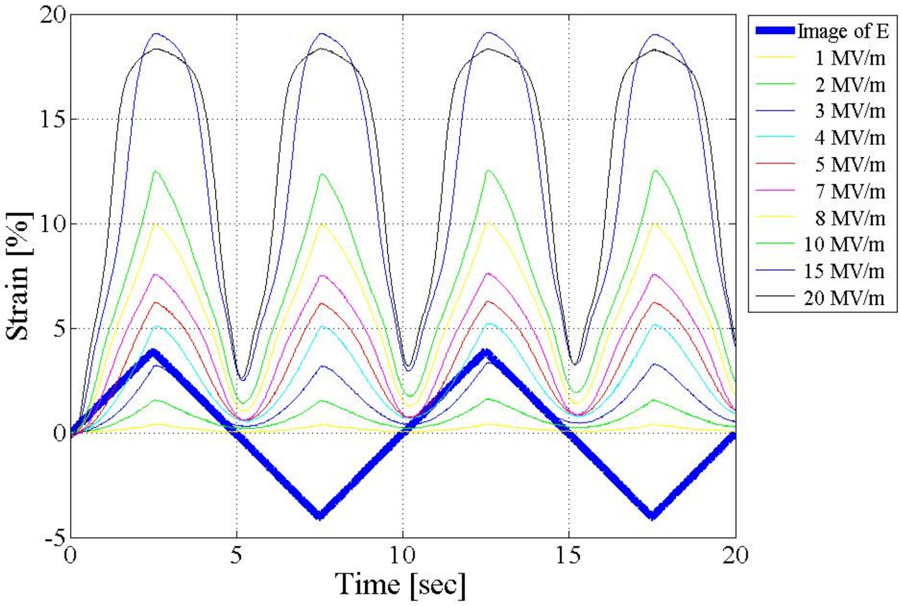

(b) 0.89 vol% composite film (40 µm)

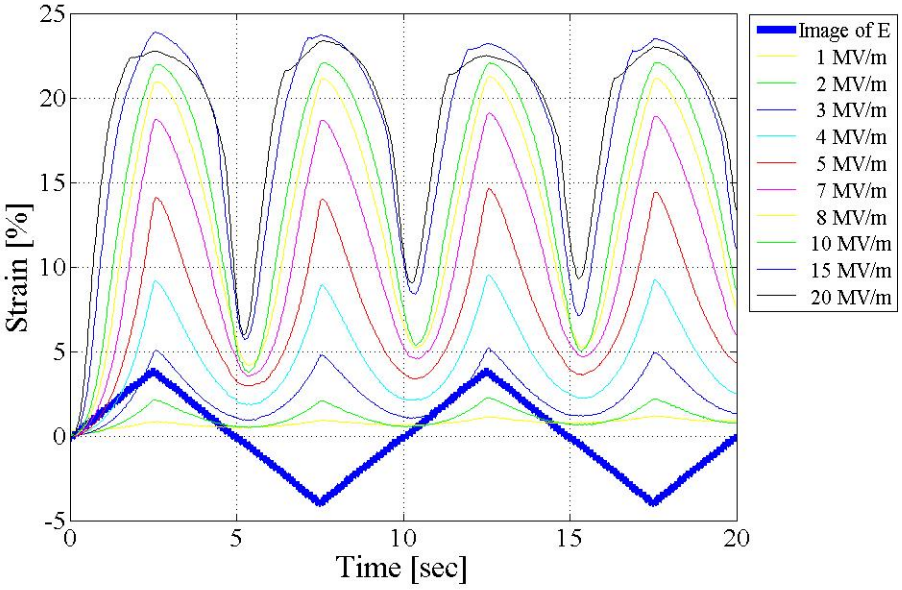

Figure 2.11 2-cycle of sawtooth wave electric field induced strain of pure PU and 0.89 vol% composite films, 40 µm.

For a two periods of electric field driving, the strain exhibits four periods. This frequency doubling can be understood easily since the strain writes $S=ME^2$ for low electric field values. M is the electrical-field-related-electrostriction coefficient of the material. The round shape aspect of the strain and the fact that the zeros of the electric field and the zeros of the strain do not coincide is due to the losses between the electric field, E, and the polarization, P, or/and the electric field and the strain. To describe this behavior, a convolutive equation must be considered.

$$S(t) = M(t) \underset{t}{*} E^2(t) \text{ or } S(t) = Q(t) \underset{t}{*} P^2(t) \qquad (2.1)$$

This residual strain is confirmed to disappear within a 150 sec after in cut off electrical field input. Figure 2.12 shows strain versus time of 40 µm pure PU films. The shape decreasing faction can be related to the *M(t)* or *Q(t)* functions previously given. From a numerical point of view, it can be referred as the relaxation function. This time-log will be explained in chapter 3.

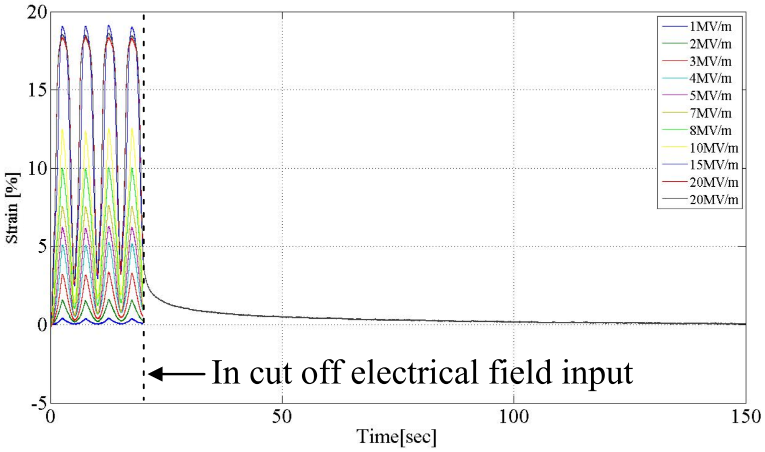

Figure 2.12 Strain versus time of 40 µm pure PU film.

2.5.2 CB doping effect

Figure 2.13 shows maximum strain, S_{max}, versus maximum electric field, E_{max}, of the pure PU and 0.89 vol% composite films. Both have the same thickness and they correspond to the films of Figure 2.11. The S_{max} is seen to have nonlinearly with the E_{max}. It can be clearly seen in Figure 2.13 that the parabolic relation of S_{max} (E_{max}) disappeared when the electric field is increased. The *S(E)* saturations are seen. Starting point of convergence occurred at a higher electric field by composite than pure PU film.

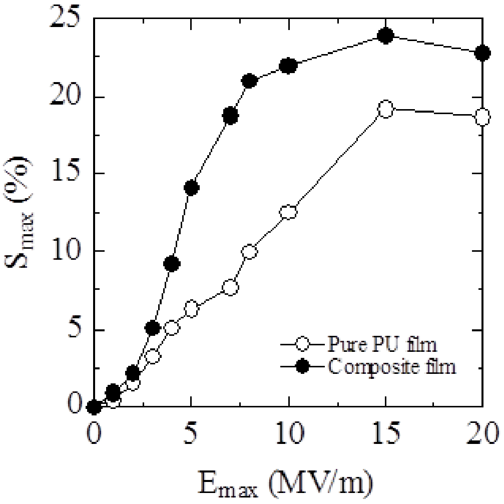

Figure 2.13 Experimental changes in maximum strain versus maximum electric field of the pure PU and 0.89 vol% composite films, 40 µm.

Beside, it is clear that the present composite film exhibited larger strains than pure PU film. Composite film was able to generate a strain of 24 % at 15 MV/m whereas 20 % by pure PU film so that the factor of 1.2 was realized by incorporating nano CB particles.

CB doping effect is the one of the first topics of the present thesis. It will be discussed in details in chapter 4.

Such strain levels, 20 or 24 %, are not surprising for ‘EAPs,’ but from the fact that EAPs in general require very high electric fields (< 150 MV/m) to obtain such strain, it is surprising. The pure PU films presented herein can generate a significant strain with moderate electric field at less than 20 MV/m. The downsizing of required electric field renders possible applications.

2.5.3 Thickness effect

Figure 2.14 shows maximum strain, S_{max}, versus maximum electric field, E_{max}, of pure PU and composite film (0.89 vol%) of thick and thin films, around 20 and 140 µm, respectively. The values S_{max} are taken at the first peak whereas E_{max} is the electric field amplitude. On both thick samples, the saturations in strain versus electrical field, *S(E)*, are clearly seen in low electric regime < 5MV/m. The values at 20 MV/m became then quite small in front of thin samples. The thin samples show the clear parabolic relations at electrical field less than 10 MV/m. The thin pure PU sample shows the start of saturation until 20 MV/m whereas the thin composite sample does not have. On the both samples, the thickness effect is obvious. The *S(E)* saturation is the second topics of the present thesis and it is well considered by simulation in the next chapter, chapter 3.

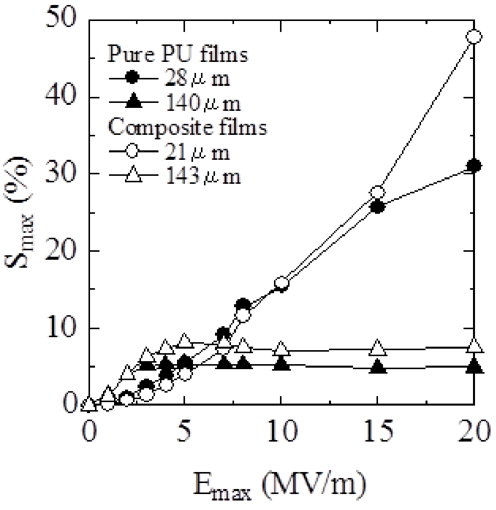

Figure 2.14 Experimental changes in maximum strain versus maximum electric field of pure PU and composite films.

2.5.4 Output current induced by electric field

In terms of the output current, the results of the 0.89 vol% composite films have also similar components to that of pure PU so that only pure PU ones will be shown here.

Figure 2.15 shows the evaluation of current of pure PU film (140 µm) under there different electric field amplitude; (a) 1 MV/m, (b) 5 MV/m and (c) 20 MV/m. The shape of induced electric field was always a 2-cycle sawtooth wave, expressed by dotted lines in figures. In the low electrical regime, total current was quite small and had rectangular shape in at low electric field, see Figure 2.15 (a). From the sawtooth wave electric field, we see that it is purely capacitive. The rectangular current, *I*, was considered according to the following **[1]**,

$$I = C\dot{V} \qquad (2.2)$$

Here, *C* is the capacitance and $\dot{V}$ is the voltage derivative.

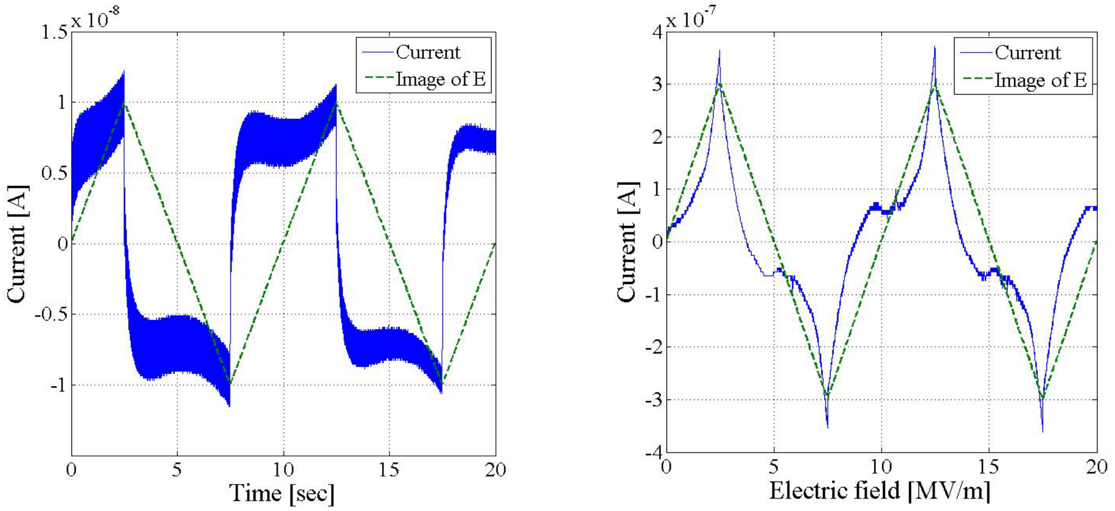

(a) 1 MV/m

(b) 5 MV/m

(c) 20 MV/m

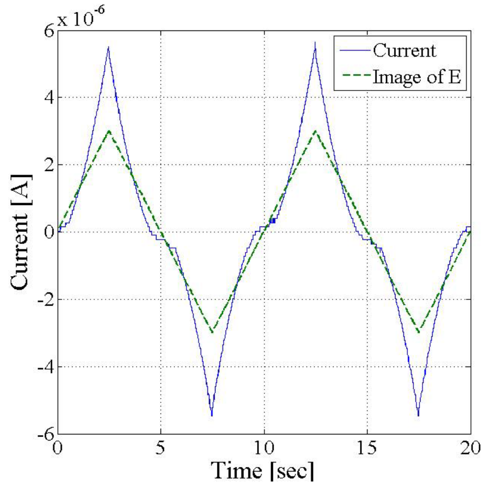

Figure 2.15 Evolution of current of pure PU film, 140 µm.

For moderate electric field values (Figure 2.15 (b)), the current undergoes sharp peaks. This trend is confirmed for high electric field values at 20 MV/m (Figure 2.15 (c)). Since the current looks like the voltage, it means that a resistive behavior takes place in this described amplitude range.

This evaluation is changed by film thickness. When film is thinner peaks appear in smaller electric field regime and peak's top evolution is more active. When film is thicker, comet stays in capacitive rectangular shape until amplitude of electric field is highly increased. The discussion part of resistive properties, it is shown in chapter 3.

2.5.5 Polarization induced by electric field

In terms of the polarization induced by electric field, the results of the 0.89 vol% composite films have also similar components to that of pure PU so that only pure PU ones will be shown here.

We can define the apparent polarization, P^*, writes from the measured current using the following equation **[1]**:

$$P^* = \frac{1}{A}\int I dt \qquad (2.3)$$

where A and I are the area of surface and current, respectively. This apparent polarization does not correlate directly to the real polarization. The measured current is $I_{measured} = I_{capacitive} + I_{resistive}$, and it is difficult to separate into to two terms. Here, we show the apparent polarisation calculated from the total of current, $I_{measured}$.

Figure 2.16 shows the apparent polarization in time domain at three different amplitudes of electric field of pure PU film, 140 µm. The data was obtained at (a) 1 MV/m, (b) at 5 MV/m and (c) 20 MV/m of maximum electric field induction. The shape of induced electric field was always a 2-cycle sawtooth wave, expressed by dotted lines in figures.

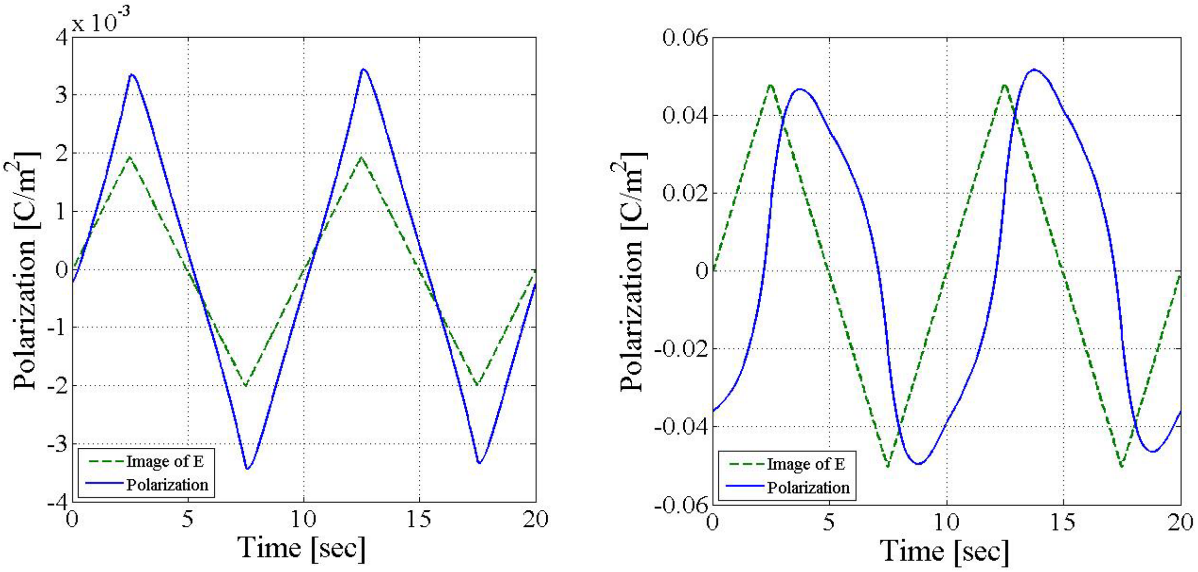

(a) 1 MV/m

(b) 5 MV/m

(c) 20 MV/m

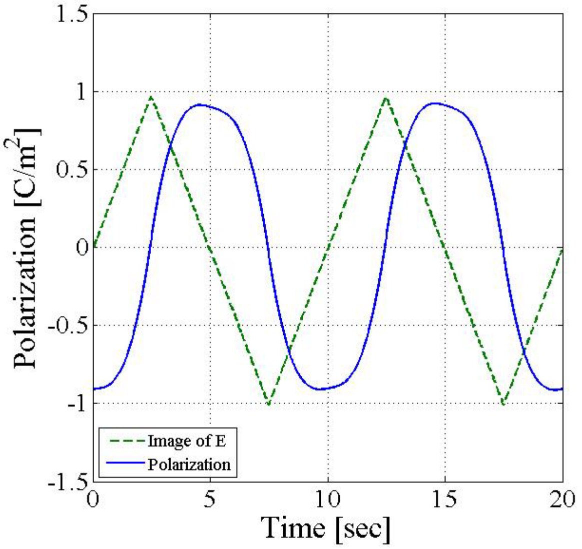

Figure 2.16 Change of the form of current and apparent polarization with maximum electric field of pure PU film, 140 µm.

When the amplitude of input electric field is quite small, as shown in Figure 2.15 (a), the current has rectangle shape. The increasing oscillation is seen in each stage of increase amplitude of electric field. The polarization has triangle shape. When the amplitude of input electric field is increased, as shown in Figure 2.15 (b) then (c), the current is strongly deformed. The apparent polarizations also change from triangle shape to round shape. Not on the flat slope but the edges of rectangle shape of Figure 2.15 (a) increases. The edges at peak of electric field increase much more than the other edges and the current to peak~~s~~ shape.

Figure 2.17 shows the result of the apparent polarization, P^*, as a function of the electric field for the 0.89 vol% composite film. The curves are closed and present almond shapes. We see that $P^*(E)$ surface increased a lot at high electric field amplitude domain. The discussion will be done in chapter 3.

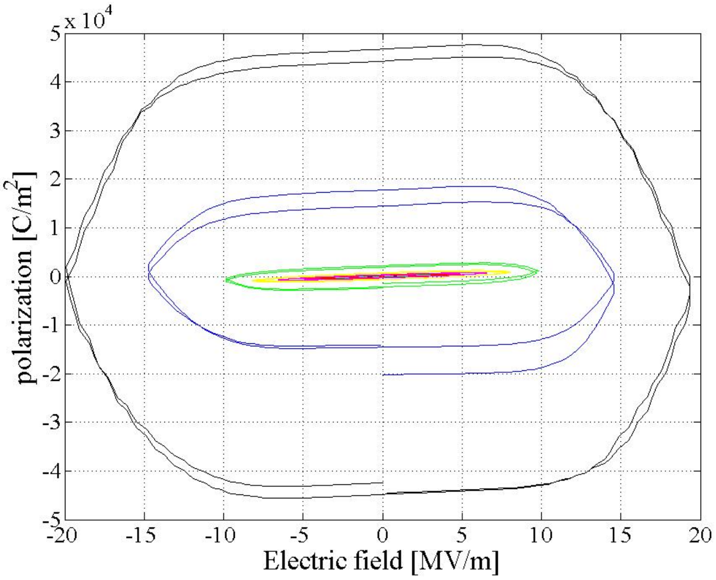

Figure 2.17 Electric field induced apparent polarization of composite film, 21 μm.

2.6 Conclusions

The present chapter proposed a specific concept and a fabrication method of EAPs which generate large strains under a moderate electrical input. Pure polyurethane (PU) was chosen as matrices material. In addition, conductive fillers, carbon black (CB) nanoparticles, were also chosen to make composite films in pure PU matrix to increase the effectively in electroactive strain. Micelle formed CB, directly obtained from nanoink, was used in order to avoid aggregation. In this chapter, chosen materials were introduced in details. Film fabrication method and experimental setup are discussed. Then, same electrical induced outputs are given for a brief overview.

First of all, strong enhancement of strain level was obtained by CB nanoparticles doping. It thus confirmed the effectiveness of the conductive filler. By a small quantity of carbon addition, 0.89 vol%, a high strain, 24 %, was obtained at moderate electric field, 15 MV/m. Such low electric input requirement can lead the possibility of EAPs to be used easily with other electrical devices. These results demonstrate the significant potential of nanoink composite polymer materials in future actuator/sensor applications. Mechanism will be discussed in the next chapter, chapter 3, and more detail results will be shown in chapter 4.

Secondly, the relation between strain and electric field was found nonlinear and a *S(E)* saturation was observed. This phenomenon occurs strongly in thick samples. Some thin samples show a start of *S(E)* saturation until 20 MV/m but some does not show. The thickness effect is obvious.

The form of the current and the apparent polarizations were shown. The current shape exhibits that the film material had changed from purely capacitive to mixture with resistive when the induced electric field amplitude is increased. It is difficult to separate them into two, so that the pure polarizations, connected to purely capacitive current, are not demonstrated here, but the apparent polarizations, obtained from the total measured current, were shown. They are closed almond shapes and the *P(E)* surface increases with electric field.

Chapter 3
Modeling the electrostrictive films behaviors

3.1 Introduction
3.2 Polarization modeling
  3.2.1 Saturation polarization
  3.2.2 Electrical/mechanical relationships in electrostrictive polymers (1D and stress free case)
    a) Relation between strain and polarization
    b) Losses effect on the strain waveforms
    c) Comment on the different equations describing the electrostrictive effect
    d) Non-linear permittivity
    e) Permittivity strain dependence
    f) Current-strain relation
    g) Influence on surface expansion on the current
3.3 Effect of thickness in electrostrictive film
    a) Experimental observation and the three-layer model with equivalent permittivity
    b) Strain curves crossing interpretation
    < Saturation electric field value significance and its evaluation >
    < Crossing conditions >
3.4 Three-layer model with force equivalent
3.5 Non-linear resistance

3.1 Introduction

The aim of the present chapter is to let the readers familiar with the physical problems related to the electrostrictive polymer film and the solutions that have been addressed. It is also an introduction to the modeling tool that we developed during the present thesis. The comparison with the experimental results will be done in the following chapters.

In the present chapter, it is assumed that the saturation of electrostrictive strain versus electric field, *S(E)*, shown in the previous chapter, chapter 2, is related to a saturation of the electrical polarization versus the induced electric field, *P(E)*. This polarization saturation may result from:

- The poled hard segment alignments along the driving electric field (a bit similar to the saturation of the ferroelectrics with the electric field)
- Others types of phenomenon

3.2 Polarization modeling

3.2.1 Saturation polarization

To model the polarization behavior in the polymer film, we consider the following function **[88]**:

$$P(E) = \varepsilon E_{sat} \tanh(\frac{E}{E_{sat}}) \qquad (3.1)$$

where ε is the permittivity at low electric field range and E_{sat} is a coefficient related to the change of behavior in the *P(E)* curves. If the electric field, *E*, is higher than E_{sat}, non-linearity takes place on the polarization. This polarization function meets the following requirements:

- It should monotonously increase (obviously, the polarization can not diminish when the field is increasing
- It should converge to the linear behavior at low electric field to describe correctly the full range of electric fields. It is the case for the selected function since $\tanh(E/E_{sat}) \approx E/E_{sat}$ and $P(E) \approx \varepsilon E$ when *E* is small enough
- It should saturate to a finite value for high electric field values. It is the case for the selected function since $\tanh(E/E_{sat}) \approx 1$ when $E/E_{sat} \to \infty$. The saturation value is $P(E) = \varepsilon E_{sat}$.
- It should be anti-symmetric versus the electric field. Positive and negative electric field must lead to opposed polarizations since there is not any preferred orientation or anisotropy in the material **[89-91]**. It is the case for the selected material since the hyperbolic tangent is anti-symmetric.
- It should not generate any hysteresis cycle. The selected function meets this requirement since the hyperbolic tangent is a single value function.

Figure 3.1 explains the idea of saturated polarization.

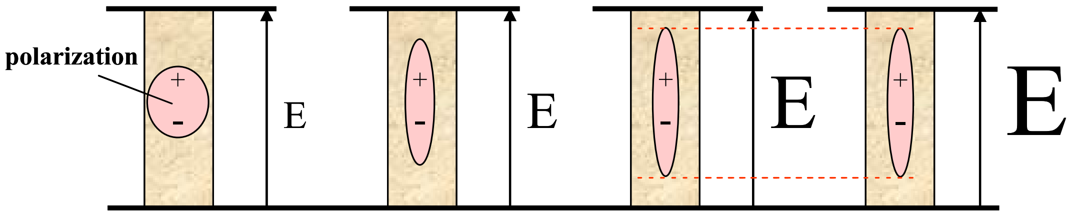

Figure 3.1 Electrical limitation caused by polarization saturation.

Clearly there is an infinity of functions which meet the above requirements and several authors have proposed different functions.

From the above polarization, a set of properties and relationships can be easily derived.

3.2.2 Electrical/mechanical relationships in electrostrictive polymers (1D and stress free case)

a) Relation between strain and polarization

From the mechanical constitutive equation of the electrostrictive material, $\tau(E) = cS(E) + \alpha P(E)^2$, I derive

$$S(E) = QP(E)^2 \qquad (3.2)$$

in 1D stress free case. The coefficient, *Q*, is the so-called electrostrictive coefficient. The electrostrictive strain, *S*, is always negative along the direction of the applied electric field.

Taking equation (3.1), $P(E) = \varepsilon E_{sat} \tanh(E / E_{sat})$, for the polarization function then the mechanical strain writes **[88]**,

$$S(E) = QP(E)^2 = Q(\varepsilon E_{sat} \tanh(E / E_{sat}))^2 \qquad (3.3)$$

Figure 3.2 depicts the polarization and strain versus the electric field for two values of E_{sat}, 7e6 V/m in dotted line and 15e6 V/m in continuous line. The values are arbitrary on the strain.

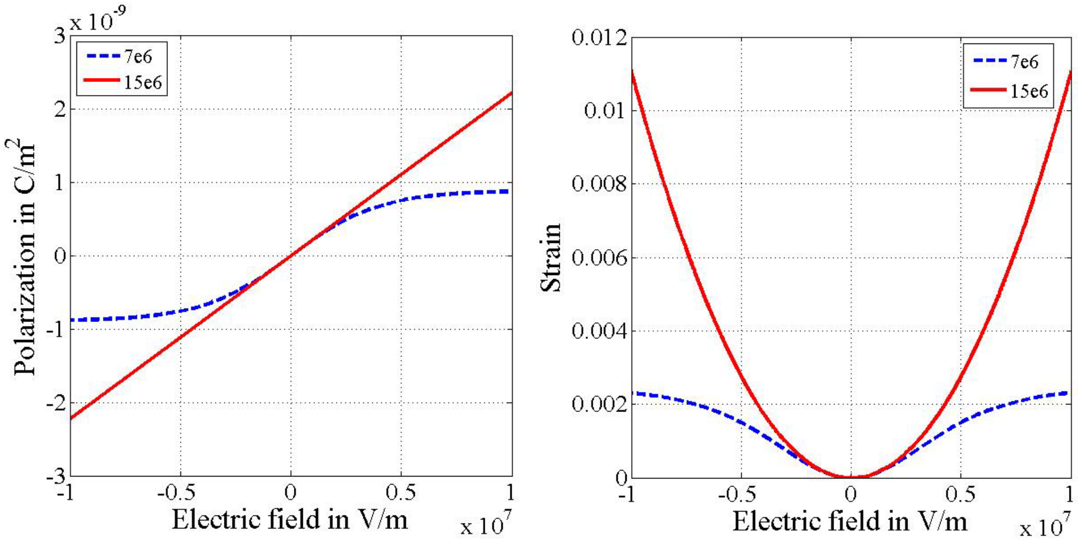

Figure 3.2 Polarization and strain versus the electric field for two values of E_{sat} (7e6 V/m in dotted line and 15e6 V/m in continuous line).

Figure 3.3 shows the strain waveforms in time domain for different values of E_{sat}, 7e6 V/m in dotted line and 15e6 V/m in continuous line, corresponding to the ones of Figure 3.1. The saturation effect becomes clearly visible in this way. The continuous fine line curve corresponds to the electric field in arbitrary units. The period doubling effect results from the squaring of the polarization.

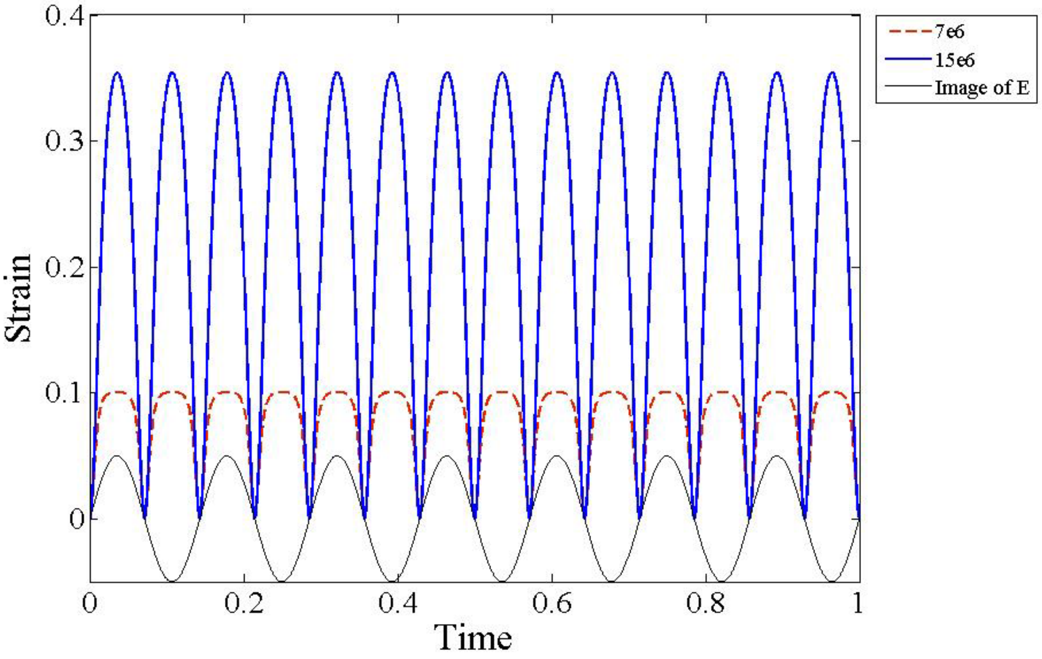

Figure 3.3 Strain waveforms versus time for different values of E_{sat}, 7e6 V/m (dotted line) and 15e6 V/m (continuous line).

b) Losses effect on the strain waveforms

Since it is not easy, due to the non-linearities, to accurately describe the losses effect, I decided to model them in a crude manner by convolving the strain function with a relaxation function. This function is

$$H(t)\exp(-\frac{t}{\gamma}) \qquad (3.4)$$

where γ is a coefficient. It is difficult to separate the electrical losses from the electrostrictive losses **[92]**.

Figure 3.4 shows the strain with and without losses versus time, in continuous line and dotted line, respectively. The electric field (expressed in continuous fine line curve which has arbitrary units) is given to mark the time lag (in phase) between the applied electric field and the resulting strain. The image of the electric field is represented in the figure by a continuous fine line. As it can be seen on the Figure, the lossy curve is lagging behind. As a result, the strain variation is strongly reduced. Similar results have been experimentally obtained, as shown in the overview, Figure 2.11 in Chapter 2.

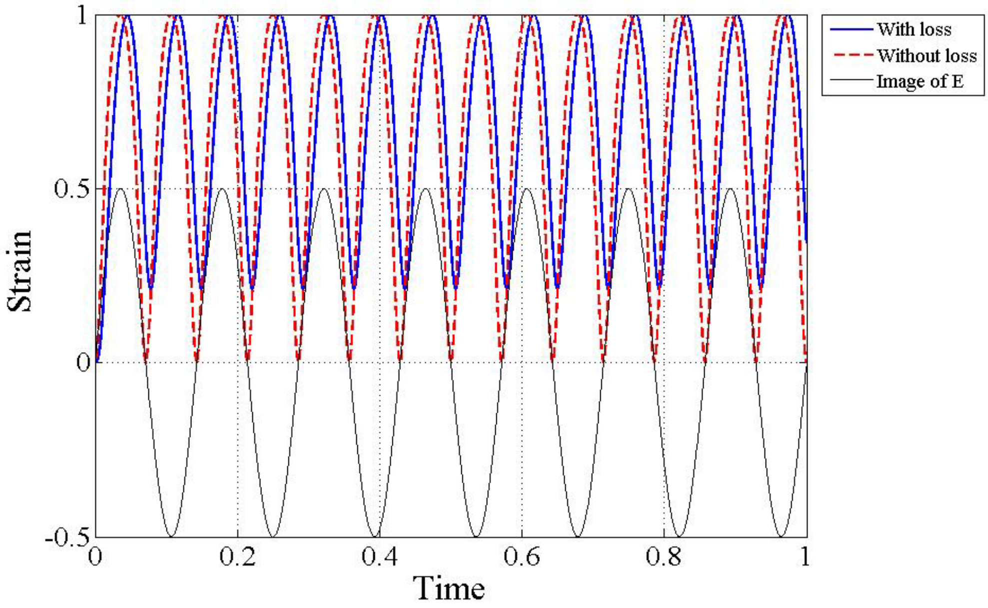

Figure 3.4 Strain with loss (continuous line curve) and without loss (dotted line curve) versus time.

c) Comment on the different equations describing the electrostrictive effect

In the literature, the free stress electrostrictive effect is often described by

$$S(E) = ME^2 \qquad (3.5)$$

where M is another electrostrictive coefficient. Even if this equation described correctly the low field case, it can not describe the full range of electric fields since it leads a quadratic behavior which does not match with the observed strain, see Figure 2.14 in Chapter 2. Since the electric field is known while the polarization is the general case, the equation (3.5) is more convenient but leads to tremendous errors at high field. From a physical point of view, it means that the electric field is the "control parameter", while the polarization is the "ordering parameter". Introducing a linear behavior of the polarization $P(E) \approx \varepsilon E$ then the strain, $S(E) = QP(E)^2$, writes, $S(E) = Q\varepsilon^2 E^2$. Consequently, $M = Q\varepsilon^2$. It should be clearly noted that this relation holds only for low field values and that the errors are quite important for high field values.

To adjust to the experimental values and to describe the concavity change on the strain function, the coefficient *M* must vary with the field which is awkward for a "coefficient". Based on our model, we derived the *M(E)* as following

$$M(E) = \frac{S}{E^2} = \frac{Q}{E^2}(\varepsilon E_{sat} \tanh(\frac{E}{E_{sat}}))^2 \qquad (3.6)$$

which is presented on Figure 3.5. There is a good agreement with experimental values **[93]**.

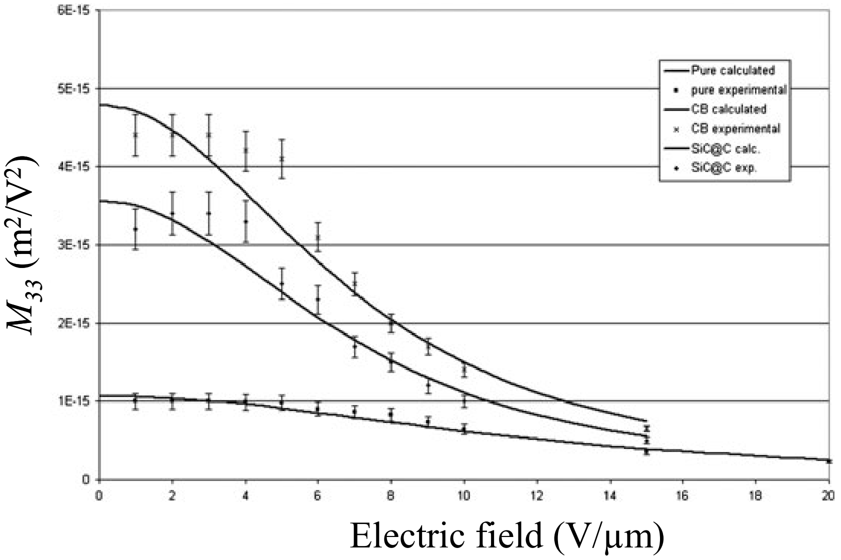

Figure 3.5 The experimental M_{33} measured on a 50-µm-thick polyurethane film, on a 50-µm-thick CB-filled polyurethane film, and on a 50-µm-thick SiC@C nanowire polyurethane film and their counterparts calculated, versus the electrical field. [93]

Figure 3.6 shows the strain versus electric field of various models. Red curve indicates the model result from equation (3.5), $S(E) = ME^2$, blue and green curves indicate the ones from equation (3.2), $S(E) = QP(E)^2$, with E_{sat} = 15e6 and 7e6 V/m, respectively. It is clearly seen that the "*M* formulation" overestimates the electrostrictive strain.

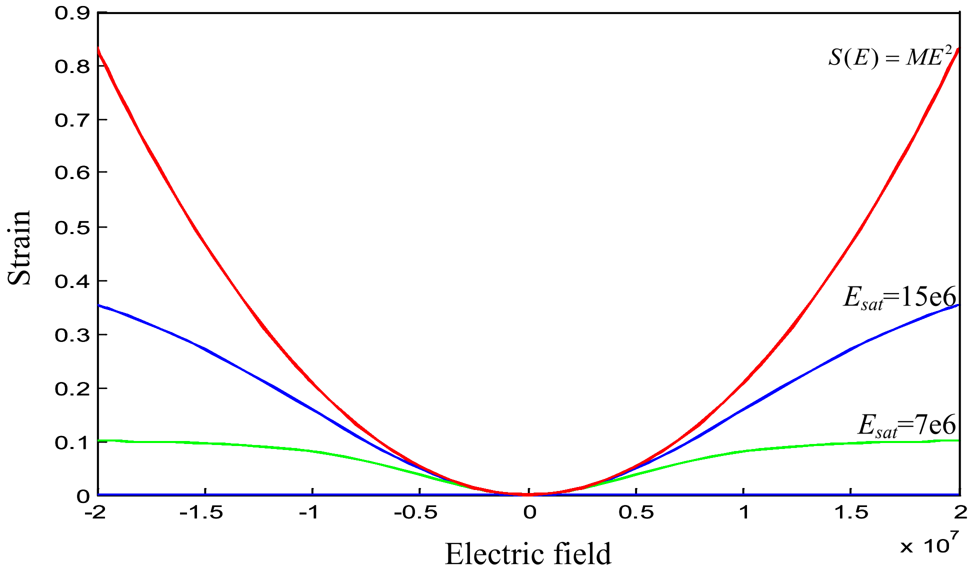

Figure 3.6 Strain versus electric field when using $S(E) = ME^2$ (red curve) and $S(E) = QP(E)^2$ for two different values of E_{sat}: 15e6 V/m (blue curve) and 7e6 V/m (green curve).

d) Non-linear permittivity

Since the polarization saturates when high electric field values, we can guess that the permittivity should decrease with the increasing electric field since it is related to the derivative of the polarization versus the electric field. Differentiating $P(E)$ versus the electric field leads to

$$\frac{dP}{dE} = \varepsilon(1 - \tanh^2(\frac{E}{E_{sat}})) = \text{Non-linear permittivity} \quad (3.7)$$

The drop of the present 'non-linear' permittivity depends on the linear permittivity coefficient and the non-linear coefficient E_{sat}. The current being the time derivative of the above equation, $I = A(dP/dt)$, it vanishes for high electric values. It means that no more current flows into the system. The saturation acts as current limiter. Unfortunately, the material exhibits small electrical losses that make the current cancellation, difficult to observe from an experimental point of view. The experimental current evolution was already shown in Figure 2.15.

Figure 3.7 shows the variation of the non-linear permittivity for two different E_{sat} values, 7e6 and 15e6 V/m. As expected, the permittivity tends to zero for electric field values much higher than the E_{sat} parameters.

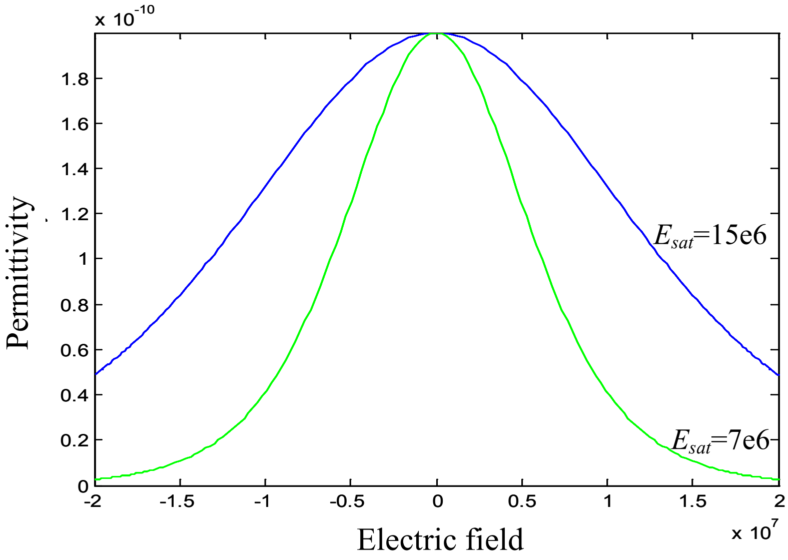

Figure 3.7 Variation of the permittivity for two different values of E_{sat}: 15e6 V/m (blue) and 7e6 V/m (green).

e) Permittivity strain dependence

Based on the above equations, the permittivity can be directly connected to the strain since equation (3.3), $S(E) = QP(E)^2 = Q(\varepsilon E_{sat} \tanh(E/E_{sat}))^2$, then

$$\tanh^2(\frac{E}{E_{sat}})) = \frac{S(E)}{Q(\varepsilon E_{sat})^2} \qquad (3.8)$$

It is easy to show that $S_{\min} = Q(\varepsilon E_{sat})^2$ when the electric field is much larger than the saturation field E_{sat} thus

$$\tanh^2(\frac{E}{E_{sat}}) = \frac{S(E)}{S_{\min}} \qquad (3.9)$$

When equations (3.7) and (3.8) are combined,

$$\frac{dP}{dE} = \varepsilon(1 - \frac{S(E)}{S_{\min}}) = \text{ Non-linear permittivity} \qquad (3.10)$$

This resulting equation illustrates the interconnection between mechanical and electrical permittivity in the electrostrictive materials.

f) Current-strain relation

From the above equation, the current is easily derived. The electrical charge, Q, writes $Q = AP(E)$, where A is the surface of the dielectric. Time differentiating the charge leads to the current so that

$$
\begin{aligned}
I &= A\frac{dP}{dt} = \varepsilon A(1-\tanh^2(\frac{E}{E_{sat}}))\frac{dE}{dt} \\
&= \varepsilon A(1-\frac{S(E)}{S_{\min}})\frac{dE}{dt} \qquad (3.11) \\
&= \frac{\varepsilon A}{L}(1-\frac{S(E)}{S_{\min}})\frac{dV}{dt}
\end{aligned}
$$

where L is the dielectric thickness, C the capacitance and V the voltage across the dielectric. So

$$I = C(1-\frac{S(E)}{S_{\min}})\frac{dV}{dt} \qquad (3.12)$$

Figure 3.8 shows the current density for two different values of the E_{sat} parameter, 7e6 V/m (dotted line) and 15e6 V/m (continuous line). The continuous fine line curve corresponds to the electric field (arbitrary units). Since the polymer film is a capacitance, the current should be a shifted sine function at low electric fields. For higher field, non-linearities occur and the current undergoes a sharpening effect that increases for small E_{sat} values.

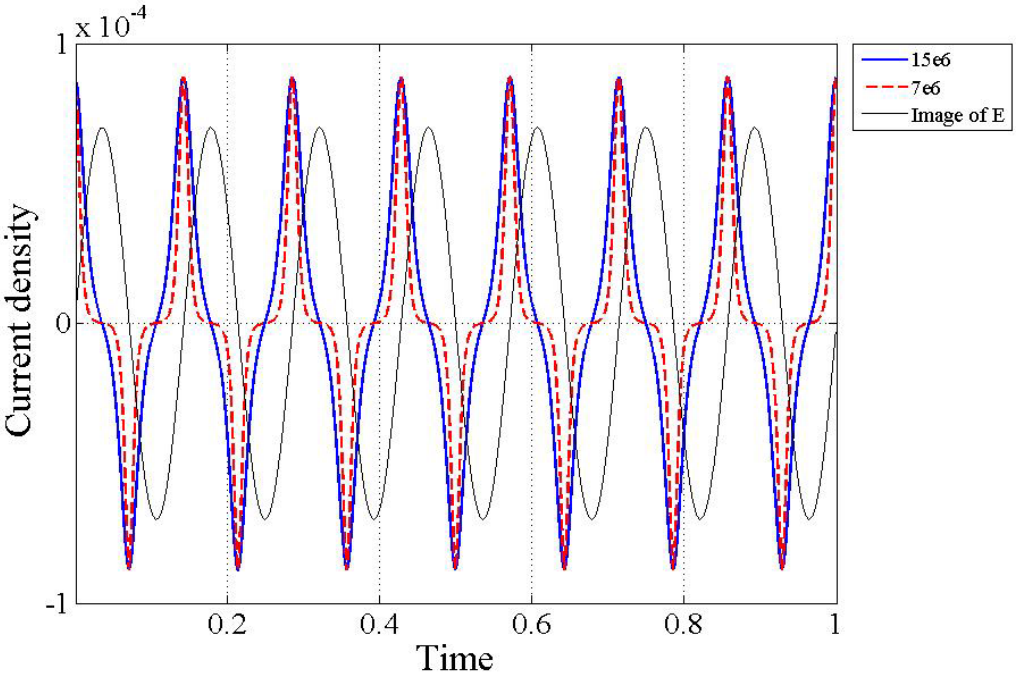

Figure 3.8 Current density for two different values of the E_{sat} parameter, 7e6 V/m (dotted line) and 15e6 V/m (continuous line).

g) Influence on surface expansion on the current

The Poisson ratio coefficient, v, in polymers is assumed to be close to 0.5. It means that there is almost no volume variation, and consequently, a deformation in one direction must lead to a deformation in the perpendicular direction. It means that the surface of the capacitance will change with the electric field. Although we could not clearly see this effect in our experiment, we still tried to relate the effect on the surface expansion on the current.

The polarization does not depend on the surface but only the charge does. The charge writes

$$Q = \int P(E, A)dA \qquad (3.13)$$

and the current becomes

$$I = \frac{dQ}{dt} = \int \frac{dP(E, A)}{dt} dA \qquad (3.14)$$

With an assumption that the polarization does not vary over the surface, *A*, then

$$I = \frac{dQ}{dt} = \frac{dP(E)}{dt} \int dA = A\frac{dP(E)}{dt} \qquad (3.15)$$

For electrostrictive polymers, the strain is such that the surface expansion can not be neglected anymore.

Let us first evaluate the surface expansion. Assuming that the width, l, remains constant, then the surface writes

$$A = (L + dL)l = A_0(1 + S_1(E)) \qquad (3.16)$$

where A_0 is the strain free surface and S_1 is the strain along the surface direction (perpendicular to S_3 which is the strain that I measure). The current writes

$$\begin{aligned} I &= \frac{dQ}{dt} = A_0 \frac{d}{dt}\left[P(E)(1 + \nu S_3(E))\right] \\ &= A_0(\dot{P} + \nu(\dot{P}S_3 + P\dot{S}_3)) \end{aligned} \qquad (3.17)$$

Since $S_3 = -QP^2$ then $\dot{S}_3 = -2QP\dot{P}$ and

$$\begin{aligned} I &= A_0(\dot{P} + \nu(\dot{P}S_3 + P\dot{S}_3) \\ &= A_0(\dot{P} - \nu(QP^2\dot{P} + 2QP^2\dot{P})) \\ &= A_0(\dot{P} - 3\nu QP^2\dot{P}) \\ &= A_0\dot{P}(1 - 3\nu QP^2)A_0\dot{P}(1 - 3\nu QP^2) \\ &= A_0\dot{P}(1 + 3\nu S) = I_0(1 + 3\nu S) \end{aligned} \qquad (3.18)$$

where I_0 is the current for the free strain case. The added multiplicative term is in the range of 30 %. This term must also generate frequencies three times higher than the fundamental one.

3.3 Effect of thickness in electrostrictive film

a) Experimental observation and the three-layer model with equivalent permittivity

For driving electrostrictive film of different thicknesses at constant electric field, the strain decreases or increases with the thickness although the driving electric field has not changed. The phenomenon has been observed by several authors but never received a satisfactory explanation. We have tried a new approach based on the introduction of a permittivity gradient along the film thickness. This new approach makes the assumption that a permittivity gradient is created during polymer processing. That might be due to the temperature on the polymer film surfaces that is different from the inner layer during the cooling and the curing thus generating skin effects. The thermal gradient may structure the material in different layers.

To take this effect into account, we developed a three-layer model with equivalent permittivity that corresponds to a discrete gradient of the permittivity, depicted in Figure 3.9.

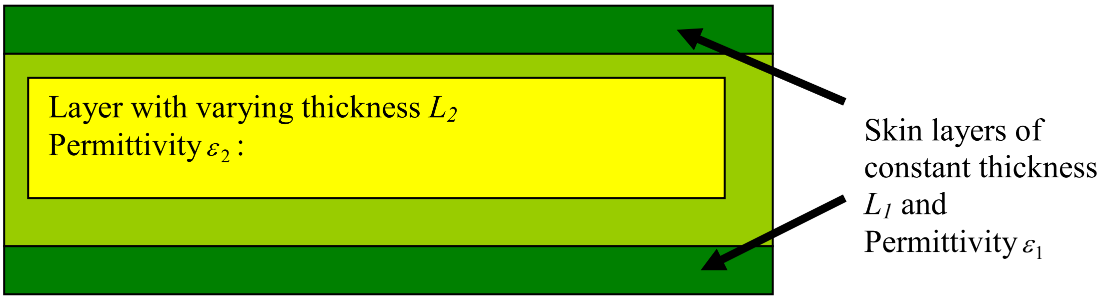

Figure 3.9 Schematic of three-layer model with equivalent permittivity.

At the beginning we assume that the polarization of a single layer system was given by equation (3.1), $P(E) = \varepsilon E_{sat} \tanh(E / E_{sat})$, where ε is the permittivity at low electric field. We can derive a similar approach for the three-layer case by replacing the permittivity, ε, by the equivalent permittivity, ε_{eq}, of the three-layer system then the polarization writes

$$P(E) = \varepsilon_{eq} E_{sat} \tanh(\frac{E}{E_{sat}}) \qquad (3.19)$$

and consequently

$$S(E) = Q(\varepsilon_{eq} E_{sat} \tanh(\frac{E}{E_{sat}}))^2 \qquad (3.20)$$

This formula introduces a direct link between the strain and the equivalent permittivity. Since the equivalent permittivity varies with the total thickness of the film, the strain will also vary with the thickness.

The computation of the equivalent permittivity is straightforward and writes

$$\varepsilon_{eq} = \frac{\varepsilon_1 \varepsilon_2}{\varepsilon_1 + (\varepsilon_2 - \varepsilon_1)\frac{2L_1}{L}} \qquad (3.21)$$

where L_1 and L are respectively the skin and total film thickness, respectively. ε_1 and ε_2 are respectively the permittivity in the skin and inner layers.

From the previous equation we can deduce that:

1) If $(\varepsilon_2 - \varepsilon_1) > 0$, then ε_{eq} increases with the thickness and, consequently, the strain increases with the thickness. The ε_{eq} converges to ε_2 for large thicknesses.
2) If $(\varepsilon_2 - \varepsilon_1) < 0$, then ε_{eq} decreases with the thickness and, consequently, the strain decreases with the thickness. The ε_{eq} converges to ε_2 for large thicknesses.
3) We conclude that there is a change of strain versus the total thickness when the sign of $(\varepsilon_2 - \varepsilon_1)$ changes.

Permittivity and strain variation versus thickness for $(\varepsilon_2 - \varepsilon_1)$ =10e-11 is shown in Figure 3.10 (a). In this case, the strain and equivalent permittivity increase. Figure 3.10 (b) shows for the case of $(\varepsilon_2 - \varepsilon_1)$ =-3e-11. In this case, both of them decrease.

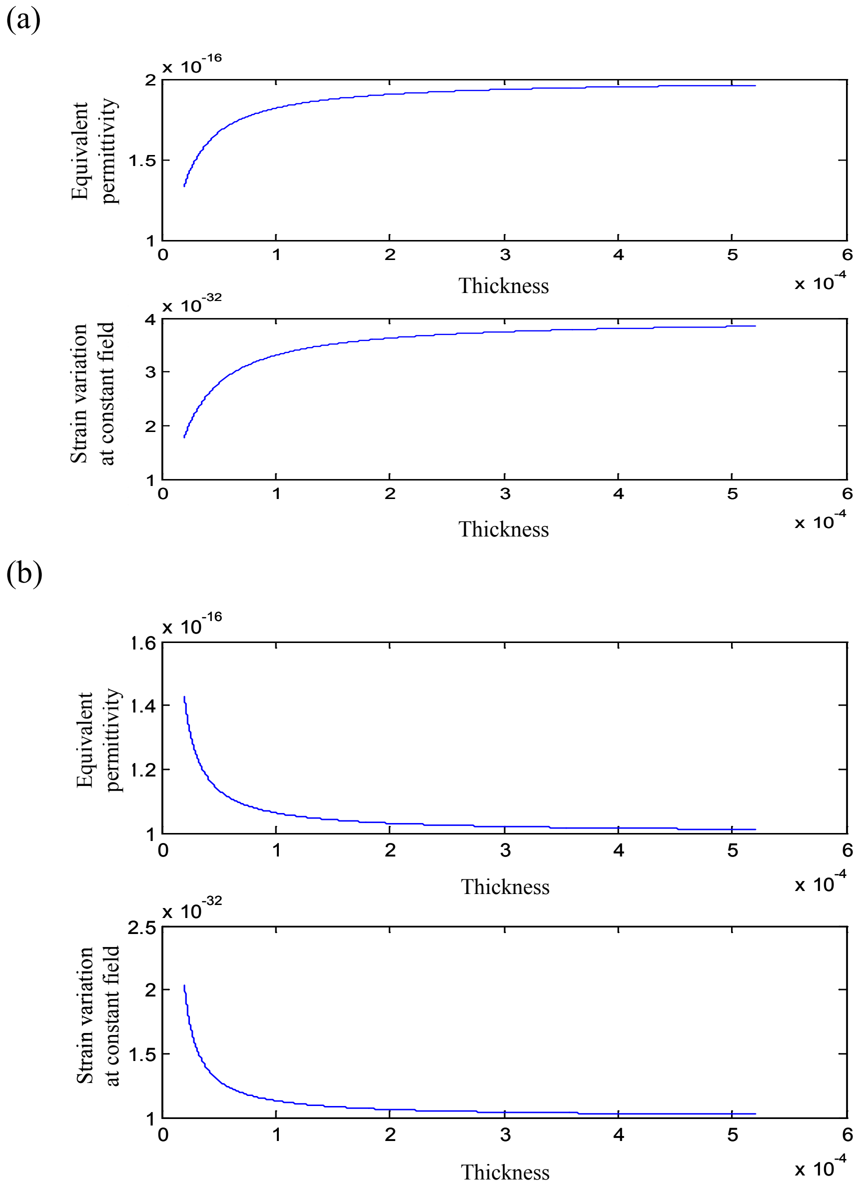

Figure 3.10 Permittivity and strain variation versus thickness (a) for $(\varepsilon_2 - \varepsilon_1)$=10e-11 and (b) for $(\varepsilon_2 - \varepsilon_1)$=-3e-11.

b) Strain curves crossing interpretation

< Saturation electric field value significance and its evaluation >

We have seen previously that the electrostrictive strain is controlled by two parameters: the equivalent permittivity and the saturation electric field, E_{sat}. The permittivity at low field is easy to measure but we can not perform a direct measurement to get the E_{sat} value.

To overcome this problem, we can use the properties of the strain function with ε_{eq}, already shown in equation (3.20), $S(E) = Q(\varepsilon_{eq} E_{sat} \tanh(\frac{E}{E_{sat}}))^2$, that is good representations of the real curves.

The strain curves undergo a change of concavity when passing from positive to negative concavity. That occurs at electric field E_{con} where the second strain derivative vanishes. An easy computation relates the E_{con} value of the E_{sat} value. This relation writes

$$E_{con}=0.6585\ E_{sat} \qquad (3.22)$$

and provides a way to get E_{sat} values. When E_{con} is reduced, the saturation occurs for lower E_{sat} value, as shown in Figure 3.11.

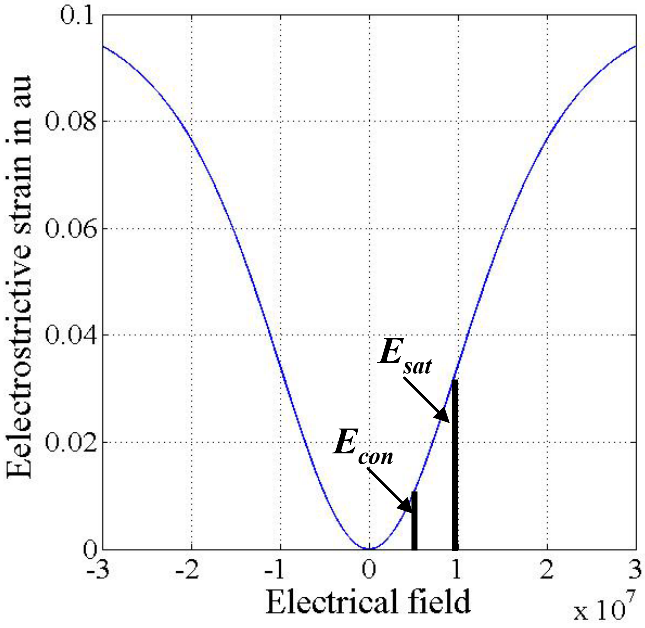

Figure 3.11 Strain curves versus electric field with indications of E_{con} and E_{sat} values.

< Crossing conditions >

Strain curves from different thickness can cross in the strain versus electric field diagram. We now discuss the conditions for the crossing occurrence in terms of E_{sat} and permittivity value.

The slope of the strain around the zero field value is $2\varepsilon^2$ where ε can either be the permittivity of a single layer system or the equivalent permittivity for a three-layer system. To get a crossing between strain curves 1 and 2 as respectively shown continuous line and continuous bold line in Figure 3.12, the permittivity of curve 2 around the zero fields should be higher than curve 1. From a practical point of view, we expect strain 2 to be higher than strain 1 but it is not since it saturates faster.

The strain amplitude for large electric field is $S_{\max 1} = Q(\varepsilon_{eq1}E_{sat1})^2$ and $S_{\max 2} = Q(\varepsilon_{eq2}E_{sat2})^2$. Let's assume that the ratio between $\alpha = \frac{S_{\max 1}}{S_{\max 2}} = \frac{Q(\varepsilon_{eq1}E_{sat1})^2}{Q(\varepsilon_{eq2}E_{sat2})^2}$ then

$$E_{sat2} = \frac{\varepsilon_{eq1}E_{sat1}}{\sqrt{\alpha}\varepsilon_{eq2}} \qquad (3.23)$$

Since $\varepsilon_{eq2} \geq \varepsilon_{eq1}$ and $\alpha \geq 1$, it means that E_{sat2} is always less than E_{sat1}. Consequently the saturation effect occurs for lower electric field values.

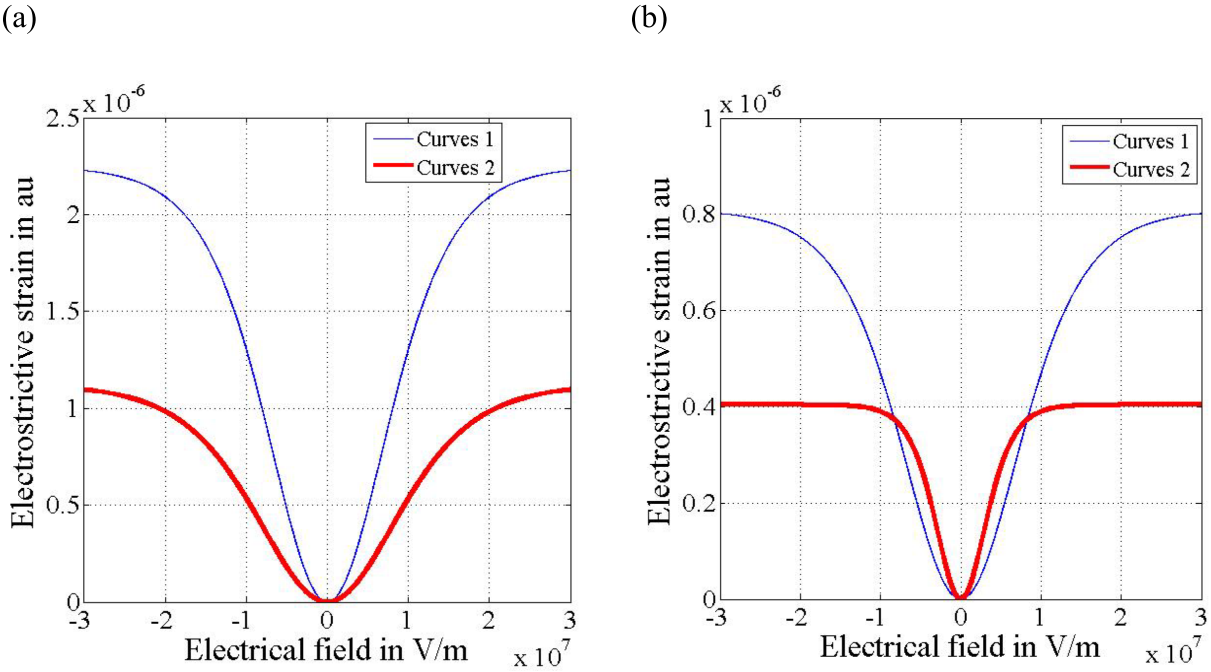

Figure 3.12 (a) Non crossing and (b) crossing strain curves.

If $\varepsilon_{eq2} \leq \varepsilon_{eq1}$, E_{sat2} is less than E_{sat1} if $\frac{\varepsilon_{eq1}}{\sqrt{\alpha}\varepsilon_{eq2}} \leq 1$ and bigger if $\frac{\varepsilon_{eq1}}{\sqrt{\alpha}\varepsilon_{eq2}} \geq 1$. In this case, the strain curve 2 (continuous bold line) remains lower than curve 1 (continuous line) all over the electric field range and never crosses the strain curve 1, as shown in Figure 3.12 (a). That seems normal since the permittivity the strain 2 is always lower that the strain 1 one. In this case no crossing will take place as shown in Figure 3.12 (b). The two different behaviors are depicted on the above figures.

To better understand the effect of the saturation field E_{sat} on the strain, the function $(E_{sat}\tanh(E/E_{sat}))^2$ is represented below, in Figure 3.13. For the sake of clearness, the permittivity is kept constant in this case.

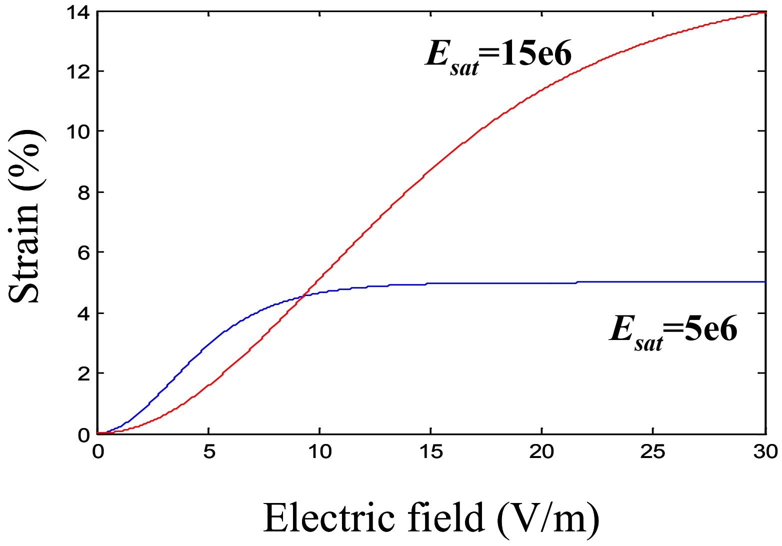

Figure 3.13 Representation of the function $(E_{sat}\tanh(E/E_{sat}))^2$ versus the electric field for two different values of E_{sat}: 15e6 and 7e6 V/m.

This introduction will not be complete without simulated but realistic images of the strain curves for various thicknesses versus the electric field can be obtained as shown in Figure 3.14. Depending on the E_{sat} values and the equivalent permittivity, ε_{eq}, the curves cross or not as discussed in this chapter.

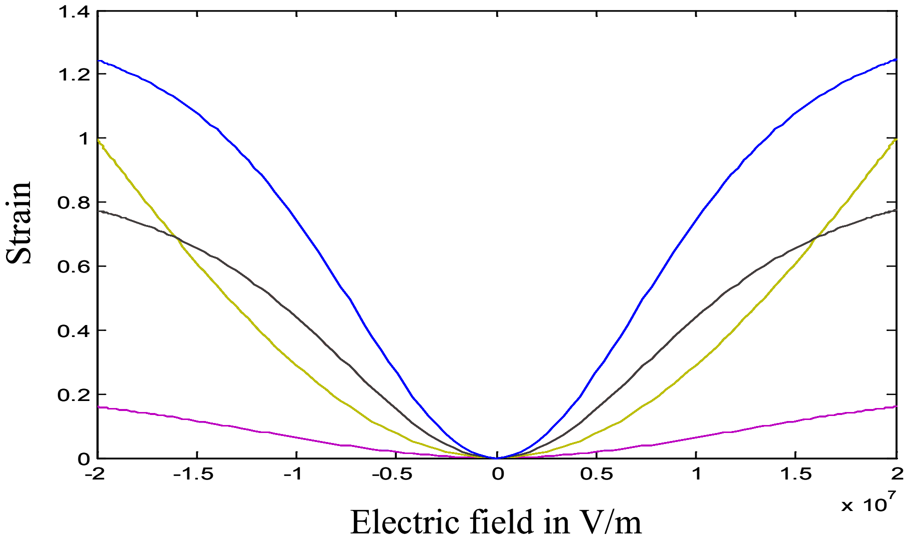

Figure 3.14 Strain curves versus the electric field for various thicknesses in arbitrary units.

3.4 Three-layer model with force equivalent

In the preceding three-layer model with force equivalent, we considered a capacitance at low electric field. Thus the equivalent capacitance can be written as $\frac{1}{C}=\sum_{k=1}^{3}\frac{1}{C_k}$. In the present work, we wanted to check on the influence of the polarization non-linearities on the equivalent capacitance and its consequences on the strain.

Due to the non-linearity of the polarization, the equivalent capacitance cannot be taken as $\frac{1}{C}=\sum_{k=1}^{3}\frac{1}{C_k}$ anymore.

Based on saturated polarization, *P(E)*, we have proposed three-layer model with force equivalent in Figure 3.9. Figure 3.15 depicts with more details with the idea of capacitance. With the equivalent permittivity, the strain curves are already able to be explained. Saturate polarization expressed by equation (3.1), $P(E)=\varepsilon E_{sat}\tanh(E/E_{sat})$, does not show clear link to the thickness, so that our first model concerns the thickness effect on strain is shown here to introduce the reader the direct connection thickness/strain. **[92]**

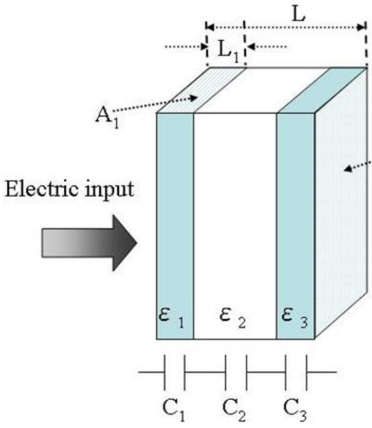

Figure 3.15 Diagram of the three-layer model with force equivalent. [92]

As formally indicated, the polymer is assumed not to be homogeneous but rather heterogeneous along the thickness direction. Electrically, each layer is considered as capacitances connected in parallel. The equivalent capacitance, *C*, cannot be taken as $\frac{1}{C}=\sum_{k=1}^{3}\frac{1}{C_k}$. Let's assume that $C_1=C_3$ and C_2 where the subscripts 1 and 3 correspond to the skin layers. Consequently, the permittivity, ε, of each layers will become $\varepsilon_1=\varepsilon_3$ and ε_2.

The input voltage, *V*, writes $V=V_1+V_2+V_3$. The electric field, applied across the sample thickness, corresponds to the constant field condition, $E=V/L$, where *L* is the sample thickness.

The current, *I*, has to be the same in all layers, thus $I=I_1=I_2=I_3$. *A* is the surface of the sample where the electric field is inputted. Assuming that the surface, *A*, variation remains small enough, the current can be written

$$I_n=\frac{\partial Q_n}{\partial t}=\frac{\partial P_n A}{\partial t} \qquad (3.24)$$

The capacitance of each layer, C_n, can be written with A according to L_n referring to layer thickness,

$$C_n = \frac{\varepsilon_n A}{L_n} \qquad (3.25)$$

With the following substitution,

$$G_n = C_n(1 - \tanh^2\left(\frac{E}{E_{sat}}\right)) \qquad (3.26)$$

the current in each layer, I_n, becomes

$$I_n = AG_n \frac{\partial V_n}{\partial t} \qquad (3.27)$$

Introducing this expression in the voltage equation leads to

$$\begin{aligned} \frac{\partial V}{\partial t} &= \frac{\partial V_1}{\partial t} + \frac{\partial V_2}{\partial t} + \frac{\partial V_3}{\partial t} \\ &= I(\frac{1}{AG_1} + \frac{1}{AG_2} + \frac{1}{AG_3}) \end{aligned} \qquad (3.28)$$

The voltage in each layer can be derived directly with

$$\frac{\partial V_n}{\partial t} = \frac{1}{AG_n(\frac{1}{AG_1} + \frac{1}{AG_2} + \frac{1}{AG_3})} \frac{\partial V}{\partial t} \qquad (3.29)$$

Since the different layers have varying characteristics, the applied voltage will generate different forces in the outer and inner layers. If we assume that no flexion takes place, then the displacements in each layer has to be identical in the 1-direction. Starting from the electrostriction equation of the first layer, $\tau_1 = c_1 s_1 + \alpha_{13} P_3^2$, the integration over the surface leads to the force of the first layer, F_1.

$$\begin{aligned} F_1 = \tau_1 A &= \frac{c_1 A_1}{L_1} u_1 + \alpha_{13} P_3^2 A \\ &= k_1 u_1 + \alpha_{13} P_3^2 A \end{aligned} \qquad (3.30)$$

Here, $k_1 = c_1 A_1 / L_1$ where u_1 is the deformation, c_1 is the Young modulus both in the first layer, and A_1 is the side surface of the first layer. The forces of the second and the third layers are obtained in the same way. Since all layers are attached together, the sum of the force in 1-direction of each layer must be zero, thus $F_2 = F_1 + F_3$. It leads

$$\begin{aligned} \sum k_n u_n + \alpha P_n^2 A_n = 0 \\ u \sum k_n + \alpha P_n^2 A_n = 0 \end{aligned} \qquad (3.31)$$

The total deformation in 1-direction, u, is then given as the function of thickness by;

$$u = \frac{-\sum \alpha_{13} P_n^2 A_n}{\sum k_n} = \frac{\alpha_{13} P_3^2 A_1 + \alpha_{21} P_3^2 A_2 + \alpha_{32} P_3^2 A_2}{\sum k_n} \qquad (3.32)$$

The strain in 3-direction is obtained with the Poisson ratio.

In the present model, four coefficients had to be determined, the permittivity, ε, and E_{sat} value of inner and outer skin layers. However ε and E_{sat} can be linked as mentioned in section 3.3 (b), it is difficult to obtain the inner and outer layers' permittivity separately. The fitting process was in fact a kind of cut and try approach. Even though, three interesting feathers were found based on the variation obtained at fitting.

- Inner layer's permittivity is assumed to be bigger than that of outer layer for my CB/PU composite and pure PU films.
- The permittivity difference between inner and skin layers is bigger in CB/PU composite films than in pure PU films.
- Almost all electric fields are concentrated in skin layers.

Figure 3.16 show the example of strain versus electric field with the variation of thickness in μm written in numbers in figure **[92]**. The outer and inner permittivity was given 2.5e-11 and 9e-11, respectively.

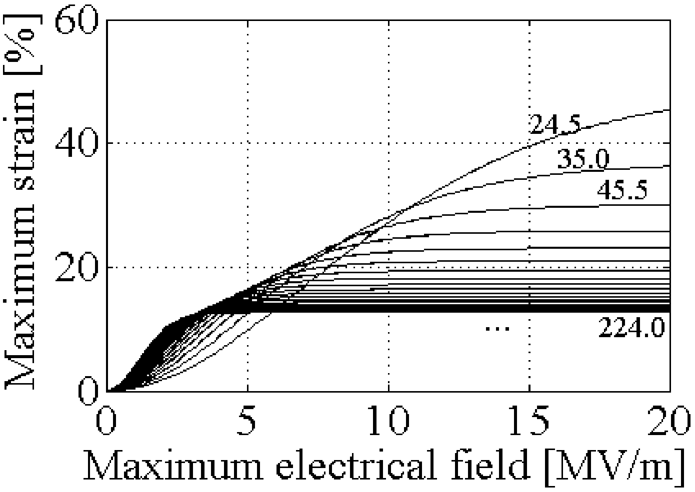

Figure 3.16 The strain with variation of thickness versus the electric field by three-layer model with force equivalent. [92]

Giving the same permittivity and E_{sat} value for inner and outer skin layers of layer model, one layer model was also effectuated considering the case if the material is completely homogeneous. The one-layer model would not give any thickness dependence in strain whereas the three-layer model with force equivalent, as shown in Figure 3.17, shows a good fit with experimental data **[92]**.

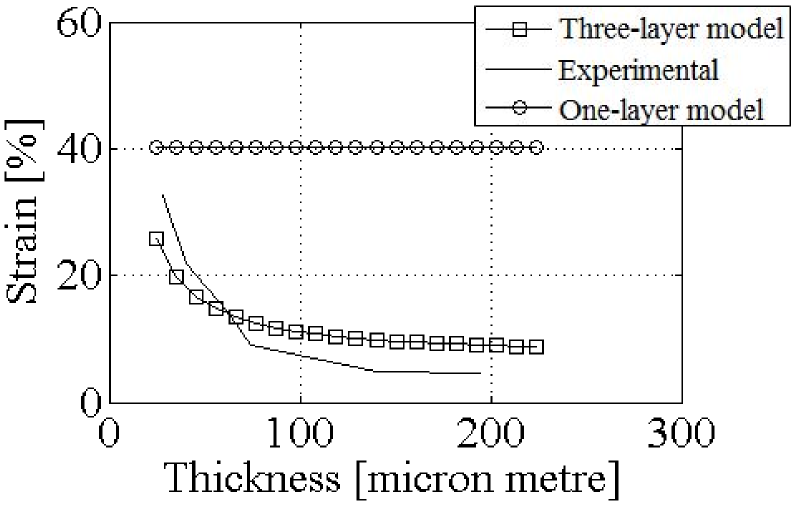

Figure 3.17 Strain versus thickness by three-layer and one-layer model with force equivalent. [92]

Many simulation results with the present three-layer with force equivalent model will be compared with experimental data in the following chapter; Chapter 4.

3.5 Non-linear resistance

As explained in the section 3.1 (f) and as shown in Figure 3.8, it is assumed that the current has a non-linearity in high electric field. In the Figure 3.15, the film was considered as capacitances in parallel. To take into account the electrical losses, a resistance is added parallel to these capacitances. The current, I, generated by induced electric field, can be separated into two parts: a capacitive part, I_C, which relates to the polarization, P, so that $I_C = A\dot{P}$, where A is the surface where the electric field is applied, and a resistive part, I_R, which corresponds to the energy losses. The resistance, R, can be related to the conductivity, σ, by $R=L/(A*\sigma)$, where L is the thickness. Here, σ is considered to have an ohmic behavior for a low electric field, but can be non-linear for higher values. To take that point into account, I introduced a non-linearity on the conductivity and it now writes $\sigma = \sigma_0 + \alpha V^2$. The total current can be calculated as follows **[94]**,

$$I_t = I_C + I_R = A\dot{P} + \frac{V}{R(V)} = A\frac{dP}{dt} + \frac{V}{R_0}(1 + \frac{\alpha}{\sigma_0}V^2) \tag{3.33}$$

The resistive current, I_R, must be converted to the energy loss. The compressive strain, S, is derived from only the capacitive current, I_C. From the fact that the current form is squared in low electric field values, the resistance is assumed to be high in front of electrical tension in such regime. Then, the resistance drop occurs with increasing field. Peaks increases in phase of electric field peaks. The Figure 3.18 shows the simulation result at (a) 5 and (b) 20 MV/m. They correspond to the experimental results shown in Figure 2.15 (b) and (c) in Chapter 2.

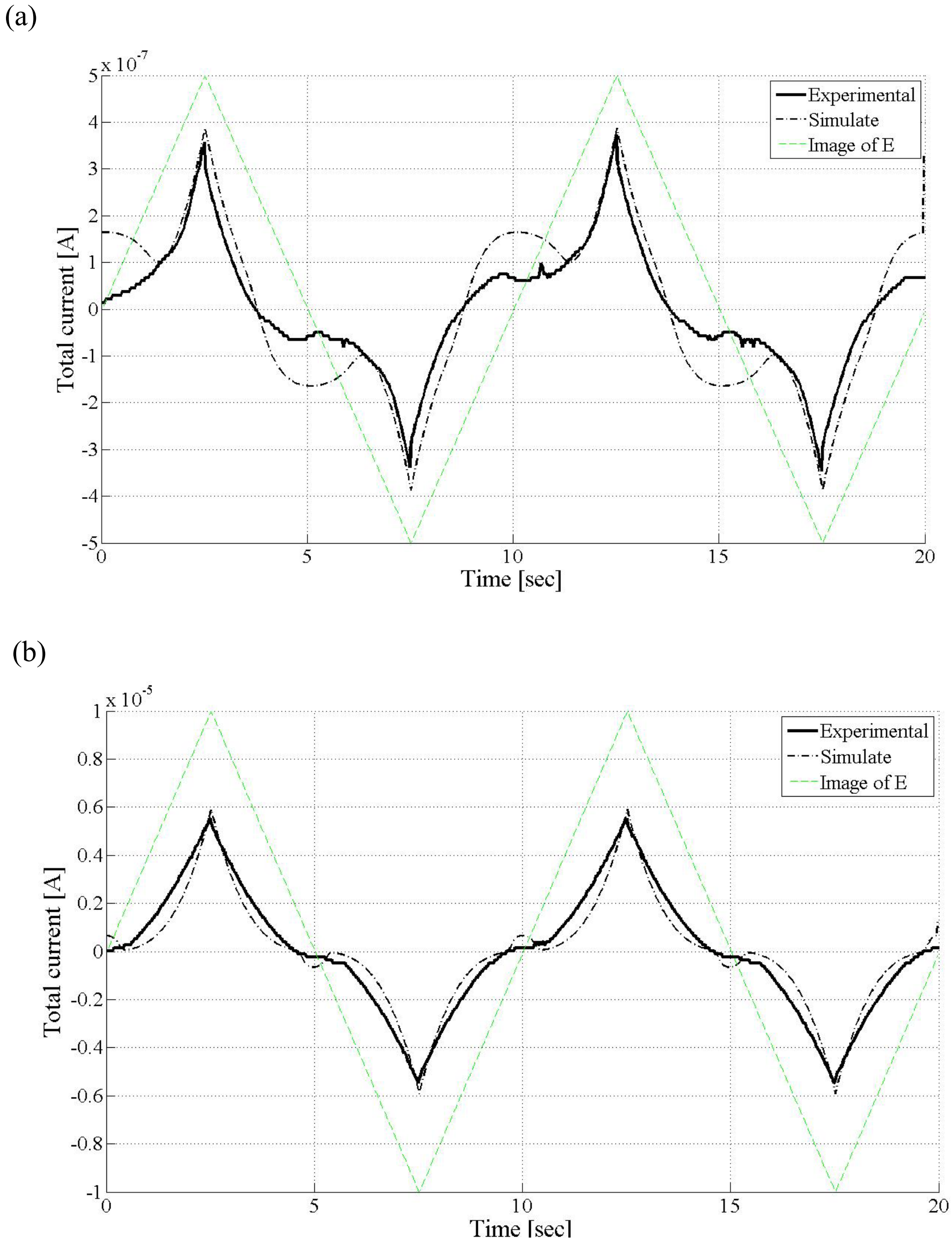

Figure 3.18 Current variation simulation with a non-linear resistance (a) at 5 MV/m, (b) at 20 MV/m.

The confirmation is tried by simulation with a linear resistance. Result is shown in Figure 3.19. As clearly seen, the peak top values of 5 and 20 MV/m stay in the same range of amplitude which is opposed to the experimental fact.

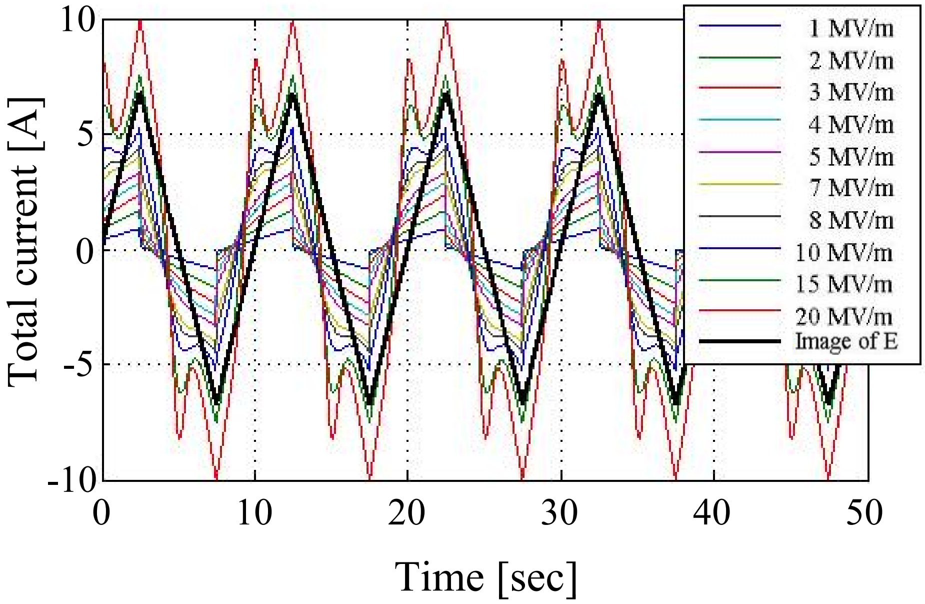

Figure 3.19 Current variation simulation with a linear resistance.

Chapter 4

Part 1: Polyurethane films

Part 2: Composites films

Part *1*: Polyurethane films

4.1 Introduction

Polyurethane (PU) is one of the most versatile materials in the world today. Their many uses range from flexible foam in upholstered furniture, to rigid foam as insulation in walls, roofs and appliances to thermoplastic pure PU used in medical devices and footwear, to coatings, adhesives, sealants and elastomers used on floors and automotive interiors **[95]**. The reasons for the choice in pure PU were already well described in chapter 2.

Over the last two decades, the field of electrically controllable polymer actuators has developed significantly because their performances are comparable to those of natural muscles. Pure PU elastomers are one of the most important class of polymers due to some remarkable electromechanical characteristics such as large electric field induced strain, high specific energy and fast speed of response **[53, 96-99]**. This makes the material very attractive for many electromechanical applications. Many electroactive strain properties of the PU were investigated but the fundamental mechanisms which are responsible for the electrostriction have not been yet well understood **[100]**.

The present part 1 of chapter 4 is dealing with the electromechanical properties of a synthesized pure PU and their dependence on the polymer film thickness.

4.2 Background of PU film thickness dependence

They are numerous researchers on PU films with the views as electroactive strain materials **[53, 100-102]**. However, only few reports are dealing with the influence of the thickness on the electroactive strain of the elastomers.

Su et al reported that the alternating electric field induced strain in unelectroded commercial PU films are dependent on the polymer film thickness **[53]**. As shown in Figure 4.1 (a) the strain of a 0.1 mm thin film is much higher than that in a 2 mm thick sample under electric field between -7 and 7 MV/m. The strain-field relationship in both samples follows perfectly $S=ME^2$, where M is the electrical-field-related-electrostriction coefficient of the material. Figure 4.1 (b) summarizes this thickness dependence behavior. Clearly seen in the figure, the strain level of the material reported is higher for thin pure PU films.

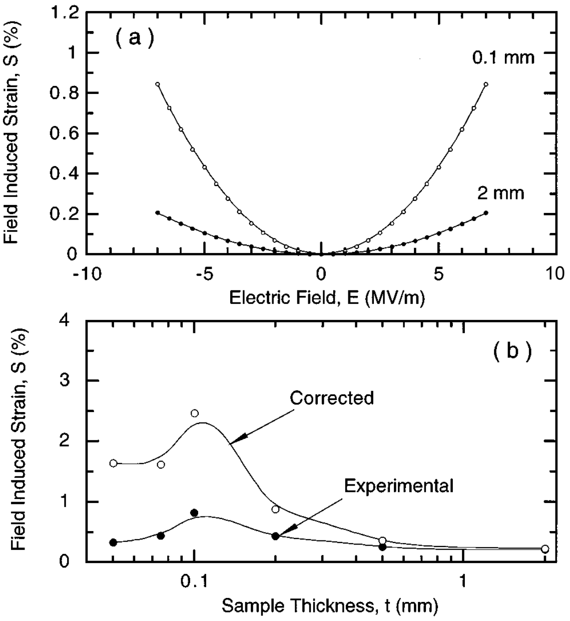

Figure 4.1 (a) Comparison of the strain response, measured at 2 Hz, from a 0.1 mm thick and 2 mm PU samples (Dow 2103-80AE). (b) The thickness dependence of the strain response in PU elastomers (measured at 2 Hz). The black dots are the measured data and the open circles are those after the correction for the gold electrode mechanical clamping effect. Solid lines are drawn to guide the eyes. [53]

Figure 4.2 depicts the strain versus electric field for 0.1 mm and 2 mm thick sample and for different frequencies ranging from 2 Hz to 1 kHz. **[53]**

As a result, the electroactive strain of 0.1 mm by thin film is influenced by the frequency slits stronger than that by 2 mm thick sample. They suggests that the electroactive strain is enhanced by the thickness effect which might include following mechanisms; charge injection, an interface effect, which results in a nonuniform space-charge distribution and, hence, a nonuniform electric field distribution across the sample thickness.

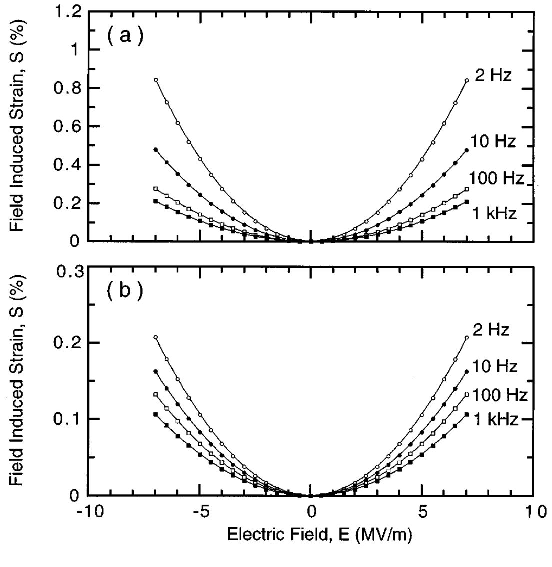

Figure 4.2 Frequency dispersion of the strain response of (a) a 0.1 mm thick sample, and (b) a 2 mm thick sample, respectively. [53]

The field induced strain by a unit external electric field increases while the film thickness decreases. Su et al reported that some nonuniform field distribution in a sample will increase the strain response. They said that the most probable cause for such a thickness dependence behavior is the existence of a surface region and an interior region, which have different electric field strength in a sample, and could be a result of charge injection and/or a nonuniform distribution of the material properties, as schematically drawn in Figure 4.3 **[98]**. They guess this schema but it was only a proposition and there were no discussion in 1997.

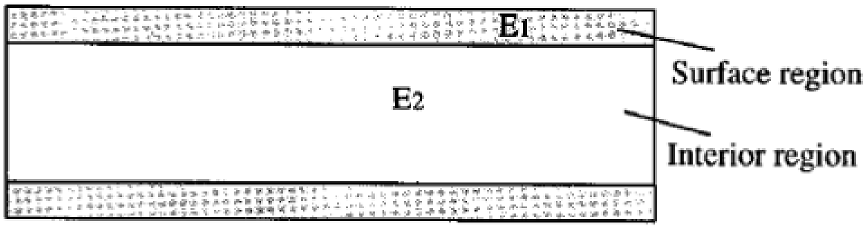

Figure 4.3 Schematically drawing of a polyurethane sample showing the surface region (hatched regions) and interior region. The electric fields E_1 and E_2 in the two regions may not be the same. [98]

Beside, they reported that the x-ray scattering result, shown in Figure 4.4, reveals that both the hard segment and soft segment are in the amorphous phase and there is no detectable crystalline phase in the material within the experimental solution. The PU used in the paper is produced by Deerfield Urethane, Inc. using Dow polyurethane (Dow 2103-80AE). The thickness of the sample was 2 mm.

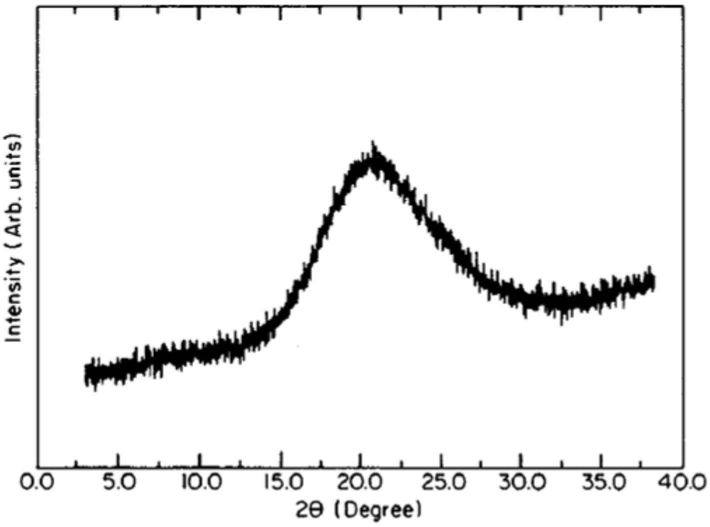

Figure 4.4 X-ray diffraction data of the polyurethane elastomer at room temperature where the broad peak near 20 degree is the atmosphere. No crystalline phase can be detected within the data resolution. [98]

Other researcher team, Diaconu et al, reported that the PU based polymer (poly(caprolactone)diol, 1,4-butane diol and isofuran diisocyanate) shows an remarkable electrostrictive behavior under static electric field and that their electromechanical parameters depend on the film thickness. Note that they mentioned remarkable for strain level around 3 % **[100, 102]**. There is peak of electrostriction at thickness of 50 µm.

Furthermore, they reported that the influence of the lithium ionic additives on the longitudinal electrostriction in the same material films of various thicknesses under static electric field. As a result, the addition of the lithium ions improves the electromechanical parameters of investigated PU films especially for thickness higher than 50 µm. (Figure 4.5) The fact could be attributed to the increased values of pure electrostrictive coefficient of hard domains.

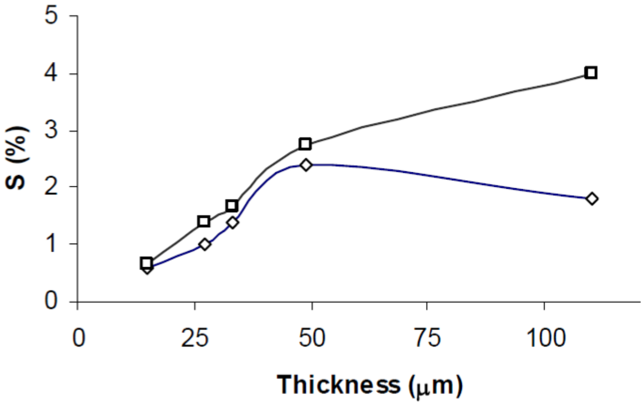

Figure 4.5 Thickness dependence of the induced strain in PU films measured at 4.5 MV/m: □ films contaminated with lithium ions and ◊ original films. [102]

Many electroactive strain properties of the PU were investigated but the fundamental mechanisms which are responsible for the electrostriction have not been yet well understood.

The present part 1 of chapter 4 is dealing with the electromechanical properties of a synthesized pure PU and their dependence on the polymer film thickness.

4.3 Results and discussion

4.3.1 Strain of thin and thick films

a) Changes in the maximum strain against electric field

Figure 4.6 shows the typical electroactive strain for two different thickness samples; (a) 28 µm and (c) 140 µm under 2-cycle of a sawtooth wave electric field with various amplitude. The image of the electric field is represented in the figure by a bold line. The upper limit of the maximum electric field, E_{max}, in the present work was 20 MV/m. Therefore, the range from 10 to 20 MV/m is called high electric field regime and 1 to 5 MV/m is called low electric field regime in the present thesis. For the sake of comparison, Figure 4.6 (b) shows the simulated results for the 24.5 µm by using three-layer method with force equivalent and Figure 4.6 (d) presents that of the 140 µm films. More adaptive parameters need to be found. Nevertheless, one can distinguish the typical behavior of these two samples. This involves:

- ➢ the strain-time curves being triangular in the low electric field regime and the peaks flatten down when the electric field is raised,
- ➢ the strain level becoming decreased when the thickness is increased.

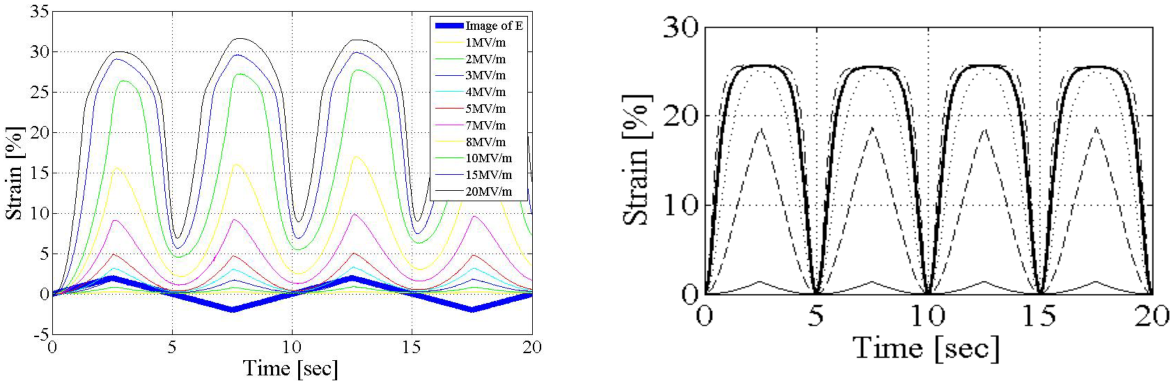

Thin pure PU film (28 µm)

(a) Experimental of thin **(b) Simulation of thin**

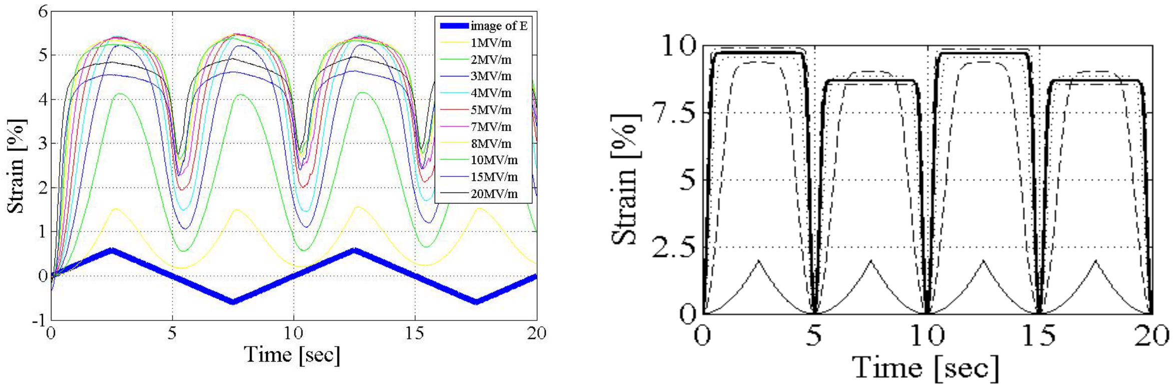

Thick pure PU film (140 µm)

(c) Experimental of thick **(d) Simulation of thick**

Figure 4.6 2-cycle of a sawtooth wave electric field induced strain of pure PU thin and thick films.

When 2-cycle of a sawtooth wave electric field was induced into the pure PU, the compressive strain in 4-semi-triangular shape appeared when the electric field was low as shown in Figure 4.6 (a). The peak tops became less sharp when the electric field was increased.

As we can see in Figure 4.7, in low electric field regime, *S(E)* is quadratic so that sawtooth wave inputs are sharper top angles. In high electric field regime *S(E)* is non-liner and has saturation resulting round shapes. In certain thick cases, a decreased strain could be seen in the high electric field regime see Figure 4.6 (a). The slope is higher with higher electric field amplitude but some peak tops became flat as the electric field increased. The maximum strain in this case was smaller than the one with lower electric field input, as it can be see on Figure 4.6 (c).

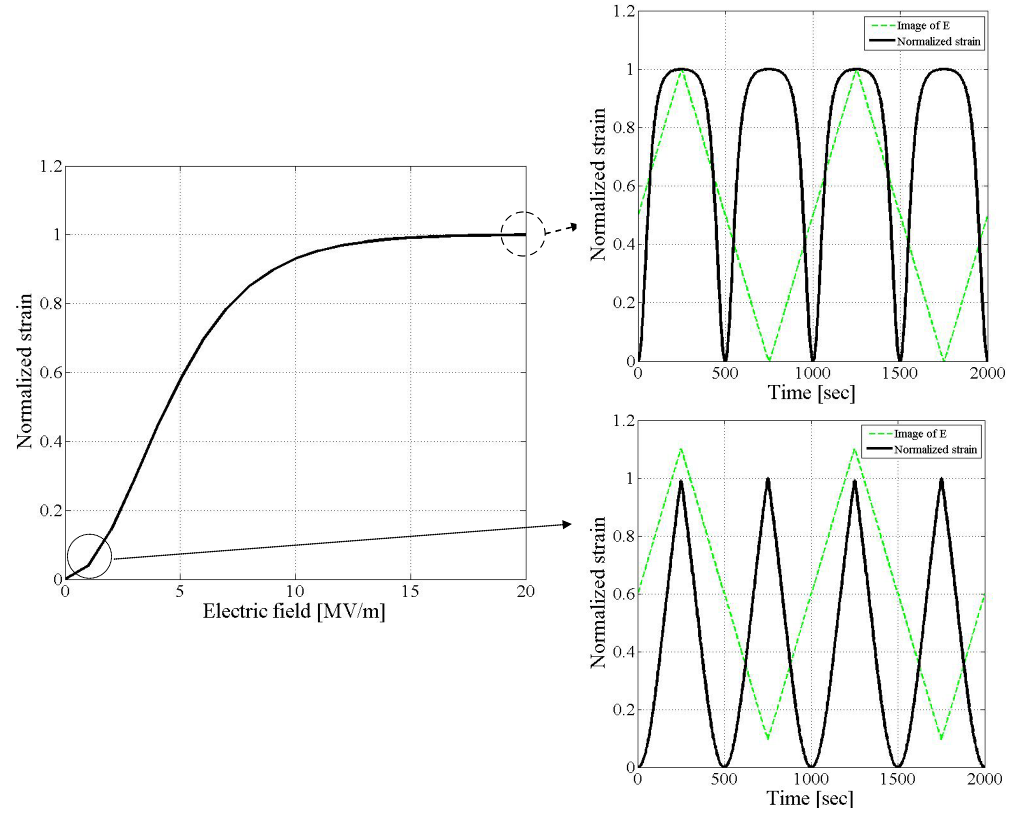

Figure 4.7 Strain forms of low electric regime and high electric regime.

Figure 4.8 shows maximum strain, S_{max}, versus maximum electric field, E_{max}, of two samples in Figure 4.6. The S_{max} was taken at the first peak of sawtooth input whereas E_{max}. The saturation in strain versus electric field on the thick sample is clearly seen.

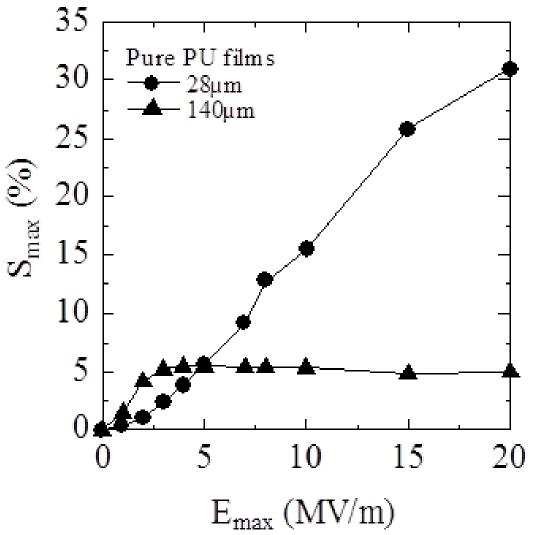

Figure 4.8 Experimental changes in maximum strain versus maximum electric field of pure PU thin and thick films.

Figure 4.9 (a) shows the strain versus the electric field of the thick film in Figure 4.6 (b). Figure 4.9 (b) shows extraction of only 1, 2 and 3 MV/m on only positive electric field side. A residual strain can be observed for a null electric field. The residual strain is related to the electrical and/or mechanical losses. It occurs also for thin film but a less extend. Since the PU is viscoelastic material at room temperature, the residual strain perfectly relaxes finally for thin and thick film when removing the applied electric field. The relaxation was already shown on time signal in Figure 2.12, chapter 2.

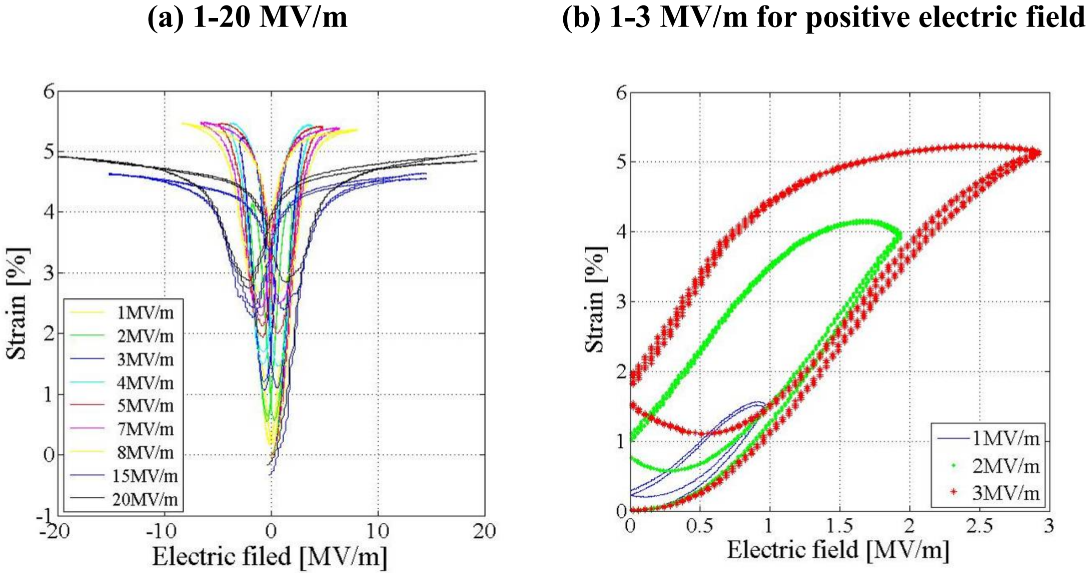
(a) 1-20 MV/m **(b) 1-3 MV/m for positive electric field**

Figure 4.9 Strain versus the electric field of the thick film.

The important thing is that a compressive strain in the thickness direction of up to around 31 % was obtained under moderate electric field < 20 MV/m by pure PU film. Such result can not be found in other researchers' works on pure PU films. Referenced works presented in section 4.2 showed only 0.85 % at 7 MV/m (0.1 mm) and 2.5 % at 4.5 MV/m (50 μm). The second we seem confirmed that our thin sample keeps the slope until higher electric field, 20 MV/m. Two factors are supposed to contribute this fact one is the selection of type of PU. The material was PU, Estane 58888-NAT021, which have higher 46 wt% of hard segments (HS) fraction then usual PU. The second reason is from the thickness of sample. It opposes to the result of Figure 4.1 but we found that thinner sample gives more than 10 MV/m because of *S(E)* saturation of thick sample. As mentioned early the thickness effect is obvious. Consequently, when electric field is 20 MV/m, thinning the films remarkably enhanced the S_{max}. When the electric field was increased, the thick film started showing a sharp increase in strain at a low electric field level. Subsequently, the saturation occurred below 3 MV/m (Figure 4.8). On the other hand, the thin film exhibited a slow raise in strain in the low electric field regime, followed by a slight saturation between 10 and 20 MV/m. Such *S(E)* saturation can be found easily in other researchers' works on polymeric material. The reason has not been well discussed yet.

b) Relationships between maximum strain versus square of the maximum electric field

Figure 4.10 shows the experimental changes in maximum strain, S_{max}, versus square of maximum electric field, E_{max}^2. The linear E_{max}^2- S_{max} relationships are obtained when electric field is low. The slope corresponds to the electrical-field-related-electrostriction coefficient of the material, *M*.

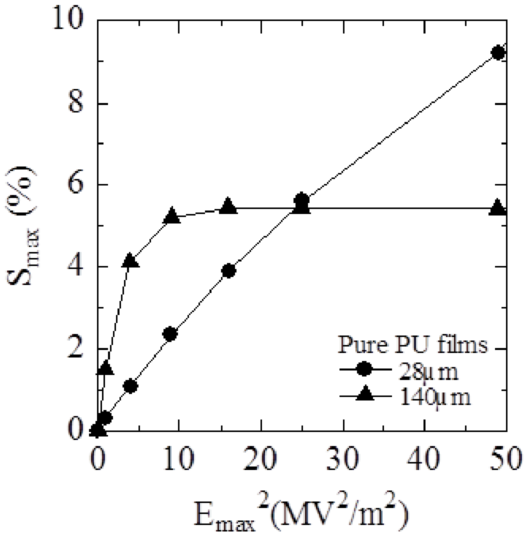

Figure 4.10 Experimental changes in maximum strain versus square of maximum electric field.

When maximum electric field, E_{max}, is low at less than the saturated electric field, S_{max} written by the following equation.

$$S_{max} = ME_{max}^2 \qquad (4.1)$$

The *M* is the important factor of strain. In general, the researchers try to increase *M* to have higher strain. However, the relation holds only for small electric fields. A simpler but more general relation writes $S=QP^2$ with a saturation on polarization for high electric field values.

4.3.2 Thickness dependent electrostriction

a) Thickness dependent strain at 20 MV/m

Figure 4.11 (a) depicts maximum strain, S_{max}, versus maximum electric field, E_{max}, for various thicknesses from 19 to 202 μm of pure PU films. Results of Figure 4.8 are included in Figure 4.11. The used driving electric fields were in a range from 0 to 20 MV/m. The thinner the thickness is, the higher the strain is in the electric field range at 10-20 MV/m. Figure 4.11 (b) shows the simulated results by three-layer model with the equivalent parameter ε_{eq}=8e-11. The values could be improved by further adjusting the parameters.

- *M* depended on the thickness: thicker films have larger *M*. In the high electric field regime until 20 MV/m,
- all samples exhibit *S(E)* saturations. The values of saturation varied as a function of the thickness.
- Smaller the thickness is the saturation starts in the higher electric field regime and the saturated strain values became bigger.

Nevertheless, the three phenomena mentioned above were well reproduced.

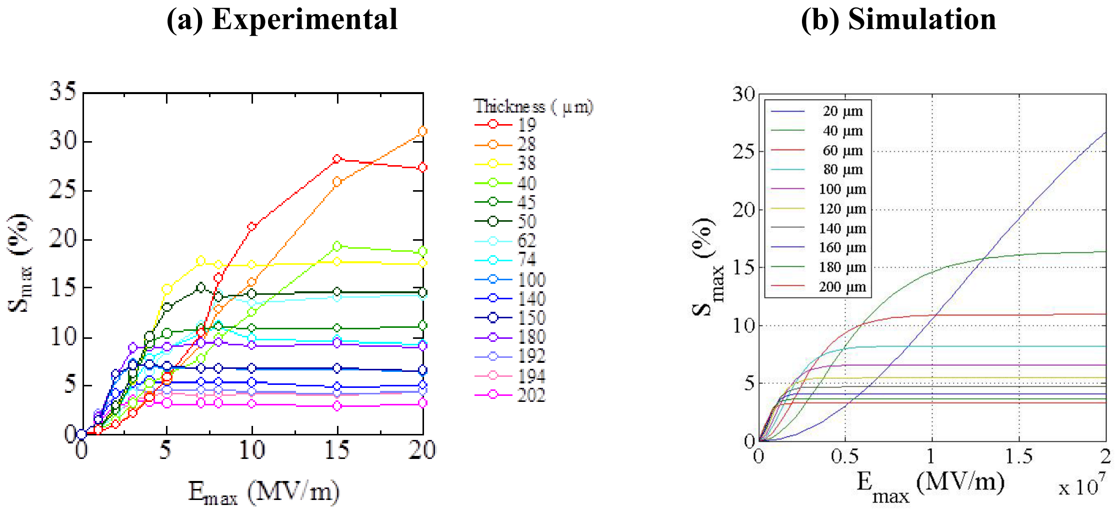
(a) Experimental

(b) Simulation

Figure 4.11 Experimental changes in maximum strain at each thickness for pure PU films against maximum electric field.

Figure 4.12 shows the relationship between thickness and maximum strain, S_{max}, at 5 and 20 MV/m, lead from Figure 4.11. Figure 4.12 (a) shows that the strain values at 5 MV/m are much smaller than that at 20 MV/m for thin films, from 10 to 50 μm. The strain at 5 MV/m is as similar as those at 20 MV/m for thick films, from 50 to 200 μm. Figure 4.12 (b) shows that the simulation results for the same data are put beside for the sake of comparison even it was already shown in Figure 3.17 of Chapter 3 **[93]**.

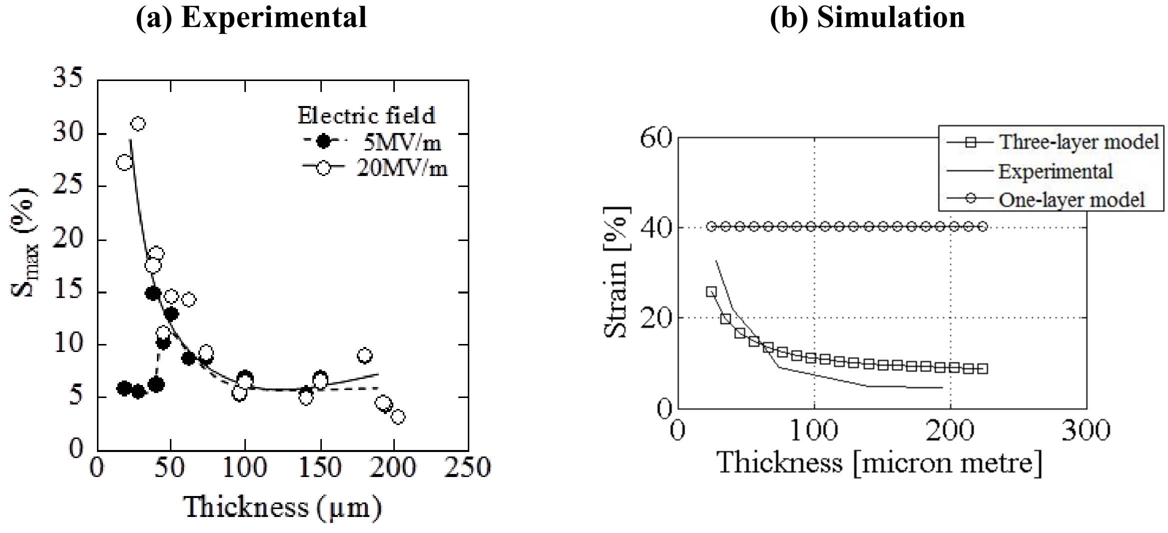
(a) Experimental

(b) Simulation

Figure 4.12 Thickness dependent maximum strain of pure PU films as a function of the thickness at 5 and 20 MV/m, (a) experimental and (b) simulation. [93]

b) Linear logarithmic relationship between thickness and maximum strain at 20 MV/m

Figure 4.13 shows the logarithmic relationship between thickness, *L*, and maximum strain, S_{max}, at 20 MV/m of pure PU films. Thinning the films remarkably enhanced the S_{max} at 20 MV/m. The S_{max} values at 20 MV/m are distributed along slope on the log-log scale from 31 % for 28 μm to 3 % for 200 μm.

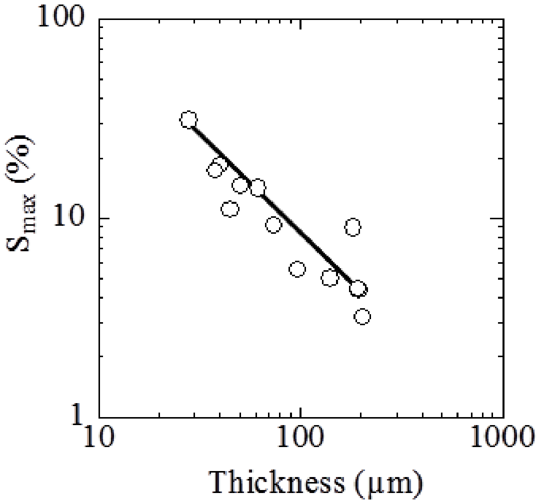

Figure 4.13 Linear logarithmic relationship between thickness of pure PU films and maximum strain (20 MV/m), which is maximum strain at maximum electric field of 20 MV/m.

The relationship between thickness, *L*, and S_{max} at 20 MV/m can be expressed by following equation.

$$S_{max\ 20MV/m} = BL^{A} \qquad (4.2)$$

where the constant *A* is the slope of the relationships between log (*L*) and log (S_{max}), and *B* is S_{max} when the log (*L*) is zero. *B* is obtained, of course, by the extension of approximation carve. It is seen at Figure 4.12 that *A* and *B* are functions of E_{max}. In the condition of pure PU at 20 MV/m, there coefficients are obtained as A= -0.91 and B= 5.42×10^{2}. The discussion will go on with coefficients of composite films in part 2 of chapter 4.

c) Inside conductive mechanism

Interesting is that the three-layer model, introduced in the chapter 3, is not only for reproducing the experimental data. Based on the variations obtained at fitting the above mentored corves, Figure 4.11, we can guess the conductive mechanism inside material as below.

Figure 4.14 (a) shows the electrical tension in material versus time for the three-layer model. The applied electric field always had a 2-cycle sawtooth wave **[93]**. The maximum was fixed at 20 MV/m. That of the inner layer, V_2, is not zero but varied with the thickness. The amplitude was raised when the thickness increased. Even though the input had a 2-cycle triangle shape, V_2 was clearly no longer triangle. Figure 4.14 (b) shows the simulated inside electrical tension, *V*, versus thickness in the case of the 224 μm thick film, using the coefficients obtained at fitting, obtained at reproductions of experimental curves **[93]**. As compared to the homogeneous case, expressed by a dotted line, the result of the three-layer model with force equivalent has a different slope between the outer and inner layers. The inclination differs in three steps from one to the other side of polymer sample. Note that the permittivity of inner layer is taken higher here.

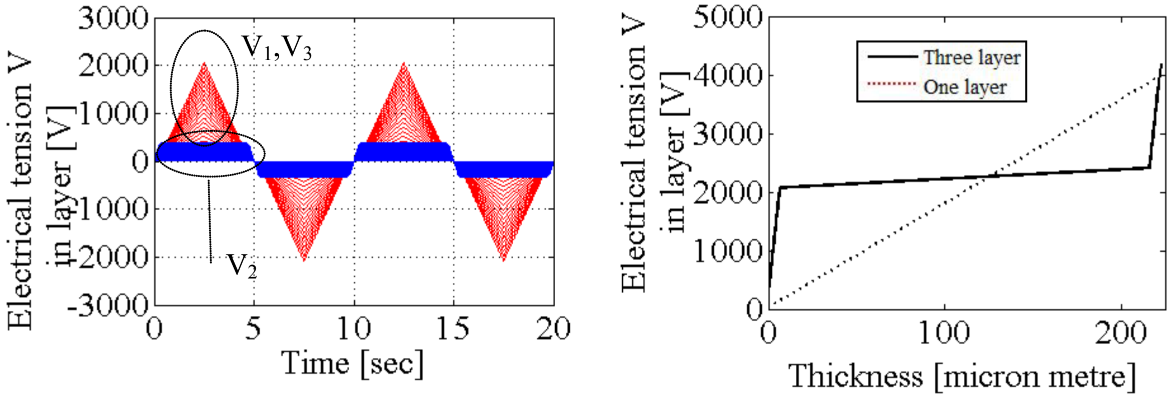
(a) Strain in time domain

(b) Function of the thickness in the case of a 224 µm film at 20 MV/m input

Figure 4.14 Simulated electrical tensions in material. [93]

The electric field, *E*, in the same cases are given in Figures 4.15. The variations in the Figure 4.15 (a) in time domain correspond to the thickness variation between 24.5 to 224 µm. The electric field of the inner layer, E_2, was almost zero for all thicknesses. Instead, the amplitude of that of the outer layers, E_1 and E_3, increased with the thickness of the sample. The triangle shapes became increasingly deformed when the thickness increased. Based on Figure 4.15 (a), the inside electric field for the same film is depicted versus the thickness in Figure 4.15 (b). For the case of a homogeneous material, the one-layer model indicates that the electric field is constant everywhere. In the case of the three-layer model, the electric field is high only in the outer layers and very low within the inner layer. We see well that almost all electric fields are concentrated in skin layers. Its maximum value increased with the sample thickness. This was due to the permittivity differing in the outer and inner layers. As can be seen above, the permittivity ε of the inner layer was taken larger than those of the outer layers, resulting from *S(E)* curves reproduction. If the permittivity of inner layer is decided smaller, strain increases with increase of thickness, which is opposed to the experimental fact.

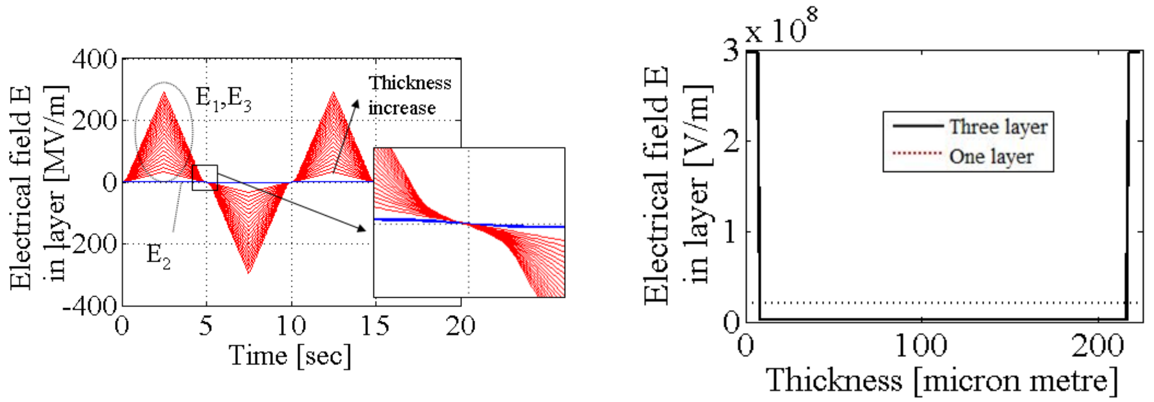
(a) Strain in time domain

(b) Function of the thickness in the case of a 224 µm film at 20 MV/m input

Figure 4.15 Simulated electric fields in material. [93]

We see that the electrical input in the inner layer is almost zero even its permittivity is larger. Consequently, the thicker the material is, the immobile layer thickness increases and it harms total elongation in 1-direction. It corresponds well to the experimental results.

4.3.3 Permittivity

The relative permittivities were measured directly by frequency response analyzer (1255, Solartron) and dielectric interface (1296, Solartron) with divers film thickness and frequency. Figure 4.16 (a) depicts them versus thickness, and (b) depicts them in terms of frequency. Except for the 0.1 Hz, the permittivity increases with the thickness and decreases with frequency.

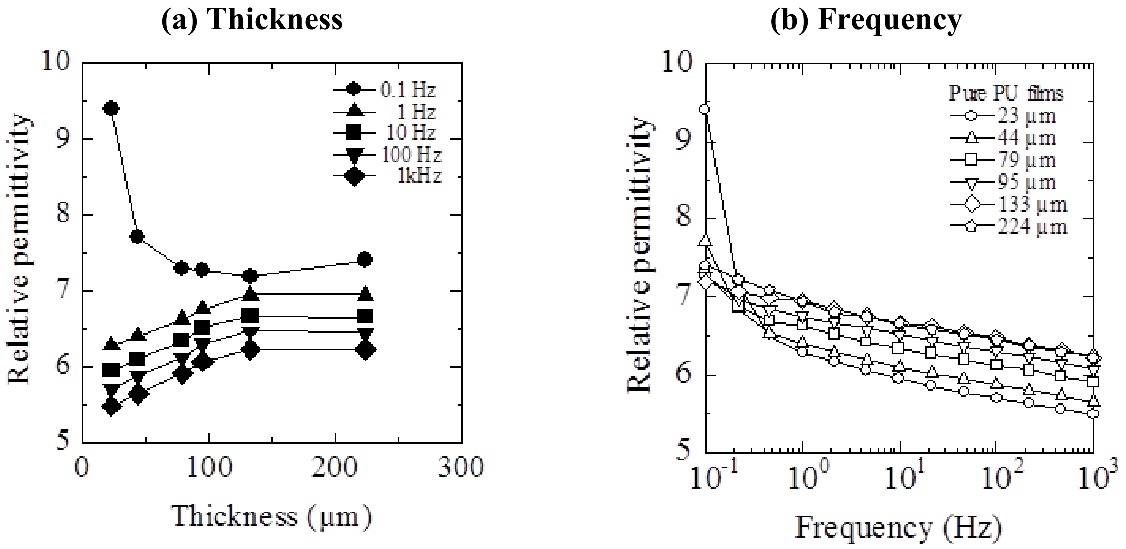
(a) Thickness

(b) Frequency

Figure 4.16 The directly measured permittivity with divers pure PU film thickness and frequency.

Figure 4.17 shows the permittivity obtained from calculation. The curve *S(E)* when electric field, *E*, linearly increased from 0 to 20 MV/m, was employed for the determination of E_{con}, where a second derivative of strain vanishes, of equation (3.22) in chapter 3. All E_{sat}, were confirmed to be less than 20 MV/m, shown in Figure 4.18. As the experimental data, I found the increasing permittivity trend is the one that I had expected.

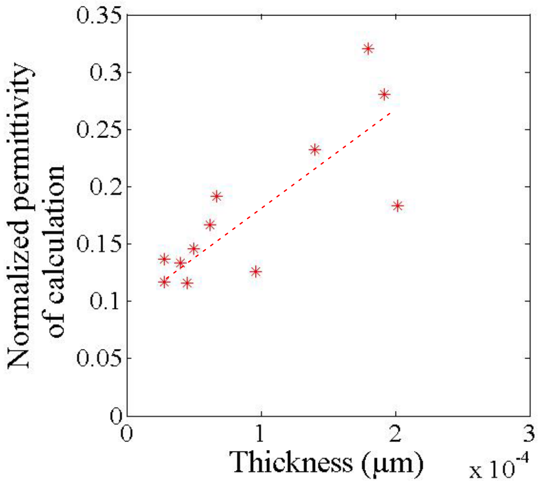

Figure 4.17 Permittivity obtained from calculation versus thickness.

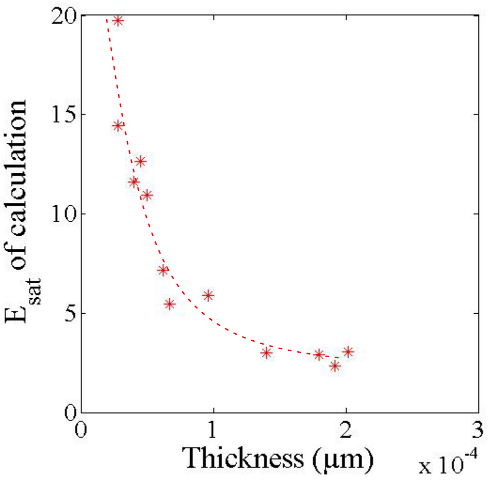

Figure 4.18 Saturation electric field obtained from calculation versus thickness.

4.3.4 Surface crystallization model from glass to crystalline form of hard segments

The results show that the maximum strain, S_{max}, of pure PU films depends on thickness. The thin pure PU film shows high strain at 20 MV/m. Differential Scanning Calorimetry (DSC) analysis and X-ray diffraction (XRD) were used to confirm the internal structures of pure PU films with different thicknesses.

a) Effects of crystallized volume fraction in material

The endothermic heat is usually generated by transformation from crystal to liquid on melting. It corresponds thus to volume fraction of crystalline form in material. Differential Scanning Calorimetry (DSC) analysis was carried out to see the fusion enthalpy value of thin and thick films, 18-22 µm and 126-135 µm, respectively. These selected thicknesses correspond to the ones of Figure 4.8 shown in Figure 4.19.

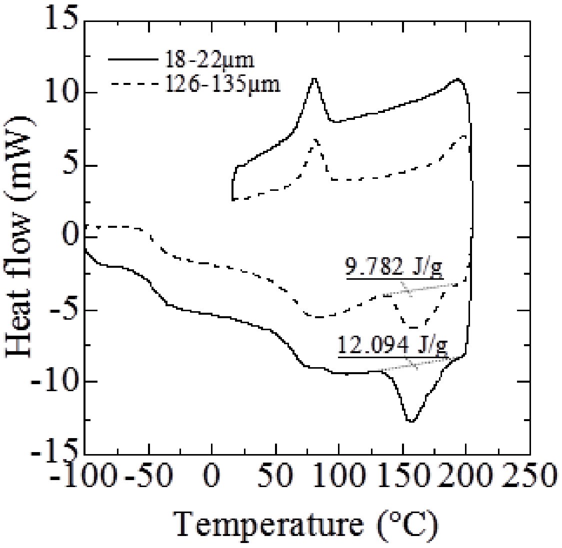

Figure 4.19 DSC analysis of thin (18-22 µm) and thick (126-135 µm) pure PU films.

The thermal analysis was performed by DSC under protective argon atmosphere. The samples (~22 mg) were placed in a closed aluminium pan and were cooled from ambient temperature down to -100 ºC then were heated to 210 ºC at heating rate of 20 ºC/min and finally were cooled again to 25 ºC at cooling rate of 20 ºC/min.

The fusion enthalpy values were obtained 12.094 and 9.782 J/g for thin and thick pure PU films, respectively. That of thin film is 1.24 times higher than that of thick film. Therefore, it is possible that high volume fraction of crystallization contribute to the high electroactive strain of pure PU thin film.

b) Crystal perfection of thin and thick pure PU films

It is possible that the change in electroactive strain strongly corresponds to the periodicity of crystalline form of hard segments as well as its crystallized volume fraction in material. The periodicity was investigated by the width of X-ray diffraction peak.

Crystal structures in thin and thick film were checked by X-ray diffractometer (XRD: D8 ADVANCE, BRUKER). All X-ray diffractions were carried out on universal XRD with copper Kα radiation (λ= 0.15418 nm) and a quartz monochrometer. The operating was performed at 40 kV and 40 mA with an interval of 1 s/step. The step size was chosen 0.02 °. To choose the angular range, an initial scan was necessary with the diffraction angle ranging from 5 to 50 ° for samples.

Figure 4.20 shows the X-ray diffraction peaks of thin and thick pure PU films. The thin film thickness is 19 µm, and the thick one is 140 µm. Most of the sharp peaks are related to thin film, whereas the broad peak is related to the thick film. No sufficient explications are found for the small peaks. Besides, the angle width of thick samples is smaller than the other one. The angle width corresponds to the crystal perfection of crystalline form of hard segments. Therefore, this result gives the conclusion that the thin sample has the more perfect hard segments than the other.

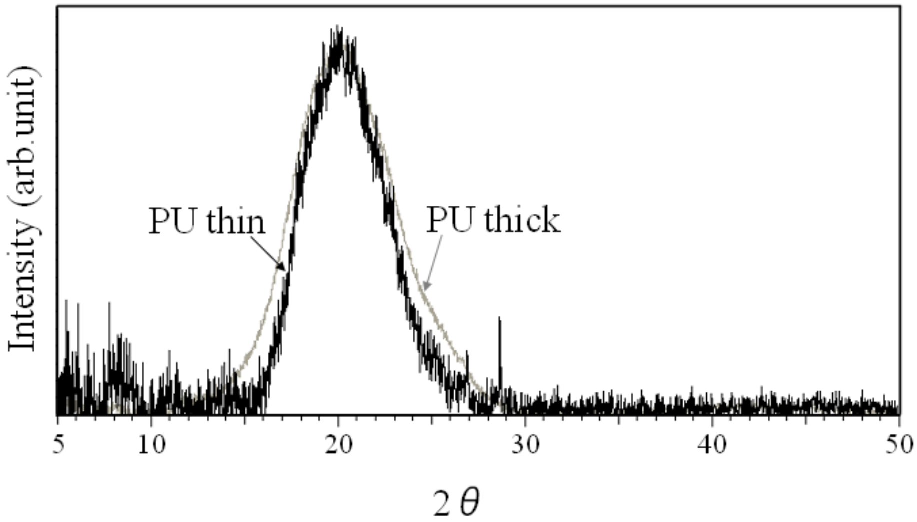

Figure 4.20 X-ray diffraction peaks of thin and thick pure PU films.

c) Layer model

The pure PU (thin and thick) films shows thickness effect. Furthermore crystallized volume fraction and crystal perfection were confirmed to have changed by thickness difference. In other terns, we can say that constituting thin film presents same differences to the material of thick film.

These films were fabricated by solution cast method. The films were solidified on a clean surface. After the films were removed from the glass plate, they were dried again in high temperature. Two surfaces were in contact with heated air at that time. Explanation can be given. One is the thermal conductivity in material and the other is the oxidation from the surfaces. It is possible that formation of a crystal starts from the surfaces due to the thermal gradients. A property gradient takes place (For instance ratio soft/hard segment…). Outside of film can have different morphology to the one of inside. In other terms, film can have skins. Neither DSC nor XRD can see the different of layers in material, but the results do not against to this hypothesis. The crystallized volume fraction and perfection of thin film is higher then thick film.

Figure 4.21 is inferred from there result. There are only skins of thin sample and there are skins and inner layer for thick sample from the fact that there were no out-plane motion when electric field was inducted, the model was done with three layers to keep the symmetry in thickness direction. In this model, the polymeric material is considered to have a skin effect that might have occurred during the fabrication processing. The large strain of thin films is estimated being generated by the strong isotropy, when the crystallization had occurred in hard segments. On the other hand, when the volume fraction of crystallization in material is not so high, as the case of the thick film, the low strain can be obtained because of its anisotropy. The layer model can be the method to explain the thickness dependence on electroactive strain.

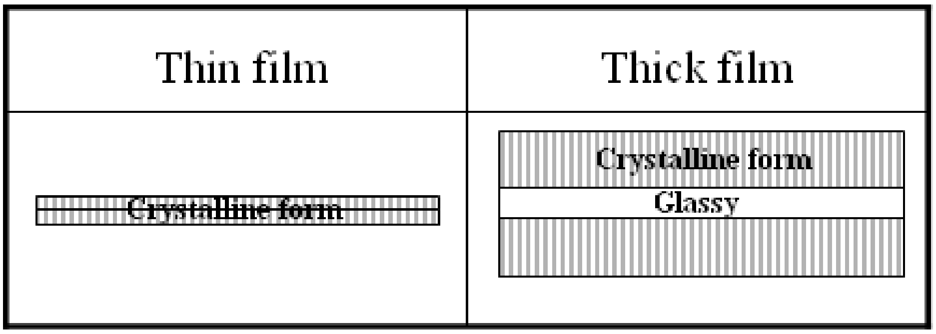

Figure 4.21 Schematic drawings of thin and thick PU films.

4.4 Conclusions

The present part 1 of chapter 4 is dealing with the electromechanical properties of a synthesized pure PU and their dependence on the polymer film thickness.

The important thing is that a compressive strain in the thickness direction of up to around 31 % was obtained under moderate electric field < 20 MV/m by pure PU film. Two factors are supposed to contribute this fact; one is the selection of type of PU. The material was PU, Estane 58888-NAT021, which have higher 46 wt% of hard segments (HS) fraction then usual PU. The second reason is from the thickness of sample. When the electric field was increased, the thick film started showing a sharp increase in strain at a low electric field level. Subsequently, the saturation occurred below 3 MV/m. On the other hand, the thin film exhibited a slow raise in strain in the low electric field regime, followed by a slight saturation between 10 and 20 MV/m.

The electrical-field-related-electrostriction coefficient of the material, M, is the important factor of strain. In general, the researchers try to increase M to have higher strain. However, M does not assure high strain. The material which has the high M has tendency to have $S(E)$ saturation easily. I recommend to use more genial relation $S=QP^2$ which is true even in high electric field regime. The thinner the thickness is, the strain becomes higher at high electric field domain from 10 to 20 MV/m.

Furthermore crystallized volume fraction and crystal perfection were confirmed to have changed by thickness difference. In other terms, I can say that the material is completely different between thin and thick films. These films were fabricated by solution cast method. The films were solidification by the surface. After the films were removed from the glass plate, they were dried again in high temperature. Two surfaces were in contact with heated air at that time. Two reasons are possible. One is the thermal conductivity in material and the other is the oxidation from the surfaces. In other terms, film can have skins. Neither DSC nor XRD can see the different of layers in material, but the results do not against to this hypothesis. The crystallized volume fraction and perfection of thin film is higher then thick film.

There are only skins for thin sample and there are skins and inner layer for thick sample from the fact that there were no out-plane motion when electric field was inducted, the model was done not for two layers but three layers to keep the symmetry in thickness direction. In this model, the polymeric material is considered to have a skin effect that might have occurred during the fabrication processing. The large strain of thin films is estimated being generated by the strong anisotropy, when the crystallization had occurred in hard segments. On the other hand, when the volume fraction of crystallization in material is not so high, as the case of the thick film, the low strain can be obtained because of its anisotropy. They layer model can be the method to explain the thickness dependence on electroactive strain.

Part *2*: Composites films

4.5 Introduction

The electric field vanishes inside the carbon black (CB) particles and consequently positive and negative charges are distributed at the interface CB/polyurethane (PU) to ensure to field cancellation in the conductive particle **[1, 56, 86, 87]**. Due to the charge distribution, a polarization takes place thus increasing the electrostrictive strain. To evaluate the effects of CB dispersion on maximum strain, S_{max}, precisely, the solidification thickness strongly contributes the experimental errors. The solidification thickness means the thickness at room temperature just after solidification from liquid to solid, and may strongly affect the perfection of the crystalline form of hard segments and its volume fraction in rubber. The purpose of the part 2 of chapter 4 is to investigate the influence of thickness on electrostriction of the composite film.

4.6 Background of CB and CB filled polymers

The chapter 2 showed the characteristic of conductive particles in micelle form CB is briefly introduced here.

CB is produced by the reaction of a hydrocarbon fuel such as oil or gas with a limited supply of combustion air at temperatures of 1320 to 1540 °C. The unburned carbon is collected as an extremely fine black fluffy particle, 10 to 500 nm in diameter.

In general, CB is used as a pigment and reinforcement in rubber and plastic products. The most common use, 70 % of CB, is as a pigment and reinforcing phase in automobile tires. CB also helps conduct heat away from the tread and belt area of the tire, reducing thermal damage and increasing tire life. CB particles are also employed in some radar absorbent materials and in photocopier, laser printer toner and inks, and surface coatings.

CB filled polymers are the most commonly used polymer composites for packaging applications. The wide use of CB as conductive filler is mainly because of its cost advantage over many other types of fillers such as carbon nanotubes, metals fibres, etc **[103]**.

When used as conductive filler, CB is characterized by its surface area, structure and surface chemistry. This is important to impart conductivity in polymer matrix at very low percolation threshold, which is the critical concentration of conductive filler necessary to initiate a continuous conductive network. To obtain this, the optimal property of conductive CB is high surface area (small particles size), high structure (branched primary aggregates) and low chemisorbed oxygen complexes. But unfortunately, CB with such characteristics is expensive. On the other hand, CB with low structure is cheaper, but high concentration is required to achieve the percolation threshold, and this affects the mechanical properties, processing ability and increases the cost of the produced composite.

4.7 Results and discussion

4.7.1 Dispersion of CB nanoparticles

a) Film morphology and structure with observations of micelle formation

In the present thesis, micelle form of carbon black (CB) nanoparticles obtained from nanoink was selected as conductive particle. In general, aggregation problem is a big issue when nanoparticles are dispersed in polymer as explained chapter 2. Therefore, the micelle form effect was checked. The composite was observed by Scanning Electron Microscope (SEM) and Transmission Electron Microscope (TEM).

Figure 4.22 shows photographs of 0.89 vol% composite films. With the CB, even without ultrasonic treatment, no large aggregations could be observed as shown in Figure 4.22 (a). Figure 4.22 (b) presents an image of large aggregates, for the sake of comparison. The latter sample was obtained with dried CB from the same ink (i.e., powder) mixed in the polymer without ultrasonic activation. Such large aggregates could be easily avoided using CB-ink in micellar form. It was thus concluded that the fabrication procedure could be simplified by selecting this type of filler **[1]**.

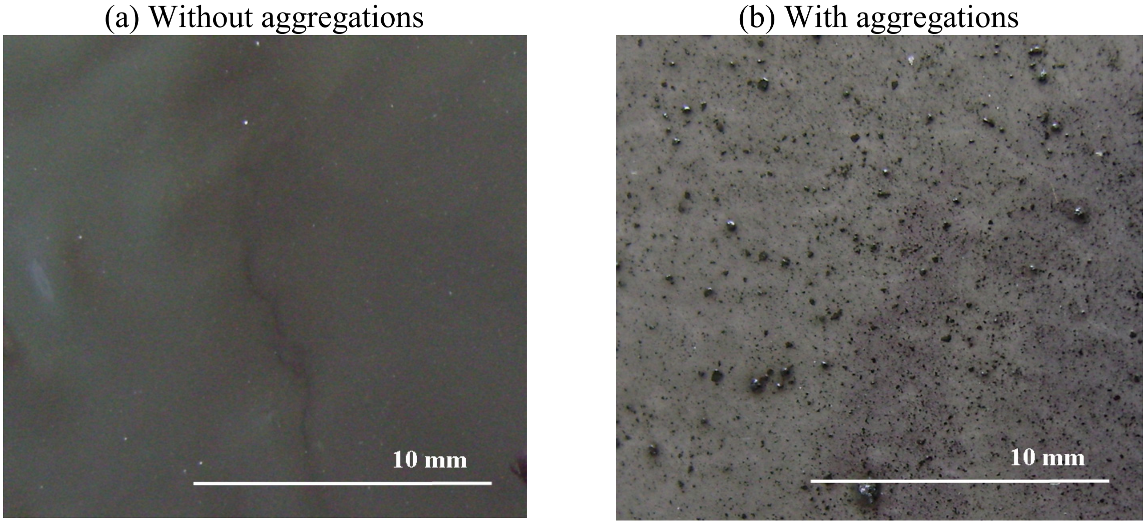

Figure 4.22 Photographs of 0.89 vol% composite films. [1]

The dispersed conditions of CB nanoparticles were observed by SEM (Supra 55 vp, ZEISS). In this case, sample was not coated to prevent the charge. Consequently, accelerating voltage was selected at 0.5 kV. The sample was frozen with liquid nitrogen. After fracture, the surface was observed by SEM.

According to Figure 4.23, the composite film exhibits a rather good CB nanoparticles dispersion within the matrix. However, few aggregates were found, as well as individualized CB nanoparticles of about 30 nm. An individual CB is marked by flesh and the small aggregation is surrounded by square in Figure 4.23.

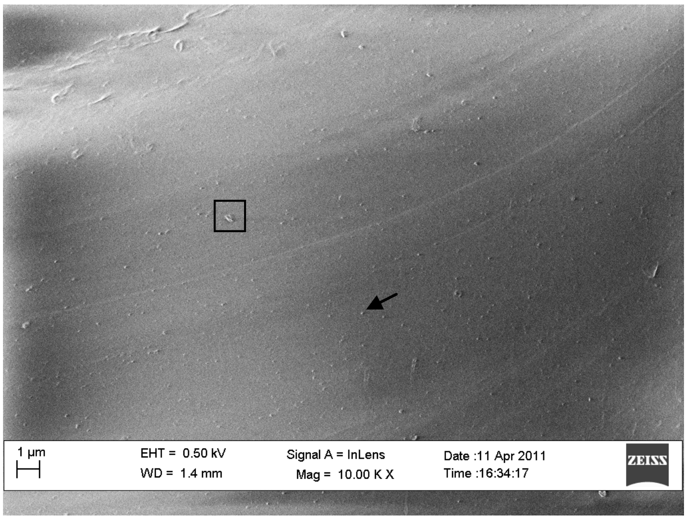

Figure 4.23 SEM micrograph of 0.89 vol% composite film.

It was also observed by TEM (HF-2200TU, HITACHI) to see more detail. Sample was coated for 30 s to prevent the charge by Au.

Figure 4.24 shows TEM micrograph of the composite film. TEM result confirmed well dispersed CB nanoparticles in PU matrix. The percolation threshold of this material is supposed around at 1.25 vol% **[104]**. In the case of 0.89 vol% composite films, the quantity of CB nanoparticles was much lower than that of percolation threshold. Thus, there was no danger of short circuiting even if some of particles are connected (aggregation) each other.

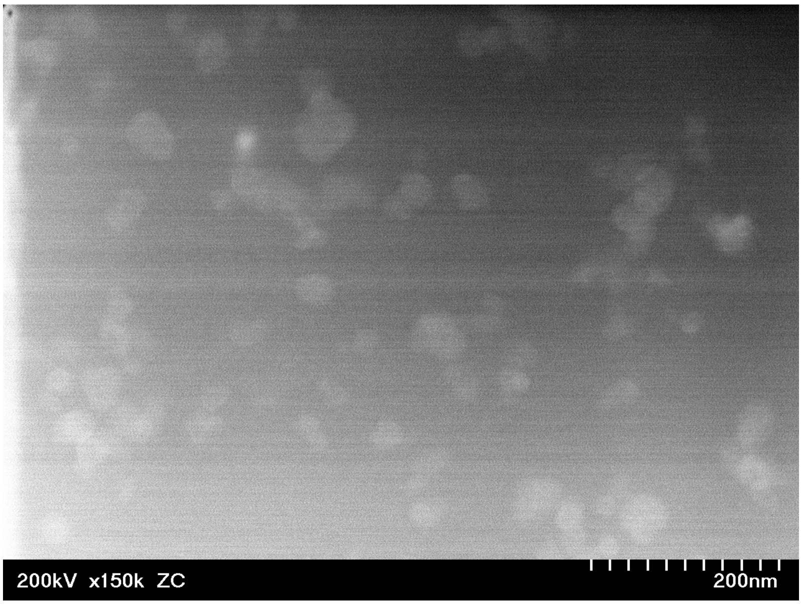

Figure 4.24 TEM micrograph of 0.89 vol% composite film.

b) Dependence of homogeneous distribution by spin-coating on electrostriction

Spin-coating is a common method for preparing a homogeneous thin film. This method was first characterized by Walker and Thompson in 1922 and is now essential to the industrial production of thin films. It is a popular deposition technique because it produces extremely uniform layers with less than 1 % non-uniformity and because the thickness of the layer is easily controlled through the concentration of solids in the liquid and the spin velocity. To see the efficient of solution casting method, spin-coating films were also prepared. Increase the homogeneity, ultrasonic treatment was also applied here.

The procedure of the preparation is shown in Figure 4.25. Only one kind of vol%, 0.89 vol%, of composite films was made by this method. An ultrasonic probe (Hielscher UP400S) was first used for 8 min to disperse the nanoink (800 μl) into the DMF (60 ml). Then, 4 g of PU granules was dissolved in mixed solution at 80 ºC for 120 min. 10 ml of the obtained composite solutions were deposited on glass disc using a spin-coating technique. The composite solution was dropped onto the glass and spun. Thickness is controllable by the spin condition. For example, film thickness of 16 μm can be obtained with the following conditions; the first step is 1000 rpm for 10 s and the second step is 1500 rpm for 10 s. It is minimum thickness sample. Sample of maximum thickness (130 μm) was spun with the following conditions; the first step is 200 rpm for 10 s and the second step is 300 rpm for 10 s. After the spin-coating, the drying process and forming process are the same to the other films.

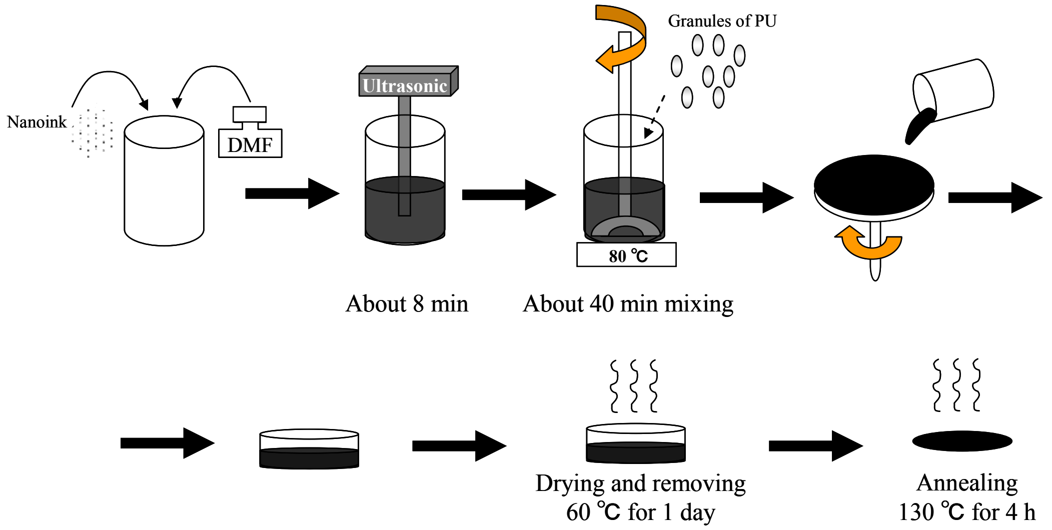

Figure 4.25 Solution casting method of spin-coating 0.89 vol% composite film.

According to SEM micrograph result shown in Figure 4.26, the 0.89 vol% composite with spin-coating treatment film exhibits a good CB nanoparticles dispersion within the matrix as well as non-treated film shown in Figure 4.26. There photos indicate that usage of micelle formed CB gives already quite high dispersion level so that complicated treatment is no more useful. Consequently, these observations demonstrated that 0.89 vol% composite obtained by introducing micelles into the polymer matrix and a solution cast film processing lead to good particle dispersion. Unlike the spin coating process, the present proposed process enables to treat a large surface and less expense.

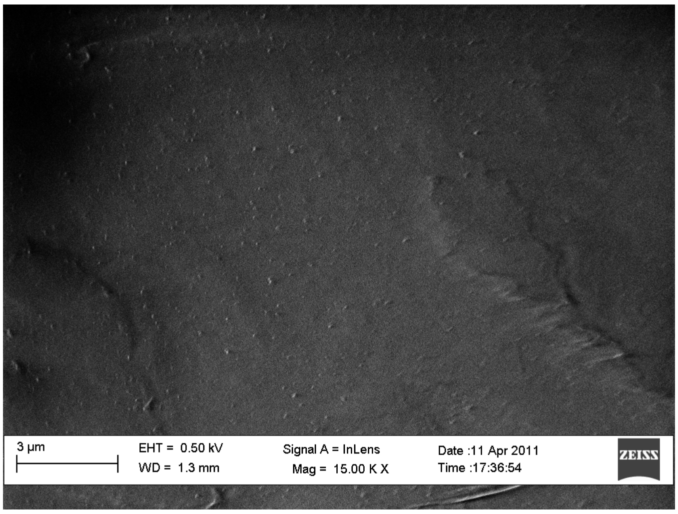

Figure 4.26 SEM micrograph of the spin-coating 0.89 vol% composite film.

Lack of aggregation problem was confirmed. It is, however, still possible that CB is not homogeneously dispersed all over the film. CB rich layer can exist by solution-cast method (without spin-coating treatment). It is difficult to see such difference by SEM observations. To check on that point I measured electroactive strain. The induced electric field, E, was a sawtooth wave for 2-cycle at 0.1 Hz. The upper limit of the maximum electric field, E_{max}, in the present work was also 20 MV/m. The maximum strain, S_{max}, was taken at the first peak of triangle input whereas E_{max}.

Figure 4.27 shows maximum strain, S_{max}, for 0.89 vol% composite with and without spin-coating treatment films versus the maximum electric field, E_{max}. They have the same thickness of 65 μm. When E_{max} is in the1-3 MV/m range, they have the almost same strain value. When E_{max} is over 3 MV/m, S_{max} of composite film without spin-coating treatment is higher than the one with spin-coating treatment, and it reaches a factor of two at 20 MV/ m.

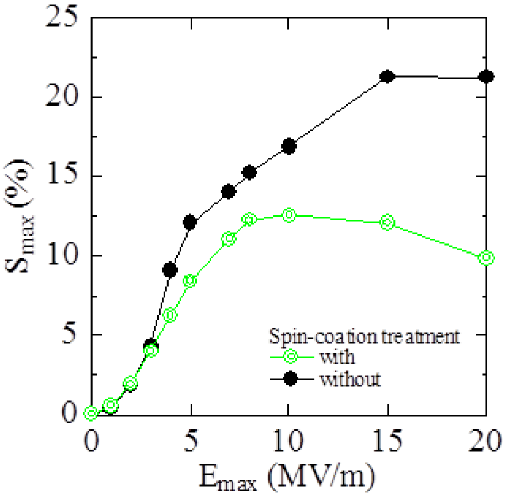

Figure 4.27 Experimental changes in maximum strain versus maximum electric field of 0.89 vol% composite with and without and spin-coating treatment films.

Figure 4.28 depicts maximum strain, S_{max}, versus maximum electric field, E_{max}, for various thicknesses from 16 to 130 µm of 0.89 vol% composite (a) with and (b) without spin-coating treatment films. As treated films, the strain of thin 16 µm film becomes higher at high electric field domain from 10 to 20 MV/m. On the contrary, the larger the thickness is, the strain at electric field from 1 to 8 MV/m, becomes higher but stay in low level at high electric field regime because of saturation. As non-treated films, the strain of thin 21µm film becomes higher at 20 MV/m.

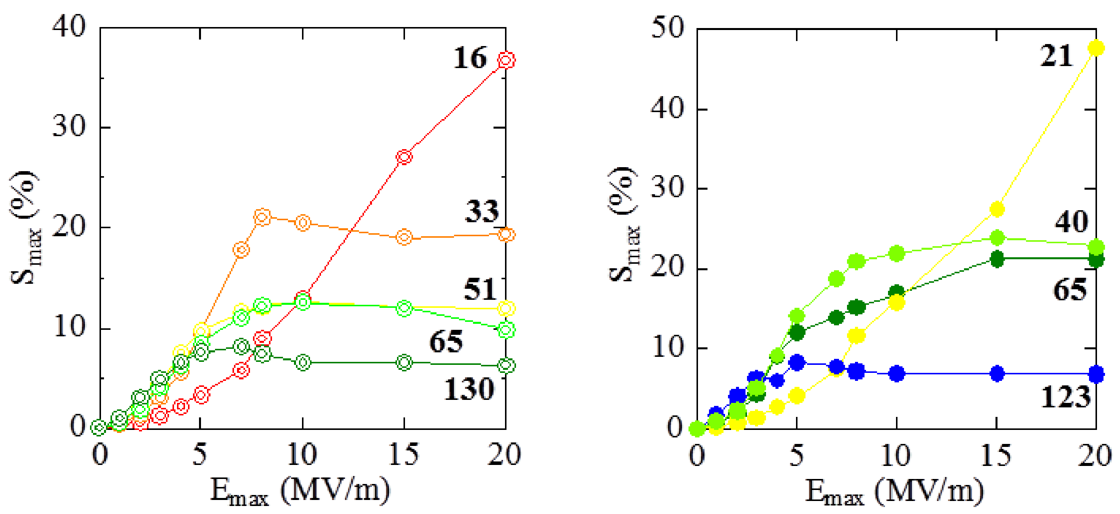
(a) With spin-coating treatment

(b) Without spin-coating treatment

Figure 4.28 Strain versus the electric field for different thicknesses of 0.89 vol% composite films.

Figure 4.29 shows the strain versus the electric field for different thicknesses of 0.89 vol% composite film, with and without spin-coating processing. In a general manner, the strains are higher for the" without spin coating" configuration. This point is confirmed on Fig 4.29.

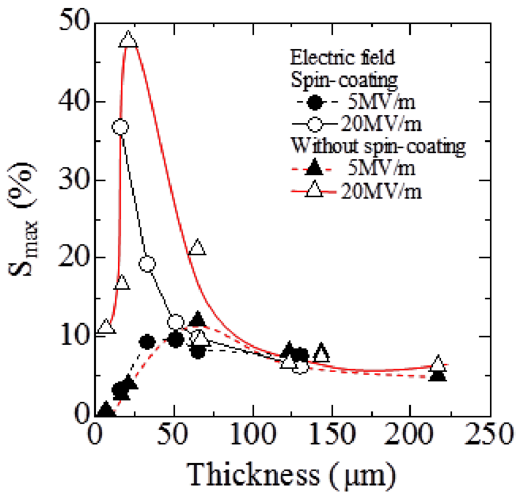

Figure 4.29 Relationship between thicknesses of 0.89 vol% composite with and without spin-coating treatment films and maximum strain at 5 and 20 MV/m.

4.7.2 Influence of volume percentage of CB nanoparticles in PU on strain

The driving electric field, *E*, was a 2-cycle sawtooth wave. Figure 4.30 shows maximum strain, S_{max}, versus maximum electric field, for different volume fraction of CB from 0 to 1.78 vol% in PU. The film thickness exhibits small thickness variation, (38.5+/-2.5 µm).

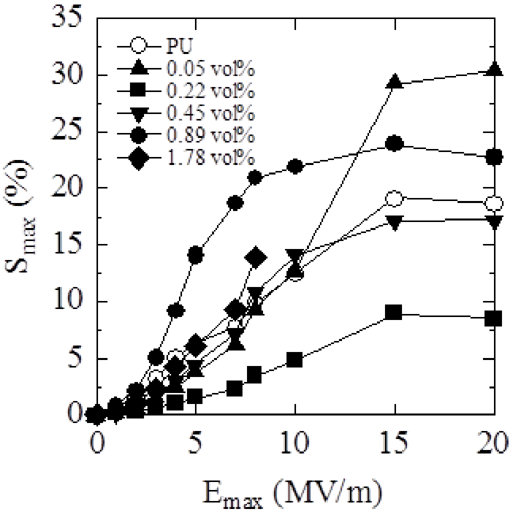

Figure 4.30 Strain versus electric field for different volume fraction.

The S_{max} of 0.05 vol% composite film is larger than pure PU film at over 10 MV/m. The S_{max} of only 0.89 vol% composite film is larger than pure PU film at over 1 MV/m. That of 0.05 vol% and 0.89 vol% composite films are 1.63 and 1.22 times higher than that of PU film at 20MV/m, respectively.

Noticeable point is that the S_{max} of 1.78 vol% composite film has many CB particles in PU, and it breaks down easily. It was impossible to obtain the curve which achieves until 20 MV/m. The percolation threshold of our material is supposed around at 1.25 vol% **[104]**. The electric break down of 1.78 vol% composite film confirms that the percolation threshold is less than 1.78 vol%.

Figure 4.31 shows maximum strain, S_{max}, versus volume percentage of CB in PU at maximum electric field, E_{max}, of 5 MV/m and 20 MV/m. The 0.05 vol% and 0.89 vol% composite films are higher than those of pure PU and other composite films at 20MV/m. When the electric field is 5 MV/m, the S_{max} of 0.89 vol% composite film is also higher than that of pure PU and other composite films. The 0.89 vol% composite film is good S_{max} at both 5 and 20 MV/m. Thus, 0.89 vol% composite films were chosen to compare with pure PU.

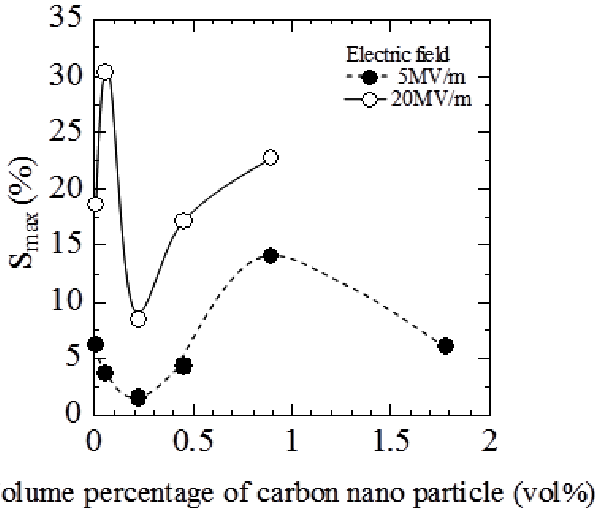

Figure 4.31 Maximum strain versus volume percentage of CB in PU at maximum electric field of 5 and 20 MV/m.

The 0.89 vol% was chosen but other volume percentages of CB composite films also show thickness effect.

Figure 4.32 depicts maximum strain, S_{max}, versus maximum electric field, E_{max}, for various thicknesses of pure PU and from 0.05 to 1.78 vol% composite films. Results of Figure 4.11 (a) are included in Figure 4.32 (a). The thickness of thin films, for examples 7 µm of 0.89 vol% and 5 µm of 1.78 vol%, gives very small S_{max}. However, thin films, for example 20 µm of 0.05 vol% and 21 µm of 0.89 vol %, lead to large S_{max}. We can not see saturation of S_{max} (E_{max}). On the contrary, the larger the thickness is, the smaller the strain is for an electric field ranging from 1 to 5 MV/m.

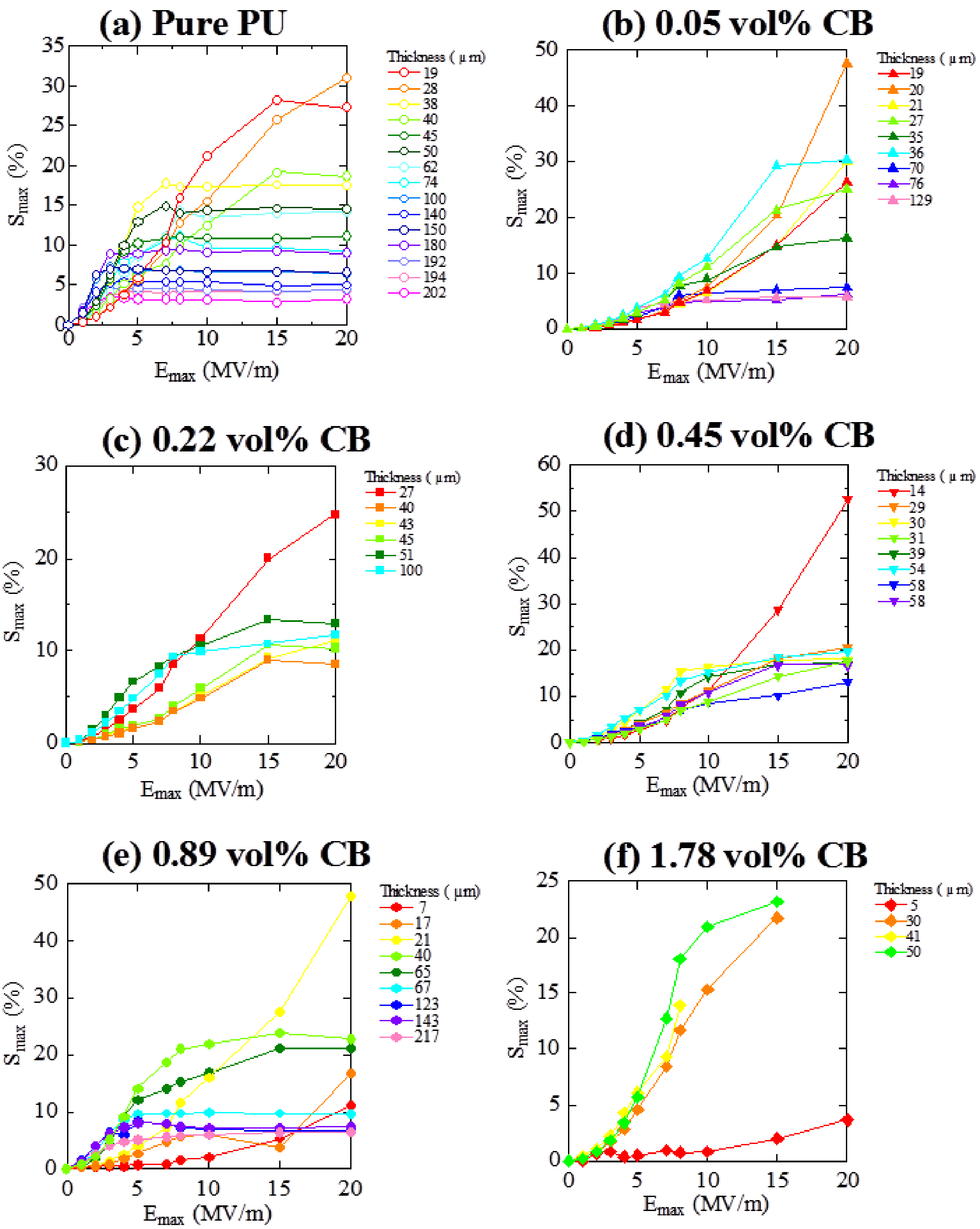

Figure 4.32 Maximum strain at different thicknesses for pure PU and composite films versus electric field.

Figure 4.33 shows the relationship between thickness and maximum strain, S_{max}, at 5 and 20 MV/m, lead from Figure 4.32. The strain values at 5 MV/m are much smaller than that at 20 MV/m for thin films. The strain at 5 MV/m is as similar as those at 20 MV/m for thick film. Consequently, pure PU and 0.05 to 1.78 vol% composite films have strong thickness effect.

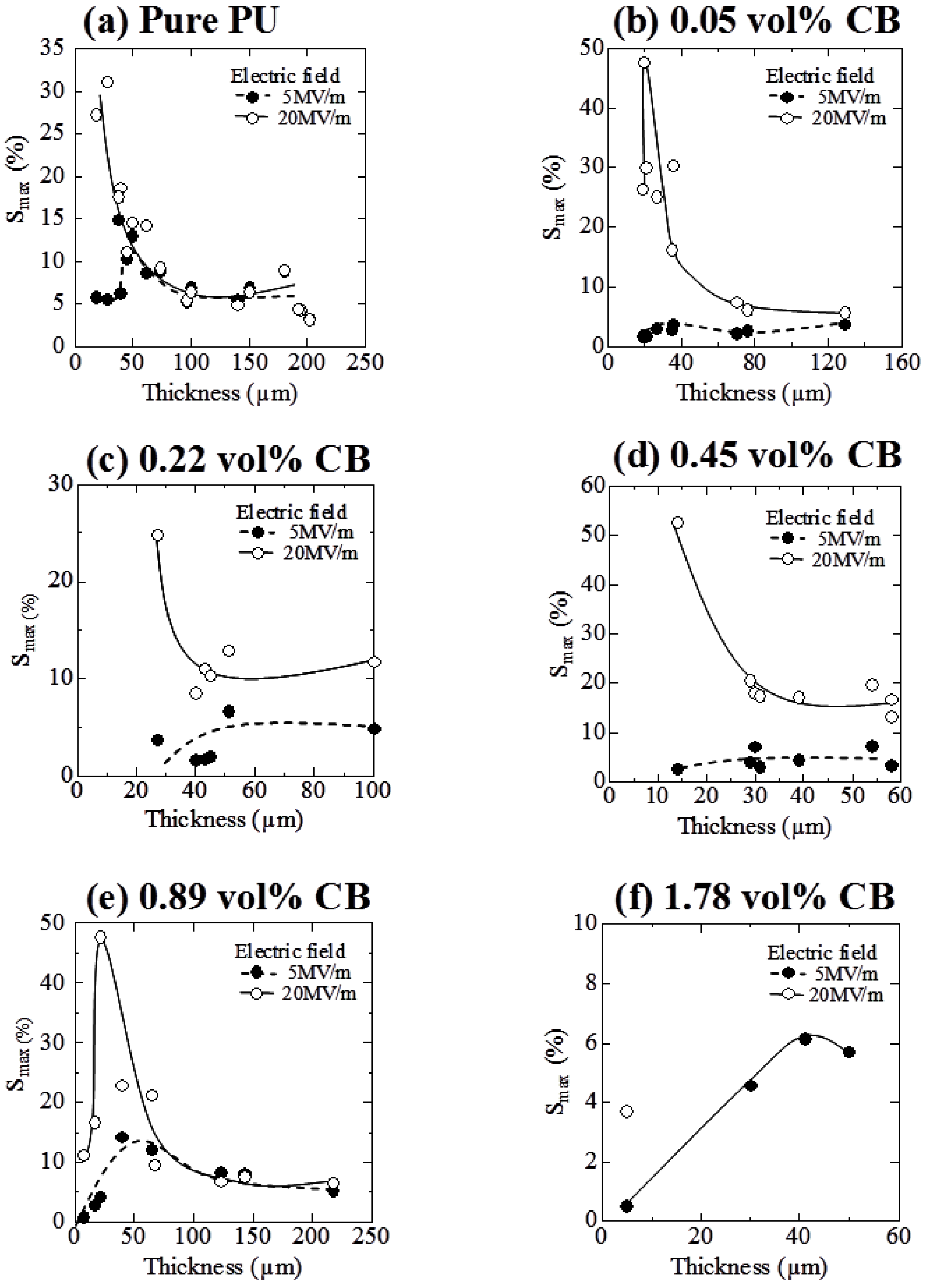

Figure 4.33 Thickness dependent maximum strain of pure PU and composites films as a function of the thickness at 5 and 20 MV/m.

4.7.3 Strain of thin and thick 0.89 vol% composite films

a) Changes in the maximum strain versus electric field

Figure 4.34 shows the typical electroactive strain for two different thickness samples; (a) 21 µm and (b) 143 µm driven by a 2-cycle sawtooth electric field with various amplitude. The image of the electric field is represented in the figure by a bold line. The upper limit of the maximum electric field, E_{max}, was 20 MV/m.

(a) Composite thin film (21 µm)

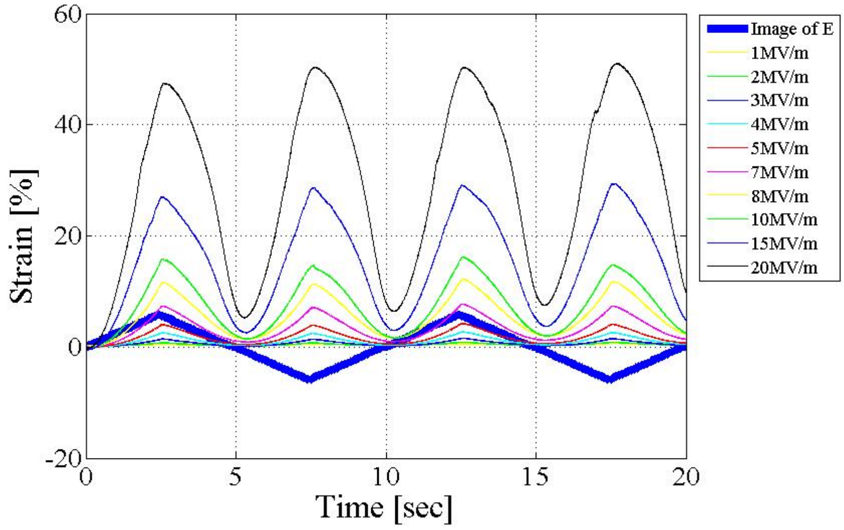

(b) Composite thick film (143 µm)

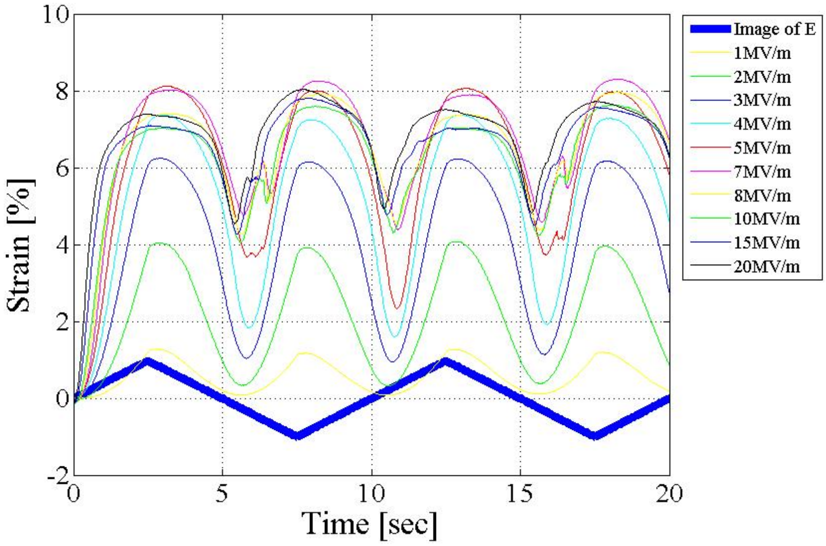

Figure 4.34 2-cycle of a sawtooth wave electric field induced strain of 0.89 vol% composite thin and thick films.

When 2-cycle of a sawtooth electric field was induced into the 0.89 vol% composite, the compressive strain in 4-semi-triangular shape appeared when the electric field was low as shown in Figure 4.34 (a). The peaks became less sharp when the electric field was increased. In certain thick cases, a decreased strain could be seen in the high electric field regime see Figure 4.34 (b). The slope is higher with higher electric field amplitude but some peaks became flat as the electric field increased. The maximum strain in this case was smaller than the one with lower electric field input, it can be seen as seen in Figure 4.34 (b). Explanation of these phenomena was given in the chapter 3.

Figure 2.14 already showed maximum strain, S_{max}, versus maximum electric field, E_{max}, of pure PU and 0.89 vol% composite films. The results of pure PU films were already shown in Figure 4.8. Two composite films correspond to the ones of Figure 4.34. Figure 4.35 shows the simulated results by non-linear three-layer model with force equivalent as followings; $\varepsilon_1=\varepsilon_3$=11.5e-11 and ε_2=25e-11 for pure PU films and $\varepsilon_1=\varepsilon_3$=12e-11 and ε_2=27e -11 for composite films. Note that the permittivity of both inner and outer layers and the difference in permittivity between the outer and inner layers had to be increased for composite films, compared to pure PU films, shown in Figure 2.14. The values of strain still needed to be adapted. The phenomenon of a non-saturated strain up to 20 MV/m for the thin films and a saturated strain for the thick ones are, however, well represented.

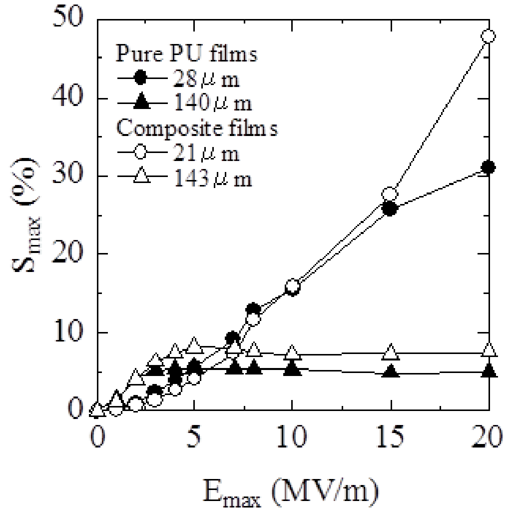

Figure 2.14 Experimental changes in maximum strain versus maximum electric field of pure PU and composite films.

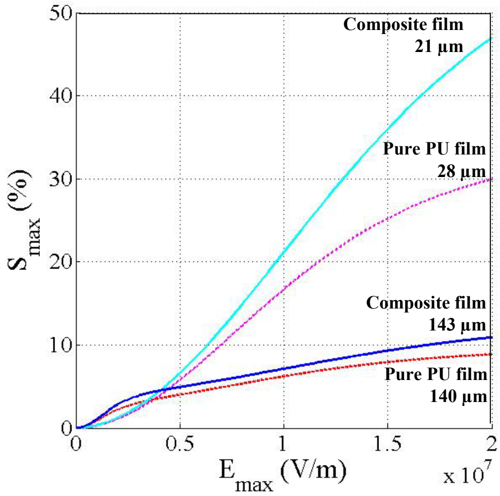

Figure 4.35 Simulated results by three-layer model with force equivalent.

Strains of both thin and thick composite films are higher than pure PU films. The effect of CB doping is clearly seen.

As mentioned earlier, the thickness effect is important and has been described and interpreted in Chapter 3. The saturation in strain versus electric field by both thick samples is clearly seen in this way. Consequently, for electric field at 20 MV/m, thinning the films remarkably enhanced the electroactive strain.

b) Linear logarithmic relationship between thickness and maximum strain at 20 MV/m

Figure 4.36 shows the logarithmic relationship between thickness, L, and maximum strain, S_{max}, at 20 MV/m of 0.89 vol% composite films, expressed by open circles and line. For a shake of comparison, the result of pure PU is also expressed by broken line. We see again that thinning the films remarkably enhanced the S_{max} at 20 MV/m. The S_{max} at 20 MV/m are distributed along a line the log-log scale from between 47.7 % for 21 µm down to 7.5 % for 150 µm film thickness.

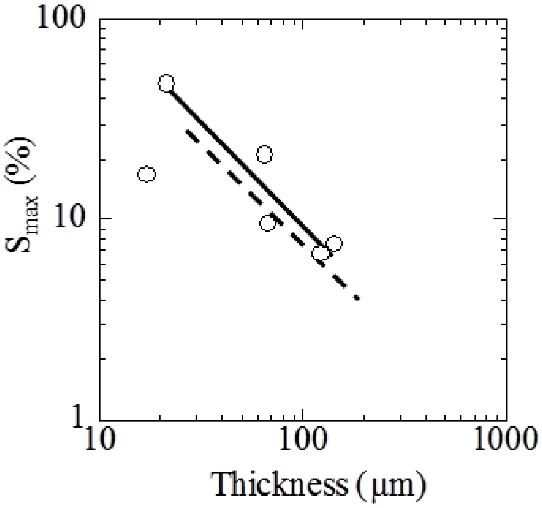

Figure 4.36 Linear logarithmic relationship between thickness of pure PU (broken line) and composite (open circle and line) films and maximum strain (20 MV/m), which is maximum strain at maximum electric field of 20 MV/m.

From Figure 4.35 (e), A and B of equation (4.2) in part 1 of chapter 4 are obtained whereas A=-0.91 and B= 5.42×10^2 of pure PU obtained in part 1 of chapter 4 A=-1.10 and B= 1.37×10^3. The log (L) dependent log (S_{max}) of the composite film is parallel to that of pure PU film. The slope of composite film is higher than that pure PU one.

4.7.4 Non linear resistance in current outputs

Figure 4.36 shows the experimental current curves versus electric field. Note that there is order difference in current for these three figures. The factor 500 is shown between the figure (a) and (c). The dependence of resistance on electrical input is clearly shown in these figures which were explained in the section 3.5 in chapter 3.

(a) E=1,2,3MV/m **(b) E=4,5,7,8MV/m**

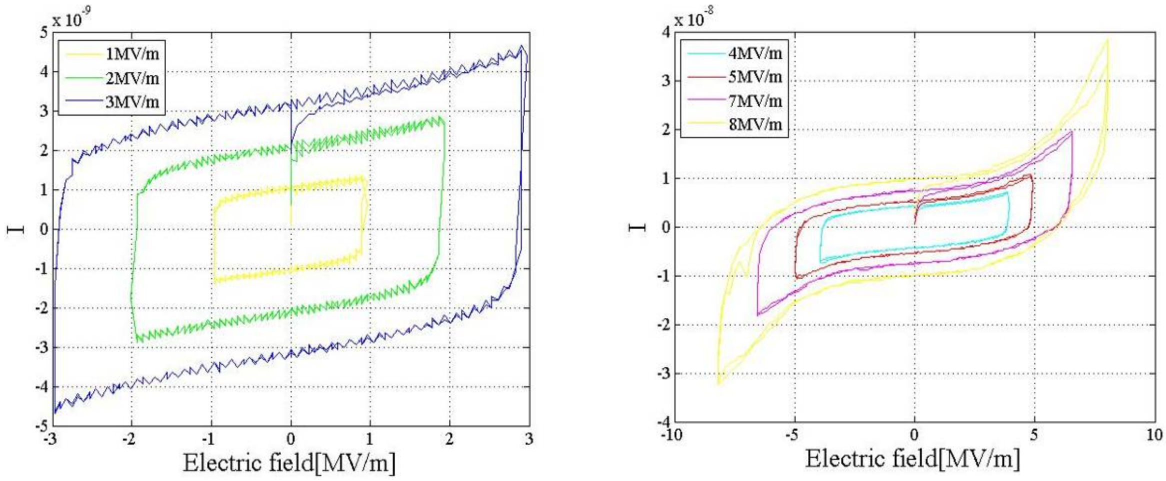

(c) E=10,15,20MV/m

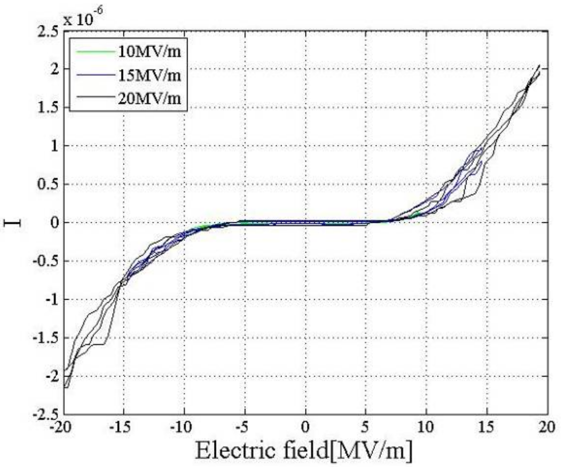

Figure 4.37 Typical outcome of electric field-induced current of composite film versus maximum electric field.

4.7.5 Permittivity

Figure 4.38 shows the directly measured relative permittivity by frequency response analyzer (1255, Solartron) and dielectric interface (1296, Solartron) with divers film thickness and frequency. Figure 4.38 (a) depicts them versus thickness, and (b) depicts them in terms of frequency. In the comparison with pure PU sample results, shown in Figure 4.17, we can see that the permittivity values increased and the difference between them of thin and thick samples becomes bigger by CB doping, which correlate well to the permittivity values obtained at fitting by three-layer model with force equivalent simulation, see Figure 4.35.

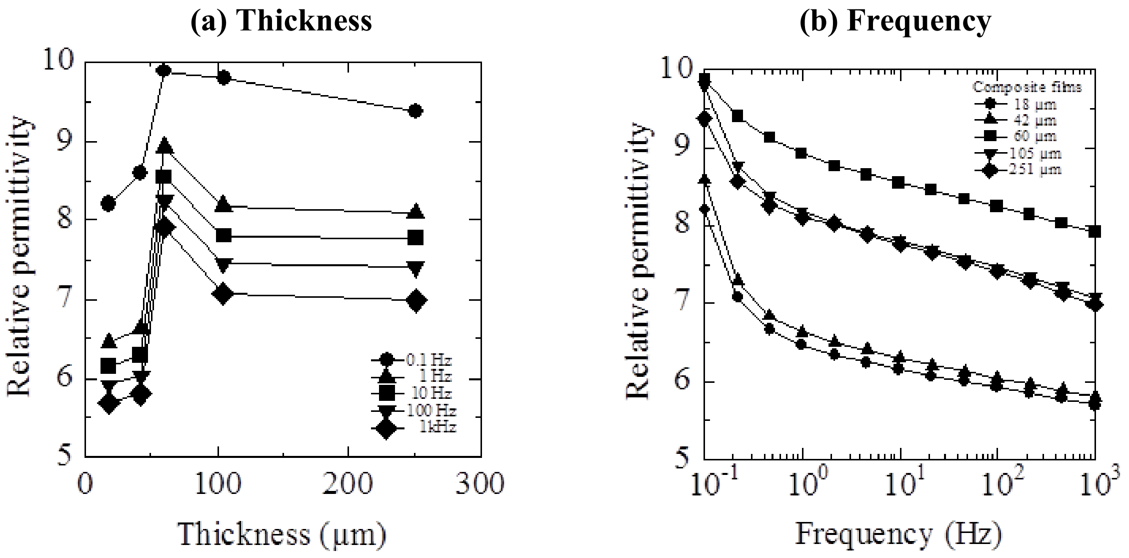
(a) Thickness

(b) Frequency

Figure 4.38 The directly measured permittivity with divers composite film thickness and frequency.

4.7.6 Surface crystallization model from glass to crystalline form of hard segments

We see well the thickness effect on composite films as well as pure PU films. The thin composite film shows high strain at 20 MV/m. Differential Scanning Calorimetry (DSC) analysis and X-ray diffraction (XRD) were used to confirm the internal structures of composite films with different thickness.

a) Effects of crystallized volume fraction in material

Differential Scanning Calorimetry (DSC) analysis was carried out to see the fusion enthalpy value of thin and thick films, 25-29 μm and 140-149 μm, respectively, shown in Figure 4.39. These selected thicknesses correspond to the ones of Figure 2.14.

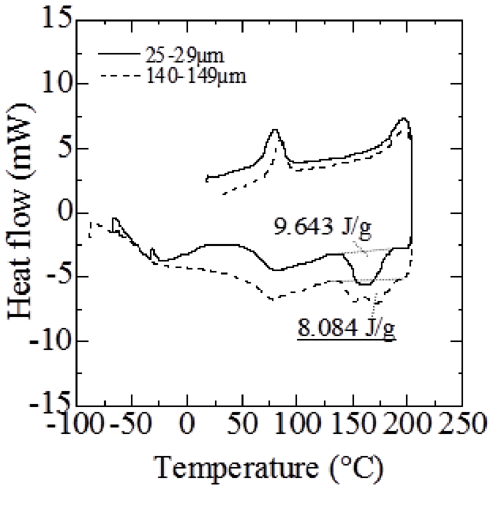

Figure 4.39 DSC analysis of thin (25-29 μm) and thick (140-149 μm) composite films.

The same thermal analysis to the one of part 1, chapter 4, was performed by DSC under protective argon atmosphere.

The fusion enthalpy values were obtained 9.643 and 8.084 J/g for thin and thick pure PU films, respectively. That of thin film is 1.19 times higher than that of thick film. Therefore, it is possible that high volume fraction of crystallization contribute to the high electroactive strain of composite thin film.

b) Crystal perfection of thin and thick composite films

Crystal structures in thin and thick film were checked by X-ray diffractometer (XRD: D8 ADVANCE, BRUKER). The conditions were the same to the ones of part 1, chapter 4

Figure 4.40 shows the X-ray diffraction peaks of thin and thick 0.89 vol% composite films. The thin film thickness is 21 µm, and the thick one is 143 µm. Most of the sharp peaks are related to thin film, whereas the broad peak is found in the thick film. No sufficient explications are found for the small peaks. Besides, the angle width of thick samples is smaller than the other one. The angle width corresponds to the crystal perfection of crystalline form of hard segments. Therefore, this result gives the conclusion that the thin sample has the more perfect hard segments than the other.

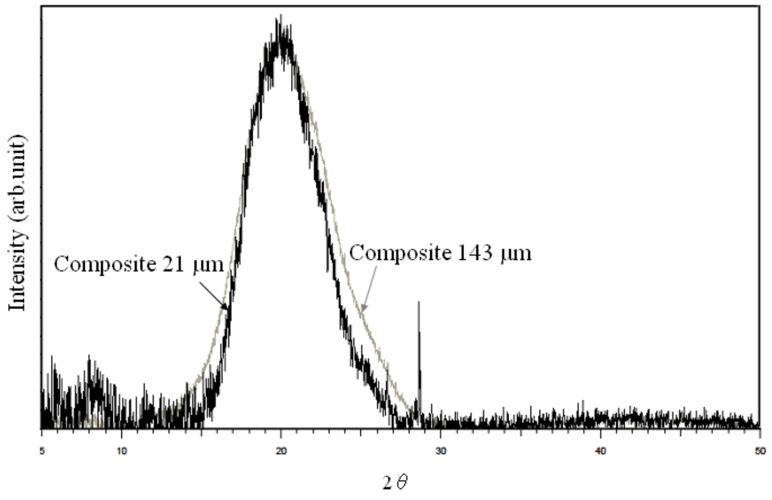

Figure 4.40 X-ray diffraction peaks of thin and thick composite films.

c) Layer model

Composite films also exhibited the thickness effect. Furthermore crystallized volume fraction and crystal perfection were confirmed to have change by thickness difference. The layer model of pure PU film was already explained and demonstrated in chapter 3 and part 1 of chapter 4. The composite films are assumed to have the same type of model. Composite films have the particles inside and their distribution was not confirmed, i.e. I am not sure if CB rich layer exists. But the results obtained with the three-layer model that fits quite well the experimental data seems to confirm the physical existence of skin layers.

4.8 Conclusions

The present part 2 of chapter 4 is dealing with the electromechanical properties of a synthesized composite and their dependence on the composite film thickness.

A compressive strain in the thickness direction up to 47.7 % was obtained at 20 MV/m with 0.89 vol% composite 21 μm thin film. The strain of composite film is generally higher than that of pure PU. Therefore, CB doping effect is confirmed. As well as pure PU, composite films undergo thickness effect and thick films exhibit saturation in strain versus electric field.

Even if SEM results shows micro-aggregates form, well dispersed CB nanoparticles was confirmed. The percolation threshold of thesis material is supposed around at 1.25 vol% **[104]**. In the case of 0.89 vol% composite films, the quantities of CB nanoparticles were much smaller than that of percolation threshold. Thus, there was no danger of short circuiting even if some of particles are connected (aggregation) each other.

The 0.89 vol% composite with spin-coating treatment film exhibits a good CB nanoparticles dispersion within the matrix as well as non-treated film. There photos indicate that usage of micelle formed CB gives already quite high dispersion level so that complicated treatment is no more useful.

Furthermore crystallized volume fraction and crystal perfection were confirmed to have change by thickness difference. The layer model of pure PU film was already demonstrated in part 1 of chapter 4. The composite films are assumed to have the same type of model. Composite films have the particles inside and their distribution was not confirmed, i.e. I am not sure if CB rich layer exists.

Chapter 5

Effect of injecting a charge of film on electroactive strain

5.1 Introduction

The new type of dielectric EAP which is able to generate a large strain (> 30 %) while requiring only a medium electric field (< 20 MV/m) were shown in chapter 2 to 4.

As these outstanding properties seem to be linked to the space charge distribution, it seems interesting to evaluate the actuation performance of a dielectric material in which electrical charges have been injected **[56, 105]**.

The most well known technique for injecting a charge is the corona treatment **[106-108]**. As other method of injecting a charge, there is electron beam irradiation **[43, 109-112]**. As explained in chapter 1 (section 1.3.4, Piezoelectric polymer), one thing that I want to note is the studies of the effect of electron irradiation. In 1998, Zhang et al. reported that high-energy electron irradiated P(VDF-TrFE) copolymers exhibit higher electrostrictive response (~ 5 %) **[42-44]**.

The electron beam irradiation with more than one MeV-class high voltage easily induces radiation damage **[113]**, whereas electron beam irradiation with an extremely low voltage of less than a 0.30 MeV simply charges materials. When 0.10 MeV-class electron beams homogeneously irradiate at the optimum absorbed dose, I speak of homogeneous electron beam irradiation (HEBI). This often induces a fracture strain of the polymer sheet to occur in a homogeneous irradiation **[114-116]**. It can be said that HEBI is a good tool for generating dangling bonds **[117-120]**.

The purpose is to evaluate and explain the effect of corona treatment and HEBI on the electroactive strain. Two types of films were selected for the purpose: pure polyurethane (PU) thick film because pure PU thick film leads to strain saturation. It would be very interesting if beam irradiation could cancel the saturation mechanism. The second chosen sample is a 0.45 vol% composite thin film (14 μm), because the composite thin film exhibits high strain value as explained in chapter 4 (section 4.3.2, Figure 4.12 (d)). Clearly it would be interesting to see that beam irradiation would enhance the already large strain in thin film.

5.2 Experimental setup

5.2.1 Corona setup

The sample was charged using a corona triode, which is schematically presented in Figure 5.1. The charged films were coated with a gold electrode on one surface (20 nm thickness) under high vacuum by a high resolution sputter coater (208 HR, Cressington) for 10 mm of diameter and 20 nm thicknesses. The electrical charges were injected for a duration of 10 min through the non-metalized surface of the sample which was placed under a stainless grid (size of nominal aperture is 0.38 mm) in order to maintain a uniform surface potential. The corona voltages were kept at -7 kV and a grid voltage of -4 kV was employed.

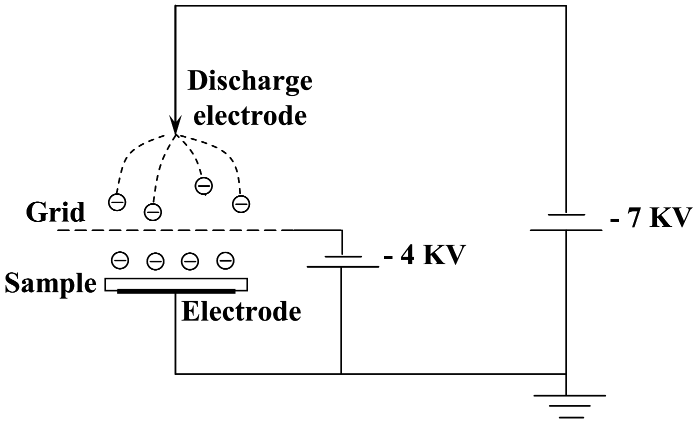

Figure 5.1 Corona discharge setup.

5.2.2 Homogeneous electron beam irradiation (HEBI) setup

The sample was homogeneous electron beam irradiation (HEBI) by using an electron-curtain processor (Type CB 175/15/ 180L, Energy Science Inc., Woburn, MA, Iwasaki Electric Group Co., Ltd., Tokyo), as show in Figure 5.2 **[109-112]**.

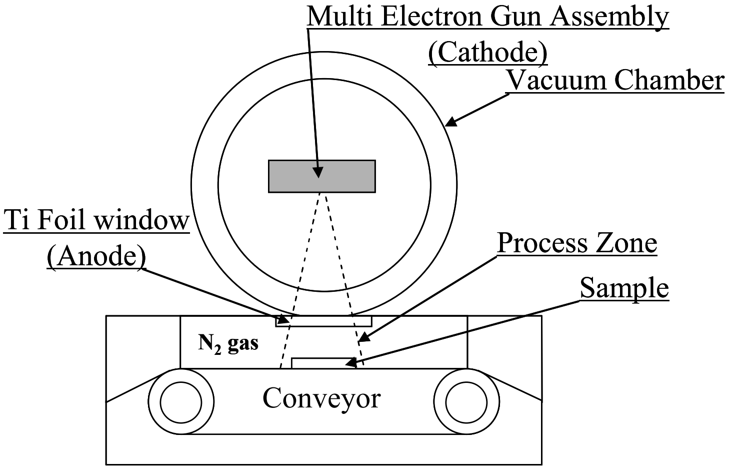

Figure 5.2 Schematic diagram of electron curtain processor. (Iwasaki Electric Co. Ltd.)

The irradiation was performed with an electron beam through a titanium window attached to a 240 mm diameter vacuum chamber. Table 5.1 shows condition of EB irradiation. A tungsten filament in a vacuum was used to generate the electron beam with an electrical potential of 170 keV and an irradiating current of 2.0 mA. To prevent the oxidation gas, the samples were kept in a nitrogen gas of 0.1 MPa with a residual concentration of oxygen gas of less than 300 ppm. The flow rate of the nitrogen gas was 1.5 Ls^{-1}. The sample was positioned in an aluminum plate holder (0.15 m × 0.15 m), and was transported on a conveyor at a speed of 9.56 m/min. Since the minimum dose of EB irradiation was 43.2 kJg^{-1} (1.13×10^{13} em^{-2} = 43.2 kGy), each burst of irradiation was performed for a short time (0.23 s) at 0.043 MGy to avoid excessive heating of the sample. As a result, the temperature of the sample surface remained below 323 K just even after irradiation.

Table 5.1 Condition of EB irradiation.

Electrical potential	170 keV
Conveyor speed	9.56 m/min
Short time (Once)	0.23 sec
EB irradiation (Once)	0.0432 MGy
Flow rate of the nitrogen gas	1.5 Ls^{-1}

Both sides of the samples were repeatedly irradiated to increase the total irradiation dose. One surface irradiation becomes 86.4 kGy. The total irradiation on both sides is then 172.8 kGy (43.2 kGy × 4 times). The interval between the end of one period of irradiation and the start of the next was 30 s. The dosage was proportional to the yield determined from the irradiation current, conveyor speed, and number of irradiations. The yield dosage was calibrated using dose-meters with radio chromic nylon film (FWT-60-00: Far West Technology Inc., Goleta, CA, USA). The electron number density (em^{-2}) was expressed by the following equation, which is often used in metals **[121]**.

$$Ng = DE/Cg \qquad (5.1)$$

Here, Ng (em^{-2}) is the irradiation dose, DE (Svs^{-1}) is the dose equivalent, and Cg is the dose equivalent per transferred coefficient of particle flux $\{0.1649 \times 10^{13}\ [(Svs^{-1})/\ (e\ (m^2s)^{-1})]\}$ **[121]**.

5.3 Thick pure PU film of corona treatment and electron beam irradiation

5.3.1 Results

a) Corona treatment

Pure PU film of 194 µm thick film is chosen. The induced electric field, *E*, was a triangle wave for 2-cycle. The upper limit of the maximum electric field, E_{max}, in the present work was 20 MV/m. Therefore, the range from 10 to 20 MV/m is called high electric field regime and 1 to 5 MV/m is called low electric field regime in the present thesis. The maximum strain, S_{max}, was taken at the first peak of triangle input whereas E_{max}.

Figure 5.3 shows maximum strain, S_{max}, versus maximum electric field, E_{max}, of 194 µm pure PU film. The strain of before and after corona treatment films are similar results. The S_{max} is seen to have nonlinearly with the E_{max}. It can be clearly seen in Figure 5.3 that the parabolic relation of S_{max} (E_{max}) disappeared when the electric field is increased. The *S(E)* saturations are seen. Moreover, the strain decreases are seemed. Starting point of convergence at before corona treatment film is higher then after corona treatment film. However, the electrical-field-related-electrostriction coefficient of the material, *M*, of after corona treatment film is higher then before corona treatment film.

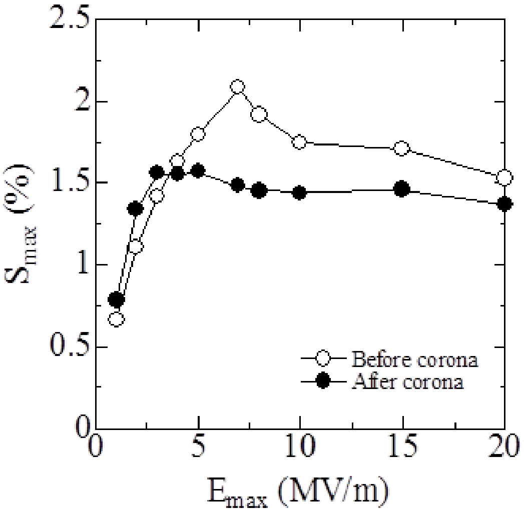

Figure 5.3 Maximum strain versus maximum electric field of 194 µm pure PU film.

b) Electroactive strain enhancement by HEBI

In order to enhance the S_{max} induced by the polarization, the pure PU thick (192 µm) film has been irradiated by homogeneous electron beam irradiation (HEBI).

Figure 5.4 shows the electric field induced strain of (a) before HEBI and (b) after HEBI under 2-cycle of a sawtooth wave electric field with various amplitudes. The image of the electric field is represented in the figure by a bold line. When 2-cycle of a triangle wave electrical field was induced into the polymer, the strain has 4-semi-triangular shape when the electric field is low. When the electric field is raised, it has round-shape.

(a) Before HEBI

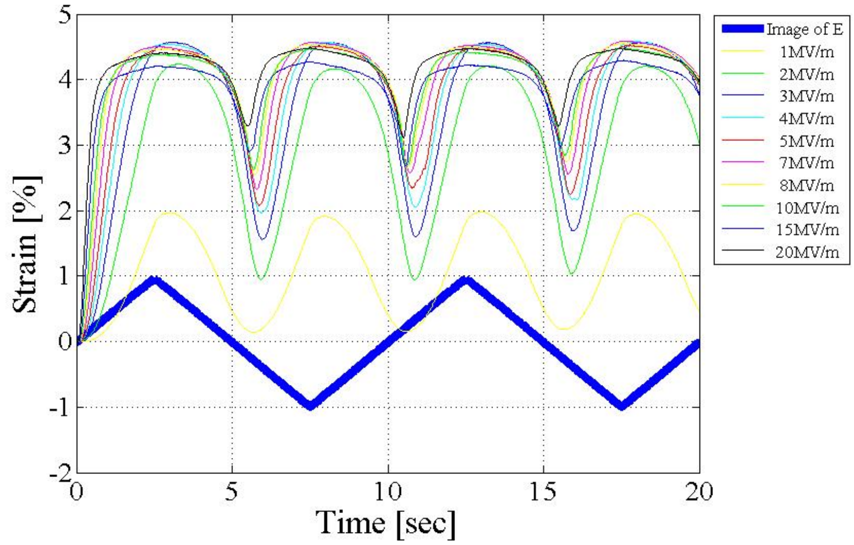

(b) After HEBI

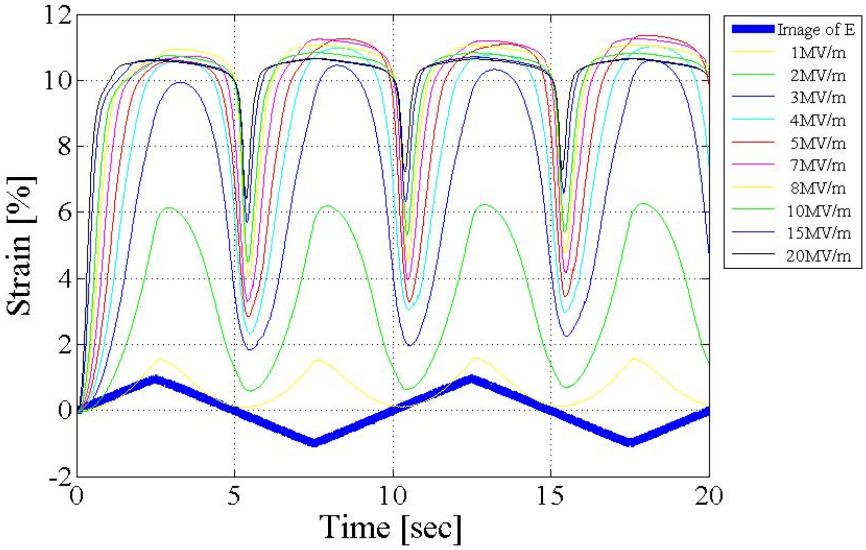

Figure 5.4 2-cycle of sawtooth wave electric field induced strain of pure PU thick film.

Looking at the position of the minima on the strain before beam irradiation, it is clear that they don't coincide with the zeros of the driving electric field, it means that the global looses are quite high. If we now look at the strain after beam irradiation, we notice first that the strain has increased by a factor 2 and, secondly that the minima of the strain function almost coincide with zero of the driving electric field. It means that the electron beam irradiation process increases the electrostrictive strain and lowered down the global losses.

Figure 5.5 shows maximum strain, S_{max}, of before and after HEBI versus maximum electric field, E_{max}, of 192 µm pure PU film. Both have the same thickness and they correspond to the specimens of Figure 5.4. The S_{max} was taken at the first peak of triangle input whereas E_{max}. The saturation in strain versus electric field by thick sample is clearly seen.

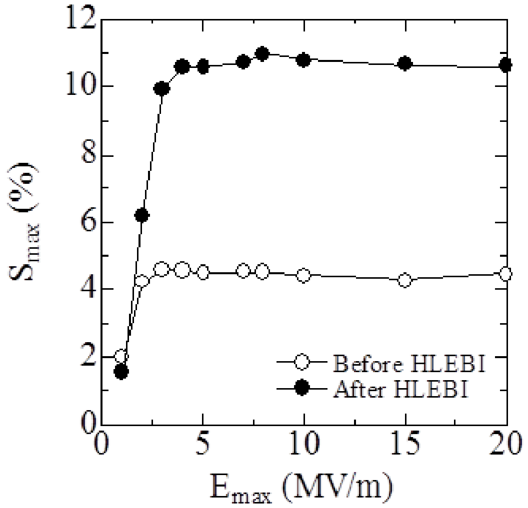

Figure 5.5 Maximum strain of thick (192 μm) pure PU film before and after HEBI at maximum electric field.

The HEBI significantly enhances the S_{max} of pure PU thick film. The S_{max} of after HEBI (6.19 %) thick film is 1.5 times higher than before HEBI (4.23 %) at low E_{max} of 2 MV/m. The S_{max} of after HEBI (10.62 %) thick film is more than two times higher than before HEBI of S_{max} (4.45 %) at 20 MV/m. The S_{max} is seen to have nonlinearly with the E_{max}. It can be clearly seen in Figure 5.5 that the parabolic relation of S_{max} (E_{max}) disappeared when the electric field is increased. The *S(E)* saturations are marked. Starting point of divergence occurred at a higher electric field after HEBI for pure PU film.

c) Electroactive strain decay by aging after HEBI

To check of the electrostrictive polymer aging, I measure the strain two months after irradiation and compare the new results with the previous ones.

Figure 5.6 shows maximum strain, S_{max}, of thick (192 μm) pure PU film before (○) and after HEBI (●) at maximum electric field, E_{max}, together with the aged film for two months after irradiation (◎). Although the HEBI strain curve has dropped by a factor of two, it remains higher than the non-irradiated strain curve (4.45 %).

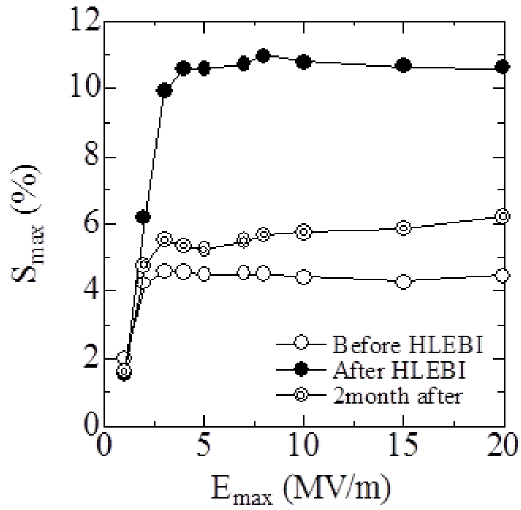

Figure 5.6 Maximum strain of thick (192 µm) pure PU film before (○) and after HEBI (●) at maximum electric field, together with the aged film for two months after irradiation (◎).

5.3.2 Discussion

a) Electroactive strain enhanced effect by HEBI

Although pure PU thick film was not changed by corona treatment, pure PU thick film was changed by HEBI. The HEBI can cut weak bonds in pure PU. Thus dangling bonds are created by HEBI. When dangling bonds are made by HEBI, there are unbounded shell electrons on terminated atoms at dangling bonds. Briefly, enhanced S_{max} is explained by unbounded shell electrons on terminated atoms at dangling. Consequently, it is possible the dangling bonds to increase the polarization sites of molecules by cutting the weak bonding in molecules. Furthermore, it is possible that injected electrons are charged and a part of trapped in the pure PU thick film. These trapped electrons probably act as polarized sites, resulting in a S_{max} enhancement.

On the other hand, the aging for two months cannot perfectly annihilate the enhancement effect of S_{max} by HEBI of pure PU thick film. The effect induced by HEBI seems to be a long term effect.

Therefore, I conclude that the S_{max} enhanced effect induced by HEBI should be a long term effect induced by dangling bonds as well as charging electrons. I am presently working on improving the process to stabilize the irradiated strain curve.

b) Penetration depth of HEBI

The penetration depth of the HEBI is always an important factor. In the present thesis, matrix of the sample film is pure PU. Thick pure PU film (192 µm) was prepared to confirm it. There exist two methods to express the penetration depth. One is the method proposed by Christenhusz and Reimer which expresses the HEBI depth, D_{th}, in meter by the density, ρ, in kgm^{-3} and by the irradiation voltage, V, in kV has been expressed by the following equation **[122]**.

$$D_{\mathrm{th}} = 66.7\, V^{5/3}/\rho \qquad (5.2)$$

The input electrical potential of 170 keV decreases when it arrives at the surface to 128 keV. It is estimated with the 10 μm thickness of the titanium (density: 4540 $\mathrm{kgm^{-3}}$) window and the 30 mm distance between the sample and the window in the nitrogen gas atmosphere (density: 1.13 $\mathrm{kgm^{-3}}$). Since the density of the pure PU is 1130 $\mathrm{kgm^{-3}}$. The HEBI depth estimated from eq. (5.2) is 192 μm. Figure 5.7 shows density dependent effective depth of HEBI for pure PU.

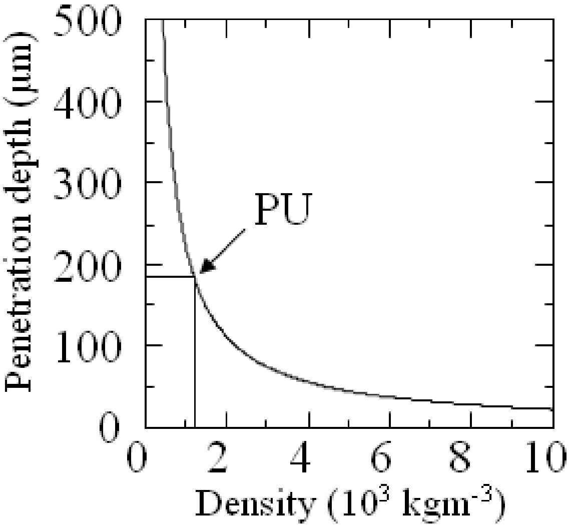

Figure 5.7 Change in penetration depth of HEBI versus density.

The second method proposed by Libby relates it to the mass thickness ($\mathrm{gm^{-2}}$), l_0, and irradiation voltage (kV), Ee, expressed by the following equation **[123]**.

$$l_0 = Ee^{5/3} / 150 \qquad (5.3)$$

The estimated mass thickness is 34.8 $\mathrm{gm^{-2}}$, when the initial irradiation voltage is 170 kV. Since both mass thickness values of Ti foil (1.78 $\mathrm{mgm^{-2}}$) and nitrogen gas (0.15 $\mathrm{mgm^{-2}}$) reduces the HEBI depth, the mass thickness of pure PU sample is 32.87 $\mathrm{gm^{-2}}$. Thus, the irradiation voltage on the sample surface is expressed by the following equation **[123]**.

$$Ee = (150\, l_0)^{3/5} \qquad (5.4)$$

As mentions above, the effective penetration depth of HEBI for pure PU is estimated as 192 μm by the first method, whereas it is 291 μm by the second. The calculated values are concerns irradiation from only one surface, but in the experiments, the irradiation is carried out on both surfaces. Nevertheless, regardless of how the depth is calculated, it is clear that the radiation has totally penetrated the 192 μm thick pure PU film.

5.4 Composite 0.45 vol% thin film of HEBI

As a result of thick pure PU, since the composites fabrication process was not charged, I could not measure them. Now, I have to evaluate and explain the effect of HEBI on the maximum strain, S_{max}, of 0.45 vol% composite thin film.

5.4.1 Results

a) Effects of HEBI on electroactive strain

In order to enhance the S_{max} induced by the polarization, the composite 0.45 vol% thin film (14 µm) has been homogeneously irradiated by HEBI.

Figure 5.8 shows the electric field-induced strain of (a) before HEBI and (b) after HEBI under 2-cycle of a sawtooth wave electric field with various amplitudes. The image of the electric field is represented in the figure by a blue bold line. When 2-cycle of a triangle wave electric field was induced into the polymer, the strain has 4-semi-triangular shape when the electric field is low. When the electric field is raised, it has round-shape.

(a) Before HEBI

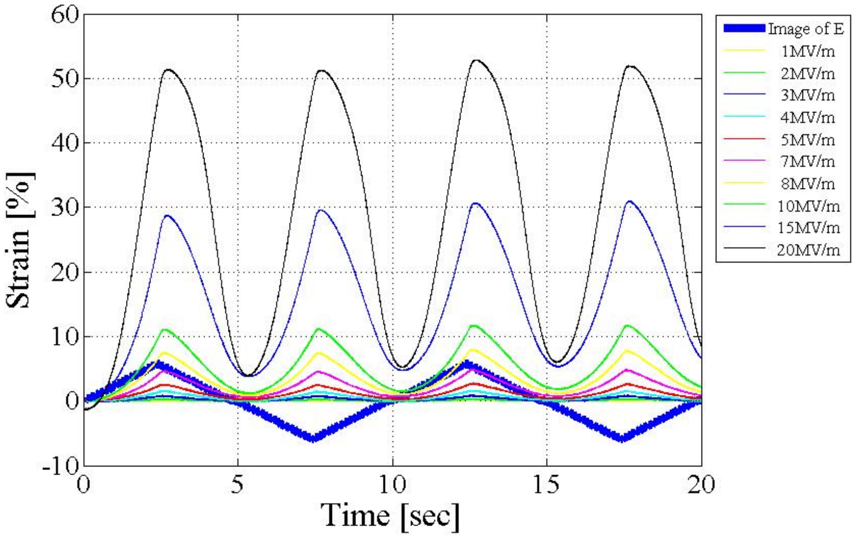

(b) After HEBI

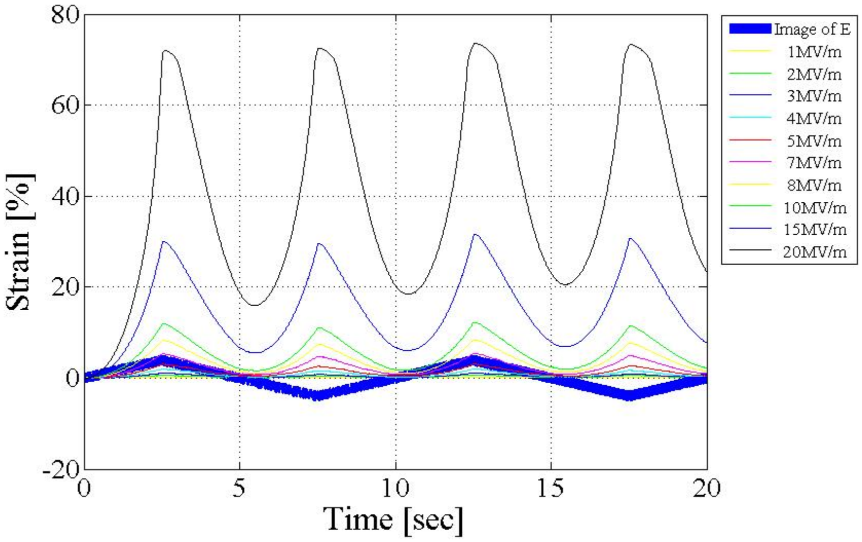

Figure 5.8 2-cycle of sawtooth wave electric field induced strain of composite 0.45 vol% thin film.

As it was for pure PU, the electrostrictive strain of the composite is significantly enhanced by electron beam irradiation as its can seen by comparing the curve before and after irradiation. The strain at 20 MV/m is 52 % before HEBI and it is boosted to 72 % after HEBI. The position of the strain minima coincide with the zero on the driving field. Consequently the strain and field are almost in phase, though the global losses very limited.

Figure 5.9 shows maximum strain, S_{max}, versus maximum electric field, E_{max}, of 14 µm composite 0.45 vol% thin film. Both have the same thickness and they correspond to the specimens of Figure 5.8. The S_{max} was taken at the first peak of triangle input whereas E_{max}.

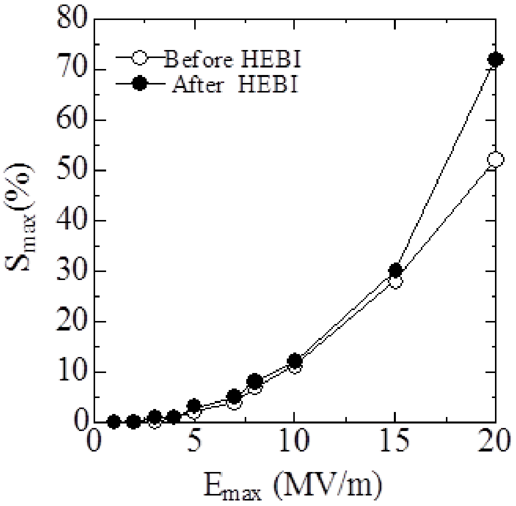

Figure 5.9 Maximum strain (S_{max}) of composite thin film before (○) and after HEBI (●) against maximum electric field (E_{max}).

In the low electric input regime, from 1 to 15 MV/m, S_{max} remains at more (slight increase less than 1 %) or less the same level even after HEBI. Although the S_{max} at 20 MV/m is already large before irradiation, a great enhancement of S_{max} is obtained after HEBI, i.e., from 52 to 72 %, or in other words a 1.3-fold increase. It is clear that HEBI generates a remarkable enhancement in S_{max}.

b) Volume expansion induced by HEBI

The HEBI often induces a large fracture strain of the polymer sheet to occur in a homogeneous fashion. It can be said that HEBI is a good tool for generating dangling bonds **[117-120]**. These, in turn, probably expand the polymer molar volume, that is generating the free volume **[124, 125]**, because of repulsive force between them **[117-120]**. Electric field is thus expected to enhance the electroactive strain by a large reduction of free volume among polymer molecules treated by HEBI.

The film thickness probably contributes to the crystalline volume fraction. The present sample thickness is only 14 µm and the volume fraction is thus estimated to be sufficiently high from the beginning. The effect of HEBI on the crystalline form has been investigated.

Figure 5.10 (a) portrays X-ray diffraction peaks of composite film before (gray line) and after (black line) HEBI. The peak height of an irradiated sample at the high angle side is lower than its counterpart before irradiation, as shown in the expanded Figure 5.10 (b).

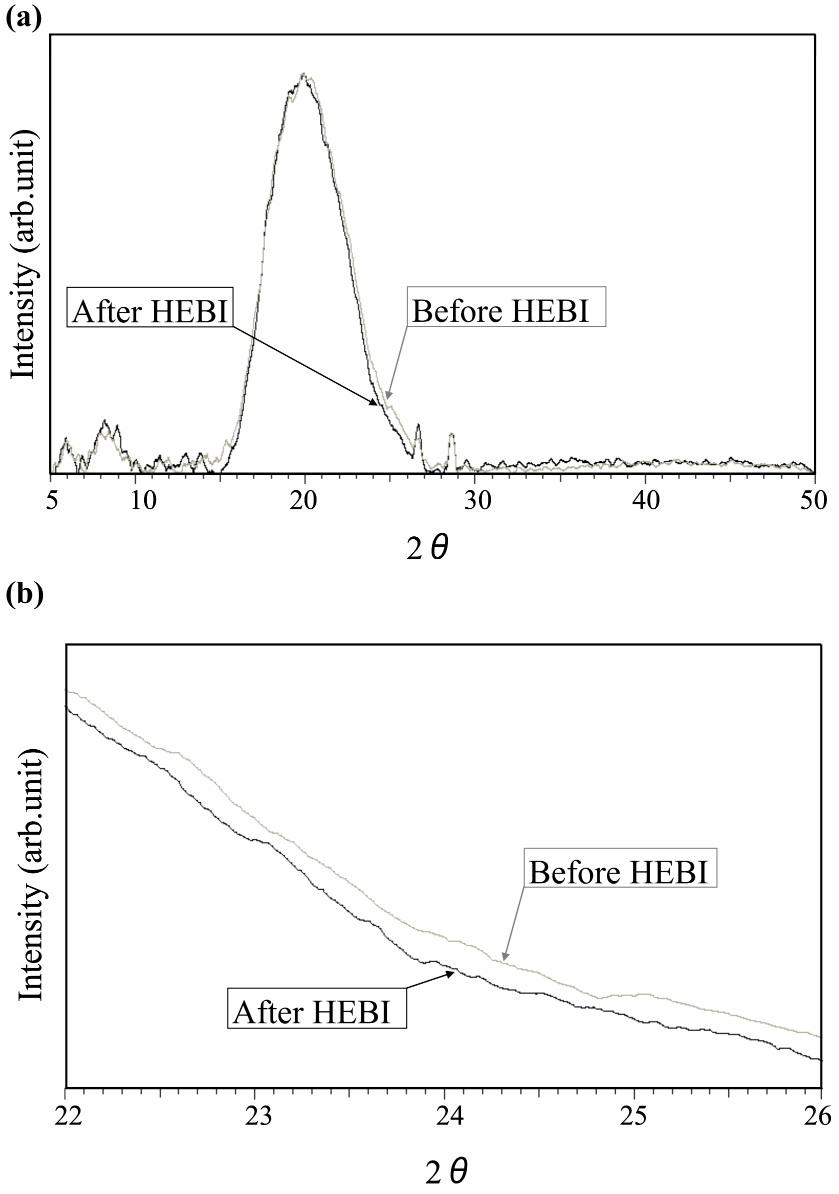

Figure 5.10 (a) X-ray diffraction peaks of composite thin films before (gray line) and after (black line) HEBI and (b) from 22 to 26 degrees.

HEBI sharpens the peak of X-ray diffraction. The sharpness of the peak corresponds to an enhancement of the periodicity perfection of the crystalline form of hard segments. Consequently, HEBI can be said to increase the perfection of the crystallites.

5.4.2 Discussion

a) Monomer arrangement model

In the low electric input regime, the Maxwell effect is in general used to explain the observations **[38]**. It gives a linear relation between the strain and squared electric field. Here, I propose the idea of free volume affecting the strain induced by the Maxwell effect.

Figure 5.11 presents a diagram of the side-by-side arrangement of monomers of an anisotropic polymer when the electric field is applied. The black circles represent CB nanoparticles and the squares correspond to polymer molecules of hard segments. Before HEBI, the atomic bonds between the polymer molecules are assumed not to be broken by either the input or increase of the electric field.

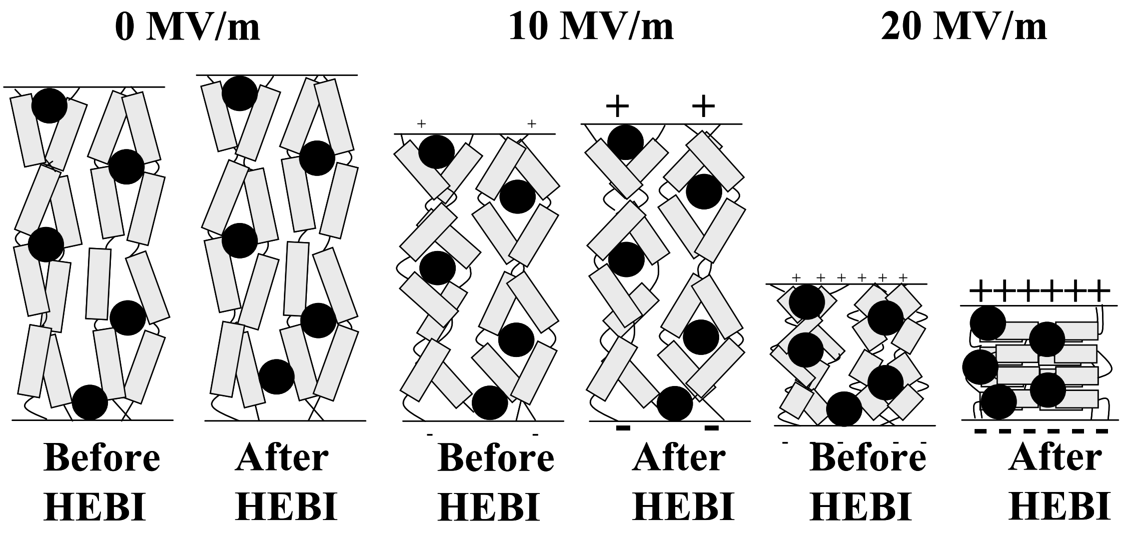

Figure 5.11 Electroactive strain model of both the Maxwell effect and polarization of composite thin films before and after HEBI at several values of S_{max}.

HEBI is in general believed to cut weak atomic bonds thus causing a great number of dangling bonds in polymers **[117-120]**. Consequently, repulsive force between these dangling bonds at terminated atoms in the polymer molecules are created and they expand with an excess free volume in polymers, as illustrated in Figure 5.11 (0 MV/m, after HEBI). With flexible dangling bonds, the compression becomes easier in the sample after HEBI, so that the difference appears to be significant in the high electrical input regime, see Figure 5.11 at 20 MV/m. This is due to the fact that the irradiation effect appears only in the high electric regime in the result of strain versus electric field shown in Figure 5.9. The peak height of an irradiated sample at the high angle side is lower than its counterpart before irradiation, as shown in the expanded Figure 5.10 (b). This fact indicates that HEBI reduces the X-ray peak angle, which represents the volume expansion, as shown in the diagram in Figure 5.11 (0 MV/m, after HEBI).

b) Polarization of the composite thin film

Bharti et al reported that P(VDF-TrFE) 50/50 mol% copolymer 25 μm films change in the polarization hysteresis loop with irradiation dose. Figure 5.12 shows the 30-Mrad-irradiated films exhibit hysteresis with a reduced remnant polarization and coercive field in comparison to unirradiated film. Interestingly, after irradiation with 60 Mrad, the X-ray diffraction peak becomes sharper and more intense in comparison with unirradiated **[43]**.

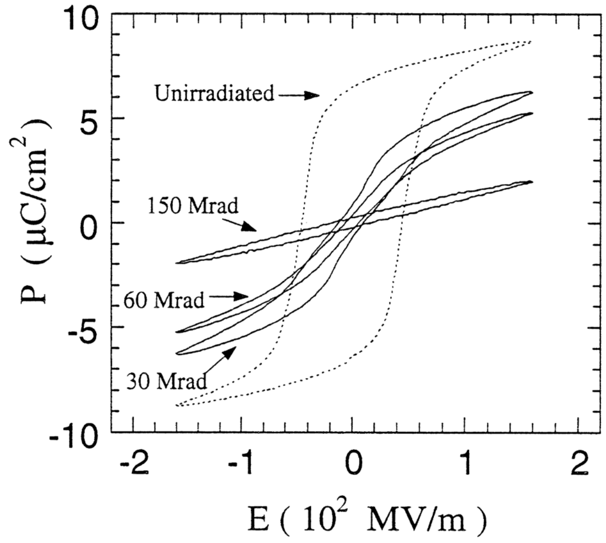

Figure 5.12 Change in the polarization hysteresis loop with irradiation dose for P(VDF-TrFE) 50/50 mol% copolymer films irradiated at 120 °C. [43]

The 0.45 vol% composite thin film (14 μm) polarization was computed by performing a straight integration of the current. This current can be split in two currents: one being the "capacitive" current and the second one the current flowing in the resistance in parallel with the capacitance. It is not possible to separate these two currents and consequently the current integration does not correspond exactly to the polarization.

Figure 5.13 shows polarization of the 0.45 vol% composite thin film (14 μm) before (a) and after HEBI (b) at several values of the E_{max}. The curves are closed and present almond shapes. As previously explained in chapter 2, the inner surface represent the energy loss.

Figure 5.13 (b) inner surface is much smaller than Figure 5.13 (a). It means that the energy losses after HEBI are smaller than before HEBI. This confirms the losses reduction due to the HEBI already mentioned previously.

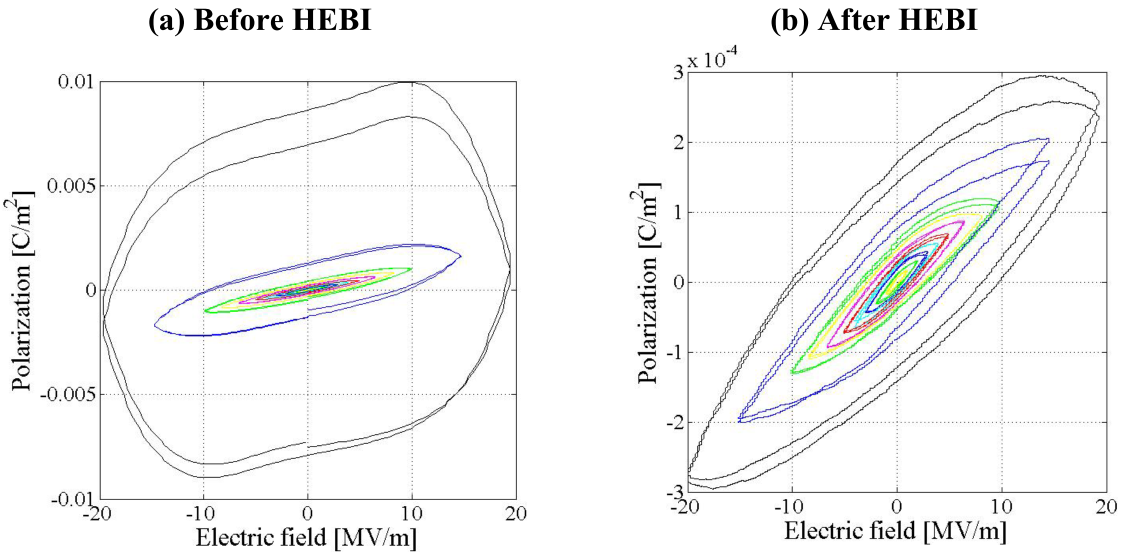

Figure 5.13 Electric field induced polarization of 0.45 vol% composite film (a) before and (b) after HEBI.

5.5 Conclusions

The purpose of the present chapter is to evaluate and explain the effect of corona treatment and HEBI on the electroactive strain.

Pure PU thick film (194 μm) was not changed by corona treatment, pure PU thick film (192 μm) was changed by HEBI. The maximum strain, S_{max}, of after HEBI (10.62 %) thick film is more than two times higher than that before HEBI (4.45 %) at 20 MV/m.

Since the estimated penetration depth is between 192 and 291 μm on both side surfaces, I conclude that the HEBI injects and implants electrons throughout the entire PU thick film.

The HEBI can cut weak bonds in pure PU. Thus dangling bonds are made by HEBI. When dangling bonds are made by HEBI, there are unbounded shell electrons on terminated atoms at dangling bonds. Briefly, enhanced S_{max} is explained by unbounded shell electrons on terminated atoms at dangling. Consequently, it is possible the dangling bonds to increase the polarization sites of molecules by cutting the weak bonding in molecules. Furthermore, it is possible that injected electrons are charged and trapped a part in the trapped in the pure PU thick film. These trapped electrons probably act as polarized sites, resulting in a S_{max} enhancement effect by HEBI on S_{max} of pure PU thick film.

On the other hand, the aging for two months cannot perfectly annihilate the enhancement effect of S_{max} by HEBI of pure PU thick film. The effect induced by HEBI seems to be a long term effect.

To summarize, I could say that: 0.45 vol% composite thin film (14 μm) undergoes a 1.3-fold increased strain for irradiated samples, compared to its non-irradiated counterpart. The free-volume was considered to be the reason for this enhancement. Since HEBI formed dangling bonds at the weak bond sites in the crystalline parts of the PU, the repulsive force between these dangling bonds of terminated atoms generated a volume expansion of the PU matrix. The extremely large S_{max} of the film treated by HEBI was explained by a Maxwell effect induced by the large volume shrinkage as well as by compressive electrostriction brought on by a perfect periodicity of the hard crystalline segments evaluated by X-ray diffraction.

Conclusions

The present thesis focuses on the so-called smart materials, especially on electroactive and / or electrostrictive polymers.

A high strain level was obtained by pure polyurethane (PU) sample, more than 30 %, at moderate electric field, less than 20 MV/m with 28 µm film thickness. Besides, a strong enhancement was also obtained by carbon black (CB) nanoparticles doping. I proposed manufacturing method enables a good dispersion of particles without recourse to the ultrasonic mixing and without using spin-coating. It is therefore an important result because it then becomes possible to obtain large area films with good conductive particles dispersion. Strains of the order of 50 % were reached (0.89 vol% CB composite, 21 µm). By such a small quantity of carbon addition, 0.89 vol%, a high strain enhancement, a factor of 1.6, was obtained at 20 MV/m. It thus confirmed the effectiveness of the conductive filler. Such low electric input requirement can lead the possibility of EAPs to be used easily with other electrical devices.

Mechanism was discussed with mathematical modeling based on saturated polarization, developed with the help of advisers. Since the simulations are in good agreement with experimental results, the hypothesis is valid. It was revealed that the strong connection occurs between the equivalent permittivity of film and its strain.

The relation between strain and electric field was found nonlinear. *S(E)* saturation was observed. This phenomenon occurs strongly in thick samples. Very thin samples show a start of *S(E)* saturation over 20 MV/m but almost all the others have it at 3-10 MV/m. The thickness effect is obvious. It seems that the crystallization depends on the film thickness. Thin films might have a hard segment rate higher than the thick films, which would increase the strain. This *S(E)* saturation can be fully explained by the model of saturated polarization with the equivalent permittivity.

Several models in linear and nonlinear developed based on that assumption were established and also confirmed.

The forms of the current and the apparent polarizations were shown. The current shape exhibits that the film material had changed from purely capacitive to mixture with resistive when the induced electric field amplitude is increased. Non linear resistance was proposed. By the comparison with linear resistance model results and with the experimental results, that effectiveness was developed.

More strain enhancement has been tried by injection of electron. Two methods were carried out; corona and homogeneous electron beam irradiation (HEBI) treatments. Corona treatment did not provide a great enhancement. Beside, the electrostrictive strain after HEBI has been multiplied the enhancement factor more than 2. It seems also that the HEBI strongly reduces the electrical losses in material. In the comparison with corona treatment of which the effect decreases within a few hours, it was confirmed experimentally that the effect by HEBI decreases less rapidly with time as I noted a substantial reduction of the effect after 2 months.

List of published

1) J. Okawa, M. Kanda, K. Yuse, D. Guyomar, H-H. Uchida and Y. Nishi
Giant Reversible Bending Motion of Unimorph Composites Driven by Hydrogen Storage Alloy Powders Dispersed Polyurethane and Supported by Titanium Thin Sheet
Sensors and Actuator B: Chemistry, submitted
2) K. Yuse, D. Guyomar and M. Kanda
Thickness effects in electroactive polymers actuators: a simple explanation and modeling
Proceeding of SPIE, San Diego, California, USA (March 2011)
Proc. SPIE 7984, 79841M
3) D. Guyomar, P.-J. Cottinet, L. Lebrun, C. Putson, K. Yuse, M. Kanda and Y. Nishi
The compressive electrical field electrostrictive coefficient M_{33} *of electroactive polymer composites and its saturation versus electrical field, polymer thickness, frequency and fillers*
Polym. Adv. Technol. (2011) DOI 10.1002/pat.1993
4) D. Guyomar, K. Yuse and M. Kanda
Thickness effect on electrostrictive polyurethane strain performances : A three-layer model
Sensors and Actuators A **168** (2011) 307-312.
5) K. Yuse, D. Guyomar, M. Kanda, L. Seveyrat and B. Guiffard
Development of large-strain and low-powered electro-active polymers (EAPs) using conductive fillers
Sensors and Actuators A **165** (2011) 147-154.
6) D. Guyomar, K. Yuse, P.-J. Cottinet, M. Kanda and L. Lebrun
Focus on the electrical field-induced strain of electroactive polymers and the observed saturation
Journal of Applied Physics **108** (2010) 114910
7) Y. Nishi, Y. Ebihara, N. Kunikyo, M. Kanda, K. Iwata, K. Yuse, B. Guiffard, L. Lebrun and D. Guyomar
High Electric Conductive PMMA Composites without Impact Value Decay by Dispersion of Copper Powder
Materials Transactions **51** (2010) 1437-1442.

Abstract

Copper powder dispersed poly-methyl methacrylic acid (acrylic resin, PMMA) composites (PMMA-Cu) were prepared by the solution cast method. The Cu addition at the critical volume fraction (15.0± 1.0vol%Cu) drastically enhanced the electric conductivity from the insulator (10^{-14} Sm^{-1}) to the electric conductor (10^{5} Sm^{-1}). The electric conductivity can be obtained by controlling the volume fraction of copper powders in PMMA polymers, as dilatation. The addition of 10vol%Cu slightly enhanced the impact value of PMMA, whereas the remarkable decrease in the Charpy impact value was found at 25 ± 5 vol%Cu. The high conductive PMMA-Cu composites (from 15 to 20 vol%Cu) with high impact value (5.5 ± 0.5 kJm^{-2}), which was higher than that of dispersed nylon6 composites (2 kJm^{-2}) utilized for practical exteriors, were obtained without impact value decay by addition of small amount of copper powders.

8) J. Okawa, M. Kanda, K. Yuse, H-H. Uchida, D. Guyomar and Y. Nishi
Reversible Bending Motion of Unimorph Composites Driven by Combining $LaNi_5$ Alloy Powders Dispersed Polyurethane and Thin Supporting Copper Sheet under Partial Hydrogen Gas Pressure
Materials Transactions **51** (2010) 994-1001.

Abstract

The polyurethane composites dispersed with powders mixture of $LaNi_S$ hydrogen storage alloy (35 vol% of $LaNi_5$) and $Pd\text{-}Al_2O_3$ catalyst powders were prepared by solution cast method, which easily controlled the shape and mixed ratio of the composites. In order to generate the bending strain of reversible up motions at vertical and horizontal directions, the unimorph ($PU+LaNi_5/Cu$) sheet constructed with the driving polyurethane composite and supporting copper thin sheet of 10 μm thickness with high specific stiffness (apparent hardening modulus per specific weight) was prepared.

Although the bending motion of the unimorph sheet operated by hydrogenation under 0.3 MPa H_2 gas was irreversible, the reversible motion was detected under 0.2 MPa H_2 gas. The maximum strain of reversible bending motion (ε^{max}) of the $PU+LaNi_5/Cu$ sheet is more than 1520 and 1120ppm on vertical and horizontal directions, respectively. The ε^{max} of the $PU+LaNi_5/Cu$ sheet at vertical direction was slightly higher than that of the ABS resin unimorph ($ABS+LaNi_5/ABS$) sheet constructed with the driving ABS resin composites and pure ABS resin supporting sheet, whereas it was slightly lower than that of the silicone rubber unimorph ($SR+LaNi_5/SR$) sheet constructed with the driving silicone rubber composites and pure silicone rubber supporting sheet. It can be estimated that the responsiveness ($d\varepsilon/dt$) of cyclic motion of the ($PU+LaNi_5/Cu$) sheet is slightly higher than $ABS+LaNi_5/ABS$ sheet.

9) Y. Nishi, N. Kunikyo, M. Kanda, L. Lebrun and D. Guyomar
Impact Value of High Electric Conductive ABS Composites with Copper Powder Dispersion Prepared by Solution-Cast Method
Materials Transactions **51** (2010) 165-170.

Abstract

Copper powder dispersed acrylonitrile butadiene styrene (ABS) composites were prepared by the solution cast method. Although the addition of Cu greatly enhanced the electric conductivity at the critical volume fraction (19.0+/—1.0 vol%Cu) from the insulator to the electric conductor, the decrease in the Charpy impact value was gradual. Since the impact value of the ABS polymer prepared by the solution cast method was 1.75 times larger than that before treatment, it is clear that the solution casting improved the impact value. When the volume fraction of Cu powders of high electric conductive ABS composites was from 20 to 30 vol%Cu, the impact value was 7 kJm^{-2}. The moderated impact value was not only 44% of that of pure ABS polymer before solution casting, but was also higher than that of dispersed nylon6 composites (2 kJm^{-2}) utilizeed for practical exteriors.

10) Y. Nishi, J. Okawa, A. Shimazu, R. Suenaga, Y. Ebihara, D. Kubo, M. Kanda, K. Yuse, D. Guyomar and H-H. Uchida
Giant Bending Strain of Reversible Motion of Uni-Morph Soft Mover Composites Driven by Hydrogen Storage Alloy Powders Dispersed in Polyurethane Sheet
Materials Transactions **50** (2009) 2460-2465.

Abstract

In order to generate the bending motion operated by pressure change in hydrogen gas, soft uni-morph composites were prepared, in which composites dispersed with not only driving particles of $LaNi_5$ hydrogen storage alloy with $Pd\text{-}Al_2O_3$ catalyst powders to get high responsiveness, were piled up on a simple polyurethane sheet. Since the highest values of irreversible bending strain at the first hydrogenation (ε^1) under 0.3 MPa H_2 gas and the maximum irreversible bending strain during hydrogenation cycles (ε^m) were remarkably obtained at the 35 vol% of $LaNi_5$ powders dispersed in polyurethane composites, the bending strain of reversible motion was detected from the first to the 8th hydrogenation (ε_r1 and ε_r^8) under 0.2 MPa H_2 gas. The bending strain of reversible motion of polyurethane composites sheet is more than 2000 ppm, which was approximately equal to that of silicone rubber composites and is extremely larger than that (300 ppm) of ABS resin composites. Responsiveness ($d\varepsilon/dt$) of cyclic motion of elastic deformed mover composites, which were constructed with 35 vol%$LaNi_5$ dispersed powder and matrix of polyurethane or silicone rubber, were more than 10 times higher than that of ABS composite.

11) M. Kanda, Y. Nishi
Effects of Water Absorption on Impact Value of Aluminum Dispersed Composite Nylon 6
Materials Transactions **50** (2009) 177-181.

Abstract

Composite polymers, which are nylon6 materials with aluminum powders dispersed homogeneously, are prepared. Influences of water absorption on Charpy impact value of composite polymers have been investigated. Although the aluminum dispersion from zero to 40 vol% Al decreases the impact value, the water absorbing treatment for 10^5 s at boiling point largely increases the impact values of all composite polymers. It is explained that water molecules in nylon6 mainly relaxes the impact force. If the water absorption also enhances the interfacial energy to form the crack in nylon 6 and its composites, the high impact value with smooth undulating surface can be explained.

International conferences

1) K. Yuse, D. Guyomar and M. Kanda
   Thickness effects in electroactive polymers actuators: a simple explanation and modeling
   SPIE, San Diego, California, USA (March 2011)
2) J. Okawa, A. Shimazu, Y. Ebihara, M. Kanda, K.Yuse, D. Guyomar, H-H. Uchida and Y. Nishi
   Giant Reversible Bending Motion of Composites Driven by Hydrogen Storage Alloy Powders Dispersed Polymer Operated by Partial Pressure of Hydrogen Gas
   ACTUATOR 2010, Bremen, Dentschland (June 2010), Poster presentation
3) J. Okawa, A. Shimazu, Y. Ebihara, M. Kanda, K.Yuse, D. Guyomar, H-H. Uchida and Y. Nishi
   Giant Revrsible Bending Motion of Hydrogen Strage Alloy Powder Dispersed Composites Polyurethane on Metal Sheet Operated by Partial Pressure of Hydrogen gas
   11th Japan International SAMPE Symposium and Exhibition, Tokyo, Japan (November 2009)
4) T. Yamamoto, Y. Ebihara, R. Suenaga, M.Kanda, K. Itou and Y. Nishi
   Mechanical Properties of Water Absorbed Nylon 6 Composites with Metal Powders Dispersion
   11th Japan International SAMPE Symposium and Exhibition, Tokyo, Japan
   (November 2009)
5) M. Kanda, K. Yuse, B. Guiffard and D. Guyomar
   Large field induced strain in carbon nano-filled composite polyurethane (PU)
   SMART'09, Porto, Portugal (July 2009)

References

1 K. Yuse, D. Guyomar, M. Kanda, L. Seveyrat and B. Guiffard, *Development of large-strain and low-powered electro-active polymers (EAPs) using conductive fillers*, Sensors and Actuators A, **165** (2011) 147-154.

2 S. Okamoto, K. Kuwabara and k. Otsuka, *Electrical stimuli-induced deformation and material properties of electro-active polymer Nafion117*, Sensors and Actuators A, **125** (2006) 376-381.

3 R. Pelrine, R. Kornbluh and J. Joseph, *Electrostriction of polymer dielectrics with compliant electrodes as a means of actuation,* Sensors and Actuators A, **64** (1998) 77-85.

4 R. Pelrine, R. Kornbluh, J. Joseph, R. Heydi, Q. Pei and S. Chiba, *High-field deformation of elastomeric dielectrics for actuators*, Materials Science and Engineering C, **11** (2000) 89-100.

5 Q. Pei, R. Pelrine, S. Stanford and R. Kornbluh, *Marcus Rosenthal, Electroelastomer rolls and their application for biomimetic walking robots*, Synthetic Metals, **135-136** (2003) 129-131.

6 Y. Liu, K. Ren, H. Hofmann and Q. M. Zhang, *Investigation of Electrostrictive Polymers for Energy Harvesting*, IEEE Trans Ultrason Ferroelectr Freq Control., **52** (2005) 2411-2417.

7 K. Ren, Y. Liu, H. Hofmann, and Q. M. Zhang, *An active energy harvesting scheme with an electroactive polymer*, Appl. Phys. Lett., **91** (2007) 132910.

8 L. Lebrun, D. Guyomar, B. Guiffard, P.-J. Cottinet and C. Putson, *The Characterisation of the harvesting capabilities of an electrostrictive polymer composite*, Sensors and Actuators A, **153** (2009) 251-257.

9 K. Bhattacharya and G. Ravichandran, *Ferroelectric perovskites for electromechanical actuation*, Acta Materialia, **51** (2003) 5941-5960.

10 A. J. Masys, W. Ren, G. Yang, and B. K. Mukherjee, *Piezoelectric strain in lead zirconate titante ceramics as a function of electric field, frequency, and dc bias*, J. Appl. Phys., **94** (2003) 1155-1162.

11 P. D. Wilcox, R. S. C. Monkhouse, P. Cawley, M. J. S. Lowe and B. A. Auld, *Development of a computer model for an ultrasonic polymer film transducer system*, NDT & E lnternational, **31** (1998) 51-64.

12 H. Lee, R. Cooper, K. Wang and H. Liang, *Nano-Scale Characterization of a Piezoelectric Polymer (Polyvinylidene Difluoride, PVDF)*, Sensors, **8** (2008) 7359-7368.

13 S. Sokhanvar, J. Dargahi and M. Packirisamy, *Influence of friction on piezoelectric sensors*, Sensors and Actuators A, **141** (2008) 120-128.

14 W. Wang, H. Fan, Y. Ye, *Effect of electric field on the structure and piezoelectric properties of poly(vinylidene fluoride) studied by density functional theory*, Polymer, **51** (2010) 3575-3581.

15 R. Kornbluh, R. Pelrine, Q. Pei, R. Heydt, S. Stanford, S. Oh, and J. Eckerle, to be published in Proc. SPIE, Smart Structures and Materials 2002:Industrial and Commercial Applications of Smart Structures Technologies, 4698 (2002).

16 S. P. Lacour, S. Wagner, H. Prahlad and R. Pelrine, *High voltage photoconductive switches of amorphous silicon for electroactive polymer actuators*, Journal of Non-Crystalline Solids, **338-340** (2004) 736-739.

17 R. Heydt, R. Kornbluh, R. Pelrine and V. Mason, *Design and performance of an electrostrictive-polymer-film acoustic actuator*, Journal of Sound and Vibration, **215** (1998) 297-311.

18 R. Pelrine, R. Kornbluh and G. Kofod, *High-Strain Actuator Materials Based on Dielectric Elastomers*, Adv. Mater., **12** (2000) 1223-1225.

19 S. P. Lacour, H. Prahlad, R. Pelrine and S. Wagner, *Mechatronic system of dielectric elastomer actuators addressed by thin film photoconductors on plastic*, Sensors and Actuators A, **111** (2004) 288-292.

20 R. H. Baughman, C. Cui, A. A. Zakhidov, Z. Iqbal, J. N. Barisci, G. M. Spinks, G. G. Wallace, A. Mazzoldi, D. De Rossi, A. G. Rinzler, O. Jaschinski, S. Roth, and M. Kertesz, *Carbon nanotube actuators*, Science, **284** (1999) 1340-1344.

21 Y. Bar-Cohen, *Electro-active polymers: current capabilities and challenges*, Paper 4695-02, Proceedings of the SPIE Smart Structures and Materials Symposium, EAPAD Conference, San Diego, CA, March 18-21, 2002

22 D. Hanson, G. Pioggia, Y. Bar-Cohen and D. de Rossi, *Androids: application of EAP as artificial muscles to entertainment Industry*, Proceedings of EAPAD, SPIE's 8th Annual International Symposium on Smart Structures and Materials, 5-8 March,2001, Newport, CA. Paper No. 4329-74

23 G. Nishida, K. Takagi, B. Maschke and T. Osada, *Multiscale distributed parameter modeling of ionic polymer-metal composite soft actuator*, Control Engineering Practice **19** (2011) 321–334.

24 T. Hirai, T. Ueki and M. Takasaki, *Electrical Actuation of Textile Polymer Materials*, Journal of Fiber Bioengineering and Informatics (JFBI) **1** (2008) doi:10.3993/jfbi06200801

25 K. J. Kim and M. Shahinpoor, *A novel method of manufacturing three-dimensional ionic polymer-metal composites (IPMCs) biomimetic sensors, actuators and artificial muscles*, Polymer, **43** (2002) 797-802.

26 S. Nemat-Nasser and Y. Wu, *Comparative experimental study of ionic polymer–metal composites with different backbone ionomers and in various cation forms*, J. Appl. Phys., **93** (2003) 5255-5267.

27 M. Shahinpoor and K. J. Kim, *Ionic polymer-metal composites: I. Fundamentals*, Smart Mater. Struct., **10** (2001) 819-833.

28 S. Nemat-Nasser, *Micromechanics of actuation of ionic polymer-metal composites*, J. Appl. Phys., **92** (2002) 2899-2915.

29 Y. Bar-Cohen, T. Xue, M. Shahinpoor, J. 0. Simpson, and J. Smith, *Flexible, low-mass robotic arm actuated by electroactive polymers*, Proc. of SPIE's 5 th Annual Int. Symp. on Smart Structures and Materials, San Diego, CA. 1998 pp. 1-6

30 H. Tamagawa and M. Taya, *A theoretical prediction of the ions distribution in an amphoteric polymer gel*, Materials Science and Engineering A, **285** (2000) 314-325.

31 G. Filipcsei, J. Fehér and M. Zrínyi, *Electric field sensitive neutral polymer gels*, Journal of Molecular Structure, **554** (2000) 109-117.

32 Y. Osada and J.-P. Gong, *Soft and Wet Materials: Polymer Gels*, Adv. Mater., **10** (1998) 827-837.

33 T. Shiga, *Deformation and viscoelastic behavior of polymer gels in electric fields*, Adv. Polymer Sci., **134** (1997) 131-163.

34 R. H. Baughman, *Conducting polymer artificial muscles*, Synthetic Metals, **78** (1996) 339-353.

35 Y. Bar-Cohen, *EAP actuators as Artificial muscle*, SPIE-International Society or Optical Engine, October 2001.

36 S. Iijima, *Helical microtubules of graphitic carbon*, Nature, **354 (**1991) 56-58.

37 M. Endo, T. Hayashi, Y. A. Kim, M. Terrones and M. S. Dresselhaus, *Applications of carbon nanotubes in the twenty-first century*, Phil. Trans. R. Soc. Lond. A, **362** (2004) 2223-2238.

38 T. Mirfakhrai, J. D. W. Madden and R. H. Baughman, *Polymer artificial muscles*, materialstoday, **10** (2007) 30-38.

39 K. Kwok and W. K.S. Chiu, *Growth of carbon nanotubes by open-air laser-induced chemical vapor deposition*, Carbon, **43** (2005) 437-446.

40 A. M. Vinogradov, V. H. Schmidt, G. F. Tuthill and G. W. Bohannan, *Damping and electromechanical energy losses in the piezoelectric polymer PVDF*, Mechanics of Materials, **36** (2004) 1007-1016.

41 E. Bormashenko, R. Pogreb, Y. Socol, M. H. Itzhaq, V. Streltsov, S. Sutovski, A. Sheshnev and Y. Bormashenko, *Polyvinylidene fluoride-piezoelectric polymer for integrated infrared optics applications*, Optical Materials, **27** (2004) 429-434.

42 Q. M. Zhang, V. Bharti, and X. Zhao, *Giant Electrostriction and Relaxor Ferroelectric Behavior in Electron-Irradiated Poly(vinylidene fluoride-trifluoroethylene) Copolymer*, Science, **280** (1998) 2101-2104.

43 V. Bharti, G. Shanthi, H. Xu, Q. M Zhang and K. Liang, *Evolution of transitional behavior and structure of electron-irradiated poly(vinylidene fluoride–trifluoroethylene) copolymer films*, Materials Letters, **47** (2001) 107-111.

44 Z.-Y. Cheng, V. Bharti, T.-B. Xu, Haisheng Xu, T. Mai and Q. M. Zhang, *Electrostrictive poly(vinylidene fluoride-trifluoroethylene) copolymers*, Sensors and Actuators A, **90** (2001) 138-147.

45 Y.-C. Hsu, C.-C. Wu, C.-C. Lee, G. Z. Cao and I. Y. Shen, *Demonstration and characterization of PZT thin-film sensors and actuators for meso- and micro-structures*, Sensors and Actuators A, **116** (2004) 369-377.

46 G. Rujijanagul, S. Jompruan and A. Chaipanich, *Influence of graphite particle size on electrical properties of modified PZT–polymer composites*, Current Applied Physics, **8** (2008) 359-362.

47 F. Fang, W. Yang , M. Z. Zhang and Z. Wang, *Mechanical response of barium-titanate/polymer 0–3 ferroelectric nano-composite film under uniaxial tension*, Composites Science and Technology, **69** (2009) 602-605.

48 G. D. Zhu, X. Y. Luo, J. H. Zhang, B. L. Liu and X. J. Yan, *Fabrication of submicrometer- to micrometer-scale ferroelectric copolymer particles by solution mixture method*, Thin Solid Films, **517** (2009) 5734-5738.

49 J. Su, J. S. Harrison, T. L. Clair, Y. Bar-Cohen and S. Leary, *Electrostrictive graft elastomers and applications*, MRS Symposium: FF: Electroactive Polymers, Boston, MS (1999)

50 Y. Wang, C. Sun, E. Zhou and J. Su, *Deformation mechanisms of electrostrictive graft elastomer*, Smart Mater. Struct., **13** (2004) 1407-1413.

51 P. M. Taylor, D. M. Pollet, A. Hosseini-Sianaki and C. J. Varley, *Advances in an electrorheological fluid based tactile array*, Displays, **18** (1998) 135-141.

52 H. Fröhlich, *Theory of dielectrics*, Oxford University Press, London, 2nd edition, 1958

53 J. Su, Q. M. Zhang and R. Y. Ting, *Space-charge-enhanced electromechanical response in thin-film polyurethane elastomers*, Appl. Phys. Lett., **71** (1997) 386-388.

54 J. Su, Q. Zhang, P.-C. Wang, A. G. MacDiarmid and K. J. Wynne, *Preparation and Characterization of Electrostrictive Polyurethane Films with Conductive Polymer Electrodes*, Polymers for Advanced Technologies, **9** (1998) 317-321.

55 M. Watanabe, N. Wakimoto, H. Shirai, and T. Hirai, *Bending electrostriction and space-charge distribution in polyurethane films*, J. Appl. Phys., **94** (2003) 2494-2497.

56 B. Guiffard, L. Seveyrat, G. Sebaid and D. Guyomar, *Enhanced electric field-induced strain in non-percolative carbon nanopowder/polyurethane composites*, J. Phys. D, **39** (2006) 3053-3057.

57 Y. M. Shkel and D. J. Klingenberg, *Material parameters for electrostriction*, J. Appl. Phys., **80** (1996) 4566-4572.

58 Q. M. Zhang, J. Su, and C. H. Kim, *An experimental investigation of electromechanical responses in a polyurethane elastomer*, J. Appl. Phys., **81** (1997) 2770- 2776.

59 A. O'Halloran, F. O'Malley and P. McHugh, *A review on dielectric elastomer actuators, technology, applications, and challenges*, J. Appl. Phys., **104** (2008) 071101

60 W. Ma and l. E. Cross, *An experimental investigation of electromechanical response in a dielectric acrylic elastomer*, Appl. Phys. A, **78** (2004) 1201-1204.

61 Q. M. Zhang, H. Li, M. Poh, F. Xia, Z. Y. Cheng and C. H. Xu, *An allorganic composite actuator material with a high dielectric constant*, Nature, **419** (2002) 284 - 287.

62 S. C. Stanton, C. C. McGehee and B. P. Mann, *Nonlinear dynamics for broadband energy harvesting: Investigation of a bistable piezoelectric inertial generator*, Physica D, **239** (2010) 640-653.

63 J. Nuffer and T. Bein, *Application of piezoelectric materials in transportation industry*, Global Symposium on Innovative Solutions for the Advancement of the Transport Industry, 4-6. October 2006, San Sebastian, Spain

64 Y.-J. Wang, C.-D. Chen and C.-K. Sung, *Design of a frequency-adjusting device for harvesting energy from a rotating wheel*, Sensors and Actuators A, **159** (2010) 196-203.

65 L. Mateu and F. Moll, *Appropriate charge control of the storage capacitor in a piezoelectricenergy harvesting device for discontinuous load operation*, Sensors and Actuators A, **132** (2006) 302-310.

66 M. O. Mansour, M. H. Arafa and S. M. Megahed, *Resonator with magnetically adjustable natural frequency for vibration energy harvesting*, Sensors and Actuators A, **163** (2010) 297-303.

67 E. Minazara, D. Vasic, F. Costa and G. Poulin, *Piezoelectric diaphragm for vibration energy harvesting*, Ultrasonics, **44** (2006) e699-e703.

68 K. Yuse, P.-J. Cottinet and D. Guyomar, *14. Actuators and energy harvesters based on electrostrictive elastomeric nanocomposites*, Totle of the Book: *Recent Advances in Elestomeric Nanocomposites*. (2011) in press.

69 H. Prahald, R. Kornbluh, R. Pelrine, et al., *Dielectric elastomers and their applications in distributed actuation and power generator*, In: Proceedings of ISSS 2005. International conference on Smart Materials Structures and Systems, India (2005)

70 G. Sebald, E. Lefeuvre and D. Guyomar, *Pyroelectric energy conversion: optimization principles*, IEEE Trans. Ultrason. Ferroelectr. Freq. Control **55** (2008) 538-551.

71 R. H. C. Bonser, W. S. Harwin, W. Hayes, G. Jeronimidis, G. R. Mitchell and C. Santulli, *EAP-Based artificial muscles as an alternative to space mechanisms*, ESA/ESTEC Contract No 18151/04/NL/MV, The University of Reading, Whiteknights, Reading RG6 2AY, 2004

72 M. Kapps, *Smart-Material Mechanisms as Actuation Alternatives for Aerospace Robotics and Automation*, The 25th Annual-International space development conference 2006 (ISDC06) May 4-7, ISDC06 Paper

73 Y. Bar-Cohen, S. Leary, M. Shahinpoor, J. O. Harrisonc, and J. Smith, *Flexible low-mass devices and mechanisms actuated by Electroactive Polymers*, Proceedings of SPIE's 6 Annual International Symposium on Smart Structures and Materials, 1-5 March, 1999, Newport Beach, CA. Paper No. 3669-38

74 T. Ueda, T. Kasazaki, N. Kunitake, T. Hirai,J. Kyokane and K. Yoshino, *Polyurethane Elastomer Actuator*, Synthetic Metals, **85** (1997) 1415-1416.

75 M. Watanabe, M. Suzuki, Y. Hirako, H. Shirai, T. Hirai, *Hysteresis in Bending Electrostriction of Polyurethane Films, Journal of Applied Polymer Science*, **79** (2001) 1121-1126.

76 M. Ghaffari, *Electroactive Graphene/Polyurethane Composites with High Longitudinal Strain at Low Electric Fields*, Carbon, (2010) in press.

77 V. Bharti, Z. Y. Cheng, S. Gross, T. B. Xu, and Q. M. Zhang, *High electrostrictive strain under high mechanical stress in electronirradiated poly(vinylidene fluoride-trifluoroethylene) copolymer*, Appl. Phys. Lett., **75** (1999) 2653- 2655.

78 E. G. Rightor, S. G. Urquhart, A. P. Hitchcock, H. Ade, A. P. Smith, G. E. Mitchell, R. D. Priester, A. Aneja, G. Appel, G. Wilkes and W. E. Lidy, *Identification and Quantitation of Urea Precipitates in Flexible Polyurethane Foam Formulations by X-ray Spectromicroscopy*, Macromolecules, **35** (2002) 5873-5882.

79 G. M. Estes, R. W. Seymour and S. L. Cooper, *Infrared studies of segmented polyurethane elastomers*, II. Macromolecules, **4** (1971) 452-457.

80 Z. Petrovic and J. Ferguson, *Polyurethane elastomers*. Prog. Polym. Sci., **16** (1991) 695-836.

81 H. J. Qi and M. C. Boyce, *Stress–strain behavior of thermoplastic polyurethanes*, Mechanics of Materials, **37** (2005) 817-839.

82 A. V. Raghu, G. S. Gadaginamath, N. T. Mathew, S. B. Halligudi and T. M. Aminabhavi, *Synthesis and characterization of novel polyurethanes based on 4,4'-[1,4-phenylenedi-diazene-2,1-diyl] bis(2-carboxyphenol) and 4,4'-[1,4-phenylenedi-diazene-2,1-diyl] bis(2-chlorophenol) hard segments*, Reactive & Functional Polymers, **67** (2007) 503-514.

83 A. Lapprand, F. Mechin and J.-P. Pascault, *Synthesis and Properties of Self-Crosslinkable Thermoplastic Polyurethanes*, Journal of Applied Polymer Science, **105** (2007) 99-113.

84 C. Park, J. H. Kang, J. S. Harrison, R. C. Costen, and S. E. Lowther, *Actuating Single Wall Carbon Nanotube_Polymer Composites:Intrinsic Unimorphs*, Adv. Mater., 20 (2008) 2074-2079.

85 T. Hu, J. Juuti, H. Jantunen and T. Vilkman, *Dielectric properties of BST/polymer composite*, Journal of the European Ceramic Society, **27** (2007) 3997-4001.

86 D. Guyomar, B. Guiffard, R. Belouadah and L. Petit, *Two-phase magnetoelectric Nanopowder/polyurethane composites*, Journal of Applied Physics, **104** (2008) 074902.

87 L. Petit, B. Guiffard, L. Seveyrat, et al, *Actuating abilities of electroactive carbon nanopowder/polyurethane composite films*, Sensors and Actuators A, Physical, **148** (2008) 105-110.

88 D. Guyomar, K. Yuse, P.-J. Cottinet, M. Kanda and L. Lebrun, *Focus on the electrical field-induced strain of electroactive polymers and the observed saturation*, Journal of Applied Physics, **108** (2010) 114910.

89 A. K. Zak, W. C. Gan, W. H. Abd. Majid, Majid Darroudi and T.S. Velayutham, Experimental and theoretical dielectric studies of PVDF/PZT nanocomposite thin films, Ceramics International, (2011) in press

90 J.-U. Sommer and G. Reiter, Crystallization in ultra-thin polymer films Morphogenesis and thermodynamical aspects, Thermochimica Acta **432** (2005) 135–147.

91 S. Yan and J. Petermann, Oriented recrystallization of pre-oriented thin polymer films, Polymer **41** (2000) 6679–6681.

92 D. Guyomar, K. Yuse and M. Kanda, *Thickness effect on electrostrictive polyurethane strain performances: A three-layer model*, Sensors and Actuators A **168** (2011) 307-312.

93 D. Guyomar, P.-J. Cottinet, L. Lebrun, C. Putson, K. Yuse, M. Kanda, and Y. Nishi, *The compressive electrical field electrostrictive coefficient M_{33} of electroactive polymer composites and its saturation versus electrical field, polymer thickness, frequency and fillers*, Polym. Adv. Technol. (2011) in press

94 K. Yuse, D. Guyomar and M. Kanda, *Thickness effects in electroactive polymers actuators: a simple explanation and modeling*, Proceedings of the SPIE, San Diego, USA (March 2011) in press

95 K. M. Zia, H. N. Bhatti, I. A. Bhatti, *Methods for polyurethane and polyurethane composites, recycling and recovery: A review*, Reactive & Functional Polymers **67** (2007) 675-692.

96 M. Zhenyi, J. I. Scheinbeinm, J. W. Lee and B. A. Newman, *High field electrostrictive response of polymers*, J. Polym. Sci., Part B, **32** (1994) 2721-2731.

97 T. Hirai, H. Sadatoh, T. Ueda, T. Toshiaki, Y. Kurita, M. Hirai and S. Hayashi, *Polyurethane-elastomer-actuator*, Die Angewandte Makromolekulare Chemie **240** (1996) 221-229.

98 Q. M. Zhang, J. Su, C. H. Kim, R. Ting and R. Capps, *An experimental investigation of electromechanical responses in a polyurethane elastomer*, J. Appl. Phys., **81** (1997) 2770-2776.

99 J. Su, Q. M. Zhang, C. H. Kim, R. Y. Ting and R. Capps, *Effects of Transitional Phenomena on the Electric Field Induced Strain–Electrostrictive Response of a Segmented Polyurethane Elastomer*, J. Appl. Polym. Sci., **65** (1997) 1363-1370.

100 I. Diaconu, D.-O. Dorohoi, C. Ciobanu, *Electromechanical response of polyurethane films with different thickness*, Rom. Journ. Phys., **53** (2008) 91-97.

101 M. Watanabe and T. Hirai, *Electric conduction in bending electrostriction of polyurethanes*, Appl. Phys. Lett., **74** (1999) 2717-2719.

102 I. Diaconu and D. Dorohoi, *Electrostrictive response in polyurethane films containing lithium ionic impurities*, Journal of Optoelectronics and Advanced Materials, **9** (2007) 990 -993.

103 M. H. Al-Saleh and U. Sundararaj, *An innovative method to reduce percolation threshold of carbon black filled immiscible polymer blends*, Composites A, **39** (2008) 284-293.

104 K. Wongtimnoi, B. Guiffard, A. Bogner-Van de Moortèle, L. Seveyrat, C. Gauthier and J.-Y. Cavaillé, *Improvement of electrostrictive properties of a polyether-based polyurethane elastomer filled with conductive carbon black*, Composites Science and Technology, **71** (2011) 885-892.

105 B. Guiffard, D. Guyomar, L. Seveyrat, L. Chowanek, M. Bechelany, D. Cornu and P. Miele, *Enhanced electroactive properties of polyurethane films loaded with carbon-coated SiC nanowires*, J. Phys. D: Appl. Phys., **42 (**2009**)** 055503.

106 J. A. Giacometti, S. Fedosov and M. M. Costa, *Corona Charging of Polymers: Recent Advances on Constant Current Charging*, Brazilian Journal of Physics, 29 (1999) 269-279.

107 C. Park, Z. Ounaies, K. E. Wise and J. S. Harrison, *In Situ Poling and Imidization of Amorphous Piezoelectric Polyimides*, NASA/CR-2002-211948, ICASE Report No. 2002-39.

108 W. J. Jasper, A. Mohan, J. Hinestroza and R. Barker, Degradation Processes in Corona-Charged Electret Filter-Media with Exposure to Ethyl Benzene, Journal of Engineered Fibers and Fabrics, **2** (2007) 1-6.

109 Y. Nishi and K. Iwata: Mater. Trans., *Effects of Electron Beam Irradiation on Impact Value for Soda Glass,* **46** (2005) 2241-2245.

110 Y. Nishi and K. Iwata: Mater. Trans., *Influence of Electron Beam Irradiation on the Impact Value of Alkali Free Glass,* **47** (2006) 1810-1814.

111 K. Iwata and Y. Nishi: Mater. Trans., *Effect of Electron-Beam Irradiation on Impact Value of Silica Glass*, **49** (2008) 2058-2062.

112 K. Iwata and Y. Nishi: Mater. Trans., *Effects of Electron Beam Irradiation on Impact Value of Borosilicate Glass*, **51** (2010) 121-127.

113 S. Egusa, *Mechanism of radiation-induced degradation in mechanica properties of polymer matrix composites*, J. Mater. Sci., **23** (1988) 2753-2760.

114 A. Mizutani, Y. Nishi, *Improved Strength in Carbon Fiber Reinforced Plastics due after Electron Beam Irradiation*, Materials Transactions, **44** (2003) 1857-1860.

115 T. Takahashi, T. Morishita, Y. Nishi, *Effect of Electron Beam Irradiation on Stress-Strain Curves of Tensile Test of Polycarbonate Resin*, J. Japan Institute of Metals, **69** (2005) 759-762.

116 H. Sato, Y. Inoue, K. Iwata, A. Tonegawa, Y. Nishi, *Influence of Electron Beam Irradiation on Impact Value of Acryl Resin*, J. Japan Institute of Metals, **72** (2008) 520-525.

117 Y. Nishi, H. Kobayashi, M. Salvia, *Effects of Electron Beam Irradiation on Charpy Impact Value of GFRP*, Materials Transactions, **48** (2007) 1924-1927.

118 Y. Nishi, K. Inoue, M. Salvia, *Improvement of Charpy Impact of Carbon Fiber Reinforced Polymer by Low Energy Sheet Electron Beam Irradiation*, Materials Transactions, **47** (2006) 2846-2851.

119 Y. Nishi, H. Takei, K. Iwata, A. Vautrin, M. Salvia, *Effects of Electron Beam Irradiation on Impact Value of Carbon Fiber Reinforced Thermoplastic Polyetheretherketone*, Materials Transactions, **50** (2009) 2826-2832

120 H. Takei, K. Iwata, M. Salvia, A. Vautrin, *Y. Nishi, Effects of Electron Beam Irradiation on Impact Value of Novolak-Type Phenol CFRTP*, Materials Transactions, **51** (2010) 2259-2265.

121 N. Tsuoulfanidis: Measurement and Detection of Radiation, (Houshasen Keisoku no riron to enshu, in Japanese), (Gendai Kougaku sha, 1983) pp. 543–552.

122 R. Christenhusz and L. Reimer: Z. Angew. Phys., **23** (1967) 396-404.

123 W. F. Libby, *Measurment of Radioactive Tracers*, Anal. Chem., **19** (1947) 2-6.

124 Y. Nishi, T. Yamamoto, S. Namba, H. Takei and K. Iwata, *High Impact Value of CFRP/ABS/CFRP Sandwich Structural Composite Homogeneously Irradiated with Low Voltage Electron Beam*, Mater. Trans. **52** (2011) 73-80.

125 Yu P Yampolskii, *Methods for investigation of the free volume in polymers*, Russian Chemical Reviews **76** (2007) 59-78.

List of figures

List of tables

French part

Chapitre 1

Le but de ce chapitre est de situer le travail entrepris dans le contexte scientifique actuel. Une description de l'état de l'art en matière d'actionnement à l'aide de matériaux électro-actifs est ainsi proposée. De plus il a été abordé la mise en commun de cette thématique, par la présentation de dispositif utilisant cette technologie.

Historiquement les matériaux piézoélectriques ont été les premiers à avoir donné lieu à d'importante recherche depuis leur mise en évidence par les frères Jacques et Pierre Curie. Et depuis les vingt dernière années à un grand nombre d'application commercial, en raison de leur nombreux avantages comme leur grand coefficient de couplage, leur réponse rapides, etc. Par contre cette technologie souffre d'inconvénient majeur comme leur non-linéarité sous champ électrique, et des déformations relativement faibles (<0.2 %).

Depuis un peu moins d'une dizaine d'année les recherches s'orientent sur les matériaux de type polymère :

- en raison de leur caractère souple facilitant leur intégration,
- un processus de fabrication simple limitant ainsi les coûts économiques et environnementaux,
- leur faible densité pour la réalisation de système compact,
- la possibilité de réaliser des grandes déformations (>10 %).

Au cours de ce chapitre, les différentes classes de polymères avec leurs propriétés ont été présentées de façon synthétique, dans le but de donner une vision d'ensemble du domaine. Un grand nombre de travaux se sont focalisés sur polymères électro-actifs de type élastomères diélectriques, qui consistent à un film de polymère pris en sandwich entre deux électrodes compliantes. Lorsque qu'un champ électrique est appliqué à travers l'épaisseur, le polymère se compresse dans son épaisseur. Les résultats ont prouvé la possibilité d'obtenir des déformations sur l'épaisseur comprise entre 10 et 60 %. Démontrant un intérêt pour la réalisation de muscles artificiels, en effets les déformations typiques des muscles humains sont d'environ 20 %. Par exemple des travaux réalisés sur un actionneur à base de silicone ont démontré qu'il est possible d'avoir des déformations égales à 380 %, avec une très bonne efficacité dans la conversion électromécanique, une bonne tenue en température et à l'humidité. Cependant cette technologie souffre d'un inconvénient majeur, qui réside dans le champ électrique qu'il faut appliquer pour obtenir ses grandes déformations, typiquement 150 MV/m. Limitant ainsi leur application du fait de la nécessité d'avoir une source haute tension pour l'alimentation de ces matériaux, avec tous les problèmes que cela entraine d'un point de vue des normes, ect.

Le but des recherches entreprise consiste à développer un matériau capable de générer des déformations importante de l'ordre de 20 % typiquement pour des champs électriques modéré, afin de concilier les avantages et inconvénients inhérent à chaque technologie d'actionnement. Parmi ces polymères électro-actifs, les polymères électrostrictifs montrent sous l'action d'un champ électrique une déformation importante ainsi que des densités énergétique relativement prometteuses, ce qui en fait des candidats de choix pour mener des investigations sur le développement de matériaux à haute performance, d'autant que peu de recherche ont été effectuées sur ceux-ci. Les travaux menés par la suite se focaliseront sur l'utilisation de polymère de type polyuréthane (PU), en raison de leur importante activité dipolaire et caractéristique mécanique.

Chapitre 2

Les propriétés électromécaniques des polymères électrostrictifs sont globalement régies par la permittivité du matériau. Ce paramètre contrôle la déformation électromécanique en mode actionneur. Une augmentation de la permittivité engendre une augmentation substantielle des performances. Pour cela plusieurs méthodes sont possibles, l'objectif développé dans les premières parties du chapitre est de donner un aperçu des méthodes les plus couramment mises en œuvre. Elles peuvent être classées en trois catégories :

- Composite avec particules dispersées aléatoirement (Random composite)
- Composite structuré (Field-structured composite)
- Synthèse de nouveau polymère (New synthetic polymer)

La première approche consiste à disperser des particules de manière aléatoire dans une matrice de polymère. La seconde exploite plus le principe des composites, avec un alignement des particules (dipôle) au sein de la matrice avec le champ électrique par exemple. La troisième consiste à synthétiser des nouveaux polymères pour obtenir les caractéristiques désirées.

Les travaux se sont concentrés sur la réalisation de composite. En effet depuis plus d'une trentaine d'années, en raison de leurs nombreux atouts, les matériaux composites sont étudiés par rapport aux matériaux traditionnels. Ils apportent de nombreux avantages fonctionnels qui vont de l'augmentation de la résistance mécanique à la durée de vie. Il existe différent type de particules pour la réalisation de composite. L'utilisation des matériaux inorganiques, avec de grande permittivité diélectrique, est une technique largement développée depuis une vingtaine d'année pour accroître la permittivité d'un composite. Les poudres à base de céramique ferroélectrique ou piézoélectrique en font des candidats de choix pour leur grande permittivité (2000 PMN). Malgré une augmentation importante de la permittivité en utilisant des particules de céramiques, cette méthode n'est pas optimale pour améliorer les propriétés en actionneurs des films polymères. L'inconvénient majeur de ce procédé réside dans les propriétés intrinsèques des particules. En effet les céramiques ferroélectriques sont très rigides, provoquant alors une diminution de la capacité de déformation du composite. Ce phénomène limite donc l'ajout de quantité de particules à de faible pourcentage afin d'obtenir une interaction faible entre la matrice et les charges. De plus le composite ainsi obtenu est bien plus rigide.

Les particules diélectriques à base de matériaux ferroélectriques ne sont pas les seules solutions pour accroître les propriétés électromécaniques des polymères, il est possible d'utiliser des charges conductrices. En effet l'utilisation de particules conductrices est une solution intéressante pour l'augmentation de la permittivité. La dispersion de particules conductrices provoque une accumulation de charges à la frontière entre les deux milieux (matrice, particules). Ces charges libres présentes dans le polymère ne contribuent pas seulement à la conduction, mais elles augmentent la polarisation interfaciale, donc la permittivité. L'étude expérimentale de la conduction d'un milieu statistiquement aléatoire, avec des inclusions conductrices et non conductrices, indique qu'en dessous d'une certaine concentration de ses inclusions, le milieu est isolant et au dessus de cette concentration, le système est conducteur. C'est autour de cette problématique que les travaux de recherche se sont orientés. Par le développement d'une méthode de synthèse pour la réalisation de composite chargé à base de particule conductrice.

Il a été choisi de réaliser des composites par le procédé ex-situ, en utilisant la méthode par voie solvant, pour des questions de facilité de mise en place et de polyvalence de cette technique. Le processus d'élaboration mis en place peut être décomposé en quatre étapes (dissolution des granules de PU, ajout des charges conductrices sous forme de micelle, dépôt à l'aide tournette, recuit). Afin de juger de la qualité du processus de fabrication des composites développés au laboratoire, des observations microscopiques à toutes les échelles de taille ont été utilisées ; comme la microscopie optique, le TEM (Transmission Electron Microscope), le SEM (Scanning Electron Microscope). Les différentes échelles d'observation rendent compte d'un état de dispersion à des échelles différentes.

Afin d'évaluer le potentiel des composites du laboratoire, les travaux entrepris étudie la dépendance de leur déformation avec le champ électrique, etc. En effet, de par le caractère innovant de ces matériaux, peu de données sont disponibles. C'est pourquoi une caractérisation complète est nécessaire pour une meilleure compréhension des phénomènes. Pour cela les mesures de déformation longitudinale sont réalisées dans le sens d'application du champ électrique. Le film de polymère est placé horizontalement entre deux disques de laiton jouant le rôle d'électrode, afin d'éviter de mesurer des mouvements de flexion du film. Le champ électrique est appliqué au polymère à l'aide d'un amplificateur haute tension (Trek 10/10B) commandé par un générateur de fonction (Agilent 33220A). Le courant fourni au polymère pour fonctionner est mesuré à l'aide d'un amplificateur de courant (Stanford Research Systems SR570) pour pouvoir remonter à la polarisation. Afin de mesurer la variation d'épaisseur de l'échantillon un bloc laser interférométrique (Agilent 5519A) double faisceau dont la résolution est de l'ordre de 10 nm est utilisé. L'ensemble des données est acquis sur un ordinateur.

Les mesures ont démontré l'effet bénéfique de l'utilisation des charges conductrices dans l'amélioration des propriétés en actionnement des polymères. Pour un même champ électrique un facteur trois sur la déformation a été noté entre une matrice de PU pure et une matrice de PU chargée avec 0.89 vol% de carbone. De plus des non-linéarités ont été observées concernant la déformation en fonction du champ électrique. Pour les faibles valeurs de champ électrique inférieur par exemple à 5 MV/m une déformation quadratique est observée. Par contre lorsque le champ électrique augmente la déformation sature.

Chapitre 3

A partir des résultats obtenus dans le chapitre 2, plusieurs phénomènes restent à éclaircir, tel que saturation de la déformation en fonction du champ électrique. Pour cela une modélisation de la réponse électromécanique des polymères a été réalisée. L'approche proposée est basée sur une modélisation en fonction hyperbolique, afin de déterminer la possible saturation de la polarisation avec le champ électrique.

La modélisation part du principe que le comportement diélectrique de nos polymères peut s'écrire sous la forme de l'équation suivante :

$$P = \varepsilon_0 . \varepsilon_r . E_{sat} . th\left(\frac{E}{E_{sat}}\right)$$

Avec ε_0 la permittivité de vide ε_r la permittivité relative, E_{sat} correspond au champ électrique de saturation, P et E indiquent respectivement la polarisation et le champ électrique.

La fonction en tangente hyperbolique a été choisie pour modéliser le comportement non linéaire des polymères car elle permet pour les faibles champs électriques d'obtenir une relation linéaire entre la polarisation et le champ électrique, et pour les amplitudes supérieures à E_{sat} la polarisation sature.

En modélisant la polarisation comme une fonction non-linéaire dépendant de deux variables (la permittivité bas niveau et un champ de saturation), on décrit correctement :

- les effets de saturation des niveaux
- le processus qui limite l'augmentation de la déformation avec la permittivité
- la dépendance de la déformation en fonction de l'épaisseur
- les effets liés aux pertes diélectriques et/ou électrostrictives.
- les écarts importants entre la formulation en champ électrique et la formulation en polarisation ; cette dernière respectant mieux la physique du phénomène.
- La distorsion des courants et la variation de la conductivité avec le champ électrique.
- L'évolution fortement non-linéaire de la permittivité avec le champ
- La connexion très forte entre la permittivité équivalente du film et la déformation de ce dernier.
- Les effets de croissance ou de décroissance de la déformation avec l'épaisseur de ce dernier.

La modélisation nous a amené à supposer l'existence d'un gradient de propriété dans le sens de l'épaisseur. Etant donné que les simulations sont en bon accord avec les expérimentations, on peut considérer que l'hypothèse est valide. Plusieurs modèles, en régime linéaire et non-linéaire, ont été développés à partir de cette hypothèse.

D'un point de vue microscopique, cette saturation peut prendre forme en raison de la structure des polymères. En effet les élastomères PU sont constitués de blocs de chaînes flexibles de température de transition vitreuse faible (appelés segments souples) provenant essentiellement du macrodiol et de blocs hautement polaires, relativement rigides (appelés segments rigides). Lors de l'application d'un champ électrique les segments durs ont tendance à s'orienter dans la direction du champ électrique appliqué, en raison de leur caractère polaire. Pour un champ électrique correspondant au champ de saturation ceux-ci sont parallèles. Il n'y a plus de déplacement de l'interface entre les domaines polaires (segments durs ou charge) et les segments souples, d'où la saturation de la polarisation.

Chapitre 4

Créer des muscles artificiels une ambition qui n'est pas nouvelle. Depuis plus de vingt ans, les céramiques piézo-électriques et les alliages métalliques à mémoire de forme ont déjà stimulé cette recherche. Mais ceux-ci souffrent d'un grand nombre d'inconvénients comme les faibles amplitudes de déformation, pour les céramiques, et un temps de réponse très long pour les alliages à mémoire de forme. Les polymères électro-actifs développés au cours des travaux de thèse pourraient apporter une solution au problème grâce à leurs propriétés. C'est autour de cette problématique que ce chapitre s'articule, avec l'étude de la dépendance en épaisseur et sa modélisation.

Des échantillons de différentes épaisseurs ont été réalisés. Il est intéressant de noter que, pour la matrice de PU étudiée ici, une forte dépendance de la déformation avec l'épaisseur des films est observée. En effet selon le niveau de champ électrique appliqué les résultats sont totalement différents. Pour les amplitudes de champ électrique inférieur à 5 MV/m, les films épais donnent de meilleure réponse, par contre pour des amplitudes supérieures à 5 MV/m, le phénomène inverse se produit. Pour les faibles valeurs de champ électrique la variation de déformation avec l'épaisseur peuvent s'expliquer par la structure des polymères. En effet ils sont constitués de segments durs et doux permettant ainsi de piéger les charges provoquant une distribution non-uniforme du champ électrique et une augmentation de la déformation. Mais dans le cas où les films sont minces, les espaces de piégeage se chevauchent provoquant une homogénéisation des charges d'espaces. Ce phénomène se traduit par une augmentation du coefficient d'électrostriction *M*. Mais ce coefficient n'assure pas de grande déformation pour les champs électrique important comme le montre les données expérimentales. En effet le coefficient *M* assume une dépendance linéaire entre la polarisation et le champ électrique ce qui n'est pas le cas en réalité. Il est plus correct de déterminer le coefficient *Q* qui lit la polarisation à la déformation.

Dans le but de mieux comprendre cette dépendance en épaisseur, un travail de modélisation a été entrepris. Il consiste à supposer que les polymères épais sont composés de trois couches de permittivité différentes alors que pour les épaisseurs faibles la structure est plus homogène. Cette dissymétrie dans la structure avec une phase plus cristalline sur les bords est produite par une répartition non homogène de la température lors de la phase de cuisson de l'échantillon de polymère. Cet effet est accentué dans les films d'épaisseur importante, à cause du mauvais coefficient d'échange thermique des films polymère. Une image simple est celle d'une pâte à tarte qui est moelleuse à l'intérieur et craquante à l'extérieur, lors de ça cuisson. Les couches des deux extrémités étant plus cristalline leur permittivité est plus importante. La répartition du champ électrique n'est donc pas identique dans chacune d'elle. C'est autour de cette idée que les travaux de modélisation se sont organisé, en modélisant la répartition du champ électrique à l'intérieur de la structure et la réponse électromécanique résultante. Une bonne cohérence entre les résultats expérimentaux et la pratiques ont été obtenue.

Dans l'objectif de valider l'hypothèse de la structure en couche des polymères, des mesures de DSC (Differential Scanning Calorimetry) et aux rayons X (XRD) ont été réalisées. Les mesures ont démontré une cristallinité plus importante pour les films épais, comme le laissait présager le modèle. Par contre les mesures de conductivité thermique n'ont pas révélé de différence majeure.

Des mesures analogues ont été faites sur des composites chargés à l'aide carbone, le même phénomène de dépendance a été observé. Démontrant encore la validité du modèle développé au cours de ce chapitre.

Pour synthétiser les résultats obtenus, ont prouvé l'influence du degré de cristallisation sur les performances en actionnement, l'avantage de réaliser des composites avec une augmentation de l'activité électromécanique et une facilité de fabrication.

Chapitre 5

D’un point de vue général, sur le marché émergeant des systèmes réalisés à l’aide de matériaux intelligents, les céramiques font face à une rude compétition dû à leur inconvénient majeur comme : le risque de dépolarisation, leur grande fragilité, et un processus de réalisation complexe et onéreux. Les polymères électro-actifs développés au laboratoire amènent une rupture technologique importante dans la vision des nouveaux systèmes intelligents. Les premières recherche ont prouvé la possibilité de créer des matériaux capable de générer des déformations importante (<30 %) pour des champs électriques modéré (< 20 MV/m). Les résultats ont démontré un lien entre la distribution des charges d’espace, dans le but d’organiser ses charges ont sein de la structure les travaux se sont focaliser sur la possibilité d’implanter des charges électriques par effet Corona ou par irradiation.

Dans un premier temps la méthode d’irradiation a été choisie, en effet les puissances supérieures à 1 MeV entrainent des dommages important dans la structure du matériau. Pour arriver à modifier la structure sans pour autant l’altérer, une puissance de 0.1 MeV à été choisie ce qui correspond à la technologie de type (HEBI).

Différentes série de mesures ont été réalisé, il a été observé une influence positive du traitement sur les déformations. Par exemple un film de PU pure d’épaisseur 194 μm avant traitement donnait une déformation de 4.45 % à 20 MV/m, après traitement le même échantillon avait une déformation de 10.62 % pour la même sollicitation électrique. Soit une augmentation de l’activité électromécanique d’un facteur 2. Afin de juger de la qualité d’implémentation des électrons, la profondeur de pénétration à été calculé. Il a été démontré que celle-ci était comprise entre 192 μm et 291 μm. L’injection d’électron a aussi été testé sur des composites chargé avec 0.45 vol% de carbone et ayant une épaisseur de 14 μm. Une augmentation d’un facteur 1.3 de la déformation à été noté pour un même champ électrique. Le volume libre est considéré comme source possible de cet accroissement. L’ensemble des données permettent ainsi de valider l’idée d’injecter des électrons pour accroître les propriétés en actionnement des matériaux.

A titre de comparaison avec les céramiques piézoélectriques qui nécessitent la réalisation de structures multicouches pour obtenir de fortes déformations, ce qui augmentent le poids du système et le volume du système, les composites électro-actifs développés au laboratoire permettent d’obtenir des déformations importantes de l’ordre de 20 % pour un champ électrique de 15 MV/m. Par ailleurs, les films de composites ne présentent pas de phénomène d’hystérésis observé dans les PZT ferroélectriques lorsque le champ augmente. Les déformations sous champ sont donc parfaitement reproductibles sous cyclage du champ. Par conséquent, ces matériaux démontrent bien leur avantage pour des applications de type micro-positionnement exigeant à la fois une grande précision et une très bonne reproductibilité des déplacements. En outre, les polymères électrostrictifs montrent des temps de réponses de l’ordre de la milliseconde comparé à la seconde dans le cas des actionneurs à bases d’alliages à mémoire de forme.

Les travaux présentés ici ne sont bien sûr qu’une ébauche de ce que sera probablement le futur des polymères électro-actifs pour l’actionnement. Leur développement passe par l’optimisation des composites tous d’abord sur le plan de la dispersion des charges à l’aide de copolymérisation par exemple. Mais aussi par la recherche de nouveaux agents de couplages multifonctionnels afin d’accroître la compatibilité entre la matrice et les particules pour l’amélioration des propriétés de conversion de nos matériaux. Mais aussi par une recherche en amont plus fondamentale pour comprendre les processus mis en jeux lors des déformations sous champ électrique au niveau microscopique, par la mesure des charges d’espaces par exemple.

FOLIO ADMINISTRATIF

THESE SOUTENUE DEVANT L'INSTITUT NATIONAL DES SCIENCES APPLIQUEES DE LYON

NOM : KANDA DATE de SOUTENANCE : 21 July 2011
(avec précision du nom de jeune fille, le cas échéant)
Prénoms : Masae

TITRE : **Polymères électrostrictifs à forte déformation : méthode d'élaboration et modélisation**

NATURE : **Doctorat** Numéro d'ordre : 2011 ISAL 0067
Ecole doctorale : E.E.A.
Spécialité : **ELECTRONIQUE, ELECTROTECHNIQUE, AUTOMATIQUE**
Cote B.I.U. - Lyon : T 50/210/19 / et bis CLASSE :

RESUME :

De façon générale la thèse porte sur les matériaux dits intelligents et plus particulièrement sur les polymères electroactifs et/ou electrostrictifs. Ces matériaux présentent un fort couplage electro-mécanique et sont par ailleurs très flexibles et très légers. C’est dire qu’ils peuvent être utilisés soit comme actionneurs mécaniques souples, soit en récupération d’énergie sur l’énergie vibratoire. Le sujet de thèse portait sur :

•le développement d’une méthode, peu coûteuse, pour réaliser les films électrostrictifs à partir de micelle déjà formées permettant une dispersion des particules de carbone.
•L’augmentation de la permittivité, afin d’augmenter le couplage electro-mecanique en chargeant le polymère avec des particules conductrices et/ ou par bombardement électronique.
•La modélisation mathématique des phénomènes observés et les projections afin d’améliorer les caractéristiques de ces derniers

Le premier chapitre est une introduction aux systèmes couplés reliant les propriétés mécaniques et les propriétés électriques entre-elles (piézoélectricité, polymères électroactifs, polymères ioniques…). L’objectif de ce chapitre est également de choisir le type de polymère le plus adapté à la réalisation d’actionneurs flexibles ou de récupérateur d’énergie. Notre choix s’est porté sur les élastomères diélectriques et, en particulier les polyuréthanes.

Le second chapitre porte principalement sur la réalisation des films polymères. La déformation électrostrictive augmentant, dans une certaine limite, avec la permittivité diélectrique, nous avons donc décidé d’introduire des charges conductrices dans la matrice afin d’augmenter la permittivité sans trop changer la masse. Afin de pouvoir réaliser, in fine, de films de surface importante, tout en ayant une bonne dispersion, nous avons introduit le carbone sous forme de micelles préformées. En l’occurrence nous avons mélangé des encres d’écriture avec le polyuréthane et choisi une technique de type « solution-cast » pour réaliser les films. Une amélioration de la déformation d’un facteur 1,6 a ainsi été obtenue par introduction de noir de carbone à 0.89 vol%.

Le troisième chapitre porte sur la modélisation des phénomènes, menée en collaboration avec l’encadrant, et en particulier sur la saturation de la polarisation ce qui implique directement une saturation de la déformation electrostrictive et une limitation de la course des actionneurs. En modélisant la polarisation comme une fonction non-linéaire dépendant de deux variables : la permittivité bas niveau et un champ de saturation, on décrit correctement :

•les effets de saturation des niveaux et le mécanisme de limitation des niveaux
•la dépendance de la déformation en fonction de l’épaisseur et des pertes
•les écarts importants entre la formulation en champ électrique et en polarisation
•La distorsion des courants et la variation de la conductivité avec le champ
•L’évolution fortement non-linéaire de la permittivité avec le champ
•La connexion entre la permittivité équivalente du film et sa déformation.
•Les effets de croissance ou décroissance de la déformation avec l’épaisseur

La modélisation nous a amené à supposer l’existence d’un gradient de propriété dans le sens de l’épaisseur. Etant donné que les simulations sont en bon accord avec les expérimentations, on peut considérer que l’hypothèse est valide. Plusieurs modèles, en régime linéaire et non-linéaire ont été développés à partir de cette hypothèse.

Le quatrième chapitre présente une comparaison approfondie entre les films en pure polyuréthane et ceux chargés avec des particules conductrices. En ce qui concerne les composites, nous avons montré que la méthode de fabrication proposée permet d’obtenir une bonne dispersion des particules. C’est un résultat important car il devient possible d’obtenir des films de grande surface présentant une bonne dispersion des particules conductrices. Les courbes de déformation en fonction de l’épaisseur pour différents taux de charge confirment ce résultat. De déformation de l’order de 50 % ont été obtenues.

Le cinquième chapitre porte sur l’effet lié à l’injection de charges électriques, par corona ou bombardement électronique (BE), sur la déformation electrostrictive. Si les résultats obtenus par effet Corona ne sont pas convaincants, ceux obtenus par BE sont très intéressants. En effet, on gagne un facteur 2 sur la déformation et le BE semble réduire les pertes de façon très conséquente. Par contre l’effet diminue rapidement avec le temps puisqu’on note une réduction forte de l’effet après 2 mois.

MOTS-CLES : **Polymères électro-actifs, Composites, Actionneurs, Effet d’épaisseur, Permittivité, Micelle**

Laboratoire (s) de recherche : **Laboratoire de Génie Electrique et Ferroélectricité (LGEF) INSA Lyon**
Directeur de thèse: **Prof. Daniel GUYOMAR**
Co-directeur de thèse: **Dr. Kaori YUSE MCF.**
Président de jury : **Dr. Gilbert TEYSSEDRE Directeur de Recherches au CNRS**
Composition du jury :
Prof. Daniel GUYOMAR, Dr. Kaori YUSE MCF, Dr. Gilbert TEYSSEDRE Directeur de Recherches au CNRS, Prof. Yoshitake NISHI, Dr. Yves BERNARD MCF-HDR, Dr. Eric DUHAYON MCF